UNIVERSITÉ BLAISE PASCAL

Ecole doctorale

Sciences de la Vie, Santé, Agronomie, Environnement

Numéro d'ordre : 552
D.U. : 2140

THÈSE de DOCTORAT

en « Neurosciences »

par

Benoist LEHALLIER

Traitement cérébral d'odeurs biologiquement signifiantes, révélé chez le rat par imagerie RMN fonctionnelle du manganèse

Thèse dirigée par le Dr. Jean-Marie Bonny et le Dr. Yves Maurin

Soutenue le 28 juin 2011 devant la commission d'examen composée de :

Pr Jean-Marc LOBACCARO	CNRS, Clermont-Ferrand	Président du jury
Dr Nathalie BUONVISO	CNRS, Lyon	Rapporteur
Dr Luc DARRASSE	CNRS, Orsay	Rapporteur
Dr Philippe CHEMINEAU	INRA, Tours	Examinateur
Pr Franck DURIF	CHU, Clermont-Ferrand	Examinateur
Dr Yves MAURIN	INRA, Jouy-en-Josas	Directeur de thèse
Dr Jean-Marie BONNY	INRA, Clermont-Ferrand	Directeur de thèse

Laboratoire STIM – U.R. 370 – INRA de Theix

63122 Saint Genès Champanelle

UNIVERSITÉ BLAISE PASCAL

Ecole doctorale

Sciences de la Vie, Santé, Agronomie, Environnement

Numéro d'ordre : 552
D.U. : 2140

THÈSE de DOCTORAT

en « Neurosciences »

par

Benoist LEHALLIER

Traitement cérébral d'odeurs biologiquement signifiantes, révélé chez le rat par imagerie RMN fonctionnelle du manganèse

---

Thèse dirigée par le Dr. Jean-Marie Bonny et le Dr. Yves Maurin

Soutenue le 28 juin 2011 devant la commission d'examen composée de :

Pr Jean-Marc LOBACCARO	CNRS, Clermont-Ferrand	Président du jury
Dr Nathalie BUONVISO	CNRS, Lyon	Rapporteur
Dr Luc DARRASSE	CNRS, Orsay	Rapporteur
Dr Philippe CHEMINEAU	INRA, Tours	Examinateur
Pr Franck DURIF	CHU, Clermont-Ferrand	Examinateur
Dr Yves MAURIN	INRA, Jouy-en-Josas	Directeur de thèse
Dr Jean-Marie BONNY	INRA, Clermont-Ferrand	Directeur de thèse

Laboratoire STIM – U.R. 370 – INRA de Theix

63122 Saint Genès Champanelle

Remerciements

En préambule de ce manuscrit, je tiens à remercier les membres de mon jury de thèse ainsi que le Pr. Jean-Marc Lobaccaro pour avoir accepté, en urgence, de présider ce jury. Je désire exprimer mes plus sincères remerciements au Docteur Nathalie Buonviso et au Docteur Luc Darrasse pour avoir accepté de corriger et de rapporter ce travail. Ils ont contribué par leurs remarques et suggestions à améliorer la qualité de ce mémoire, et je leur en suis très reconnaissant.

Ce travail a été réalisé au sein de l'U.R. 370 à l'INRA de Theix dans l'équipe « Structures Tissulaires et Interactions Moléculaires » (STIM). Je tiens à remercier Monsieur Jean-Pierre Renou, pour m'avoir accueilli dans son unité. Les personnes qui m'ont soutenue ou aidé pendant ma thèse sont nombreuses et j'espère être juste et n'oublier personne.

En premier lieu, je tiens à exprimer toute ma reconnaissance à mes codirecteurs de thèse, à savoir Jean-Marie Bonny et Yves Maurin. J'ai eu la chance d'être encadré par ces deux personnages si différents sur certains points mais tellement complémentaires. Ce sont deux personnes que j'estime autant scientifiquement qu'humainement et je souhaite les remercier à la hauteur de leur grande implication dans ce projet. Merci à vous deux pour toutes ces longues sessions de travail partagées ensembles ainsi que pour votre soutien tout au long de cette thèse.

Je tiens également à remercier les membres de mon comité de thèse pour l'intérêt qu'ils ont porté à ce travail et pour les remarques constructives qu'ils ont fait sur mon projet de thèse. Je tiens à remercier tout spécialement Olivier Rampin pour ses précieux conseils ainsi que pour son implication dans les différents manuscrits. Je souhaite aussi remercier Gérard Coureaud et Benoist Schaal qui ont su apporter un regard d'éthologue nécessaire à ce travail.

Il est souvent difficile pour un doctorant de voir autre chose que son propre travail de thèse. J'ai eu la chance durant ces trois années de pouvoir échanger avec des spécialistes de domaines aussi variés que le traitement d'images, l'IRMf chez l'Homme ou encore la chimie analytique. Je tiens donc à remercier Philippe Andrey pour les longues discussions que nous avons eues concernant l'analyse d'images. Je tiens également à remercier Gil Morrot pour

m'avoir fait découvrir l'olfaction humaine. Merci aussi à Erwan Engel et Jérémy Ratel pour notre collaboration, entretenue depuis plusieurs années déjà, qui restera comme mes premiers pas dans le domaine de la recherche.

Ce travail de thèse fut mené un peu à l'écart des autres thématiques scientifiques existantes dans l'U.R. 370. Néanmoins, mon travail n'aurait pu s'accomplir sans le soutien quotidien de Sylvie, Jean-louis et Abdel, mes collègues de l'équipe STIM. Merci également à mes ex-collègues Patrick, Fred, Jean-Louis et tous les autres « MASSistes » pour tous ces bons moments passés. Pour finir, merci à l'ensemble des agents de la plateforme RMSB et de l'unité QuaPA pour leur accueil.

J'ai une pensée particulière pour les autres doctorants et stagiaires : Sam, Manu, Mus, Salem, Guilhem, Jif, Souley, Cyril, Malo, Aurélie, Miguel, Juliana, Wadie, Mohammed, Gérald et j'en oublie...

Les derniers mots sont pour ma famille et Fatiha qui ont su m'encourager et me soutenir au cours de cette thèse.

Résumé

L'objectif de cette thèse est d'utiliser MEMRI (manganese-enhanced magnetic resonance imaging) pour étudier le traitement d'odeurs signifiantes dans le cortex olfactif primaire de rats dans les conditions les plus proches de la perception naturelle. MEMRI est une méthode fondée sur la détection d'un agent de contraste fonctionnel et rémanent de l'activité neuronale, le manganèse, qui a prouvé son efficacité pour montrer le traitement différencié d'odeurs dans le bulbe olfactif chez l'animal vigile. Cependant, cette technique a été surtout utilisée pour tracer les voies neuronales, mais relativement peu pour explorer des fonctions sensorielles. C'est pourquoi nous avons conduit deux études visant l'une à définir les conditions d'application du manganèse et l'autre à optimiser le traitement des images MEMRI, avant d'aborder la question biologique proprement dite. S'appuyant sur ces développements méthodologiques, nous avons ensuite utilisé MEMRI pour étudier les variations du traitement d'odeurs signifiantes (odeurs de nourriture et de prédateur comparées à une situation de contrôle) dans le cortex olfactif primaire de rats. Nous avons montré que le traitement cérébral d'une odeur de prédateur est différent de celui de la situation de contrôle dans le cortex olfactif primaire. Nous avons confirmé ce résultat par immunomarquage Fos dans le cortex piriforme. Mis ensembles, les résultats de MEMRI et Fos suggèrent que le traitement cérébral d'une odeur peut varier en termes de taille de populations de neurones recrutés ainsi qu'en termes d'intensité de l'activation de ces neurones. Enfin, les résultats MEMRI montrent qu'un message olfactif crucial, pour la survie, est traité asymétriquement dans le cerveau. Les avancées méthodologiques et scientifiques qu'apporte cette thèse ouvrent la voie à une meilleure compréhension du traitement cérébral des odeurs.

Mots-clés : MEMRI, olfaction, rat, manganèse, toxicité, normalisation, cortex olfactif primaire

Abstract

The aim of this thesis was to use MEMRI (manganese-enhanced magnetic resonance imaging) for studying the processing of behaviorally significant odors in the rat primary olfactory cortex, under conditions close to natural perception in awake animals. MEMRI is a method based on the detection of a functional and remanent contrast agent, manganese, which has proved to be valuable for studying odor processing in the olfactory bulb. However, this method has mainly been used to trace neuronal pathways, but seldom to explore sensory functions. Here, we have conducted two studies to define the conditions of application of manganese and to optimize processing of MEMRI images. Based on these methodological developments, we have then used MEMRI to investigate the activation of central olfactory structures following exposure of awake rats to biologically relevant odors (food and predator odors compared to a control situation). MEMRI revealed that a predator odor is processed differently from the control situation in the primary olfactory cortex. Fos immunolabeling in the anterior piriform cortex corroborated this result. Altogether, MEMRI and Fos results suggest that olfactory processing may rely on both the intensity of activation and the size of neuronal populations recruited. Finally, MEMRI revealed that an olfactory message, crucial for survival, is asymmetrically processed in the brain. Methodological and scientific advances brought by this thesis will be useful for better understanding brain olfactory processing.

Keywords: MEMRI, olfaction, rat, manganese, toxicity, normalization, primary olfactory cortex

Liste des publications et communications

Articles, en relation directe avec le sujet de thèse, dans des périodiques à comité de lecture

1 Lehallier B., Coureaud G., Maurin Y., Bonny J.M. Effects of Manganese dose injected into rat nostrils: implications for in vivo functional study of olfaction using MEMRI. (2011) Magnetic Resonance Imaging. *In press.*

2 Lehallier B., Andrey P., Maurin Y., Bonny J.M. Iterative algorithm for spatial and intensity normalization of MEMRI images. Application to tract-tracing of rat olfactory pathways. (2011) Magnetic Resonance Imaging. *In press, doi:10.1016/j.mri.2011.07.014.*

3 Lehallier B., Rampin O., Saint-Albin A., Jérôme N., Ouali C., Maurin Y., Bonny J.M. Central processing of behaviorally relevant odors in the awake rat, as revealed by Manganese-enhanced MRI. (2011) Cerebral Cortex. *Soumis.*

Communications, en relation directe avec le sujet de thèse, dans des congrès internationaux

4 Lehallier B., Ben Moussa A., Ben Hassen W., Coureaud G., Rampin O., Schaal B., Maurin Y., Bonny J.M. Manganese-enhanced fMRI in olfaction: optimisation of Mn dose with minimal deleterious effects upon odour induced behaviour in rats. (2009) XIXth European Chemoreception Research Organization congress, Cagliari/Italy – *Résumé et Poster*.

5 Lehallier B., Ben Moussa A., Ben Hassen W., Coureaud G., Rampin O., Schaal B., Maurin Y., Bonny J.M. Dynamic MEMRI in olfaction: optimisation of Mn dose with minimal deleterious effects upon odour induced behaviour in rats. (2009) 26th Annual meeting ESMRMB, Antalya/Turkey – *Résumé et Oral*.

6 Lehallier B., Andrey P., Maurin Y., Bonny J.M. Methods for groupwise analysis of functional MEMRI data. (2010) 17th triennual ISMAR Conference, Firenze/Italy - *Résumé et Poster*.

7 Lehallier B., Coureaud G., Rampin O., Schaal B., Maurin Y., Bonny J.M. Functional Manganese Enhanced MRI Reveals Deep Brain Regions Activations In Response to Odorant Stimuli In Rats. (2010) 10th International Conference on the Applications of

Magnetic Resonance in Food Science, Clermont-Ferrand/France – *Résumé, Poster et Oral.*

Autres articles dans des périodiques à comité de lecture

8 Morrot G., Bonny J.M, Lehallier B., Zanca M. fMRI of human olfaction at individual level: inter-individual variability. (2011) Journal of Magnetic Resonance Imaging. *Accepté pour publication.*

9 Bouhrara M., Lehallier B., Clerjon S., Damez J.L., Bonny J.M. Mapping of muscle deformation during heating: in situ dynamic MRI and non-linear registration. (2011) Magnetic Resonance Imaging. *Accepté pour publication.*

10 Lehallier B., Ratel J., Hanafi M., Engel E. Systematic ratio normalization of chromatographic signal for biological sample discrimination and biomarker discovery. (2011) Analytica Chimical Acta. *Soumis.*

Table des matières

Remerciements **2**

Résumé **4**

Abstract **5**

Liste des publications et communications **6**

Table des matières **8**

Liste des figures, tables et abréviations **10**

1. Figures 10
2. Tables 13
3. Abréviations 14

Introduction générale **15**

Chapitre I : Revue de littérature **17**

1. Rappels historiques 17
2. Anatomie et physiologie du cortex olfactif primaire 19
3. L'imagerie fonctionnelle 24
   - 3.1. Vue d'ensemble 24
   - 3.2. Imagerie fonctionnelle de l'agent de contraste manganèse (« Manganese-enhanced magnetic resonance imaging », MEMRI) 26
   - 3.3. Imagerie fonctionnelle de l'olfaction 29

Chapitre II : Travail personnel **34**
1. Objectifs de la thèse 34
Présentation de l'article #1 37
2. Effet du manganèse injecté dans les narines de rat : implications pour les études fonctionnelles *in vivo* de l'olfaction utilisant MEMRI 38
Présentation de l'article #2 53
3. Algorithme itératif pour la normalisation spatiale et en intensité des images MEMRI. Application au traçage des voies olfactives chez le rat. 55
Présentation de l'article #3 78
4. Traitement central d'odeurs biologiquement signifiantes, révélé par MEMRI chez le rat vigile. 79

Chapitre III : Conclusion générale et perspectives **97**

Bibliographie **102**

Annexe **115**
Résumé des communications dans des congrès internationaux 116

Liste des figures, tables et abréviations

1. Figures

Revue de littérature

Figure 1 : Evolution du système olfactif chez les mammifères.

Figure 2 : Neuroanatomie du bulbe olfactif de chien.

Figure 3 : Projection des neurones de l'épithélium olfactif sur le bulbe olfactif.

Figure 4 : Organisation des connexions intrabulbaires.

Figure 5 : Afférences et efférences du bulbe olfactif.

Figure 6 : Synthèse des méthodes d'imagerie.

Figure 7 : Principes de l'IRMf BOLD.

Figure 8 : Schéma du transport de manganèse dans un neurone.

Figure 9 : Images pondérées T_1 acquises à différents temps après injection systémique de Mn.

Figure 10 : Image pondérée T_1 après injection systémique de Mn et rupture de la barrière hémato-encéphalique.

Figure 11 : Cartographie R1 ($=1/T_1$) réalisée 2 jours après injection de Mn dans le cortex sensorimoteur d'un rat sain.

Figure 12 : Activations mises en évidence par IRMf BOLD dans différentes régions cérébrales suite à une stimulation olfactive chez l'Homme.

Figure 13 : Activations mises en évidence par IRMf BOLD en réponse à la TMT chez le rat vigile.

Figure 14 : Traçage des voies olfactives après injection de Mn dans une narine de rats.

Figure 15 : Images pondérées T_1 montrant l'accumulation de Mn dans le bulbe olfactif accessoire suite à l'exposition d'une souris à des phéromones.

Figure 16 : Cartographies de l'accumulation de Mn dans la couche glomérulaire suite à l'exposition de rats à différentes odeurs.

Figure 17 : Coupe coronale dans la partie médiane du cortex piriforme antérieur illustrant la résolution spatiale des études MEMRI.

Figure 18 : Coupe parasagittale d'une tête de rat révélant l'anatomie de la fosse nasale.

Travail personnel

Figure 1.1: Behavioral effects of odor stimulation on Mn-free and Mn-impregnated rats.

Figure 1.2: Effects of Mn dose on MR enhancements in the olfactory bulb and the primary olfactory cortex.

Figure 1.3: Group-averaged contrast enhancement along the olfactory pathway for different Mn doses.

Figure 2.1: Automatic segmentation strategy.

Figure 2.2: Flowchart of the iterative spatial and intensity normalization algorithm.

Figure 2.3: 3D views of the 18 anatomical landmarks distributed throughout the brain.

Figure 2.4: Effect of the choice of the ROI used for intensity normalization upon activation maps.

Figure 2.5: Effect of the choice of the ROI used for intensity normalization on the number of statistically significant voxels.

Figure 3.1: Group-averaged images in different coronal slices intercepting primary olfactory cortex for the Mn-free and the unstimulated Mn group.

Figure 3.2: Effect of odor stimulation on Mn enhancement along the olfactory pathways.

Figure 3.3: Statistical t-maps overlaid on T1 weighted MEMRI images depicting variation of Mn enhancement between odor-stimulated groups and the control group.

Figure 3.4: Variation of Mn enhancement between odor-stimulated groups and the control group in anatomical ROIs located in three successive slices corresponding to the piriform cortex.

Figure 3.5: Fos immunodetection of neurons activated by olfactory stimulation in the piriform cortex.

Figure 3.6: Number of fos-positive neurons in the anterior piriform cortex of rats stimulated by different odors.

2. Tables

Travail personnel

Table 1.1: Bibliographic survey of Mn doses injected into nostrils in previous MEMRI experiments.

Table 2.1: Results of landmark-based comparison of the spatial normalization algorithms bundled with the AIR 5.2.6 package.

3. Abréviations

µm	micromètre(s)
µmol	micromole(s)
3D	tridimensionnel
ARNm	acide ribonucléique messager
BHE	barrière hémato-encéphalique
BOLD	blood oxygenation level dependent
cm	centimètre(s)
EEG	électroencéphalographie
env.	environ
h	heure(s)
INRA	institut national de la recherche agronomique
IRM	imagerie par résonance magnétique
IRMf	imagerie fonctionnelle par résonance magnétique
MDEFT	modified driven equilibrium Fourier transform
MEG	magnétoencéphalographie
MEMRI	manganese-enhanced magnetic resonance imaging
min	minute(s)
mm	millimètre(s)
Mn	manganèse
RARE	rapid acquisition with relaxation enhancement
RSB	rapport signal sur bruit
SSFP	steady-state free precession
T	tesla(s)
TEP	tomographie par émission de positrons
U-FLARE	ultra-fast low-angle rapid acquisition and relaxation enhancement

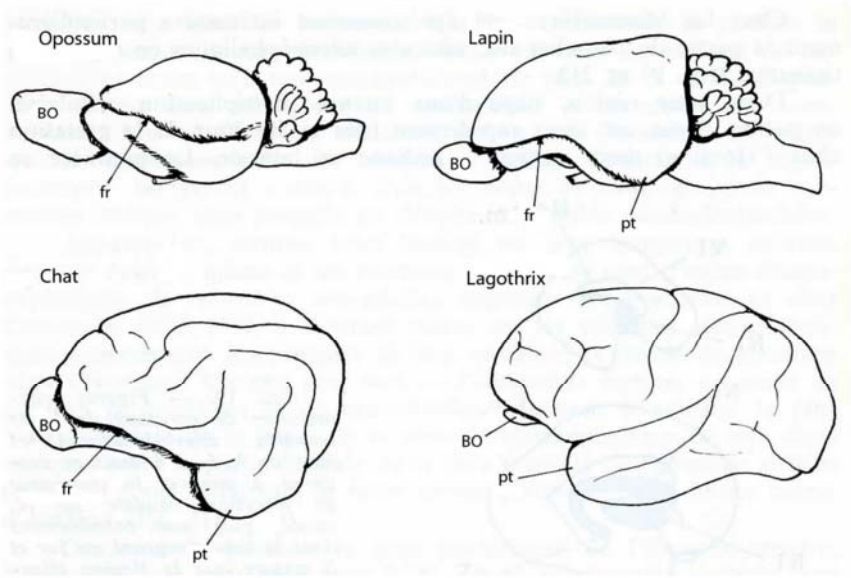

Figure 1 : Evolution du système olfactif chez les mammifères. Avec le développement du lobe temporal (pôle temporal : pt), le bulbe olfactif (BO) régresse et la fissure rhinale (fr) se déplace ventralement. [De Laget, 1976]

Introduction générale

L'olfaction est phylogénétiquement une des plus anciennes modalités sensorielles des vertébrés (Nieuwenhuys, 1967). Elle est en effet présente chez les myxines, encore dépourvues de vision et d'audition. Bien qu'au cours de l'évolution, son importance ait régressé, comme l'illustre la Figure 1, avec, notamment, le développement du néocortex chez les mammifères (Laget, 1973), elle demeure, pour de nombreuses espèces animales, un déterminant essentiel des comportements tels que la fuite devant un prédateur, la recherche d'une proie, d'un partenaire sexuel ou encore de la prise alimentaire.

Chez l'Homme, elle n'a plus une telle importance. Elle a été supplantée par la vision, et principalement la vision trichromatique (Gilad *et al.*, 2004). L'olfaction n'est sans doute plus le déterminant unique d'aucun comportement humain. En revanche, elle est étroitement liée aux processus mnésiques et cognitifs qui participent à leur élaboration (Levy *et al.*, 1999; Wilson et Stevenson, 2003; Zhou et Chen, 2009) et constitue probablement un vecteur de communication entre individus (McClintock, 1971).

Chez l'Homme, elle contribue à la prise alimentaire et à la satiété (Rolls et Rolls, 1997; Verhagen et Engelen, 2006). L'INRA, qui a mis la nutrition et la qualité des aliments au centre de ses préoccupations de recherche, s'y intéresse tout naturellement.

Il demeure que les mécanismes fondamentaux sous-jacents au rôle de l'olfaction dans les comportements sont encore très mal connus. Bien que l'Homme soit l'objectif ultime, il n'est probablement pas le meilleur sujet d'étude pour démasquer des mécanismes communs à tous les mammifères. Les lignées animales de laboratoire, génétiquement homogènes, à l'histoire individuelle connue et contrôlée, offrant de surcroît des possibilités expérimentales bien plus étendues, semblent plus appropriées aux investigations nécessaires. Le rat constitue

certainement à cet égard l'espèce de référence, tant pour les approches comportementales qu'anatomiques et physiologiques. C'est dans cette espèce que la famille des gènes codant les récepteurs olfactifs a été mise en évidence (Buck et Axel, 1991) et depuis lors, une intense activité de recherche a été développée pour élucider le codage des odeurs dans l'épithélium olfactif et dans le premier relais cérébral, le bulbe olfactif.

Il est probable cependant que ce n'est pas dans le bulbe olfactif qu'il faut espérer trouver le lieu d'une intersection fonctionnelle entre traitement central des odeurs et support physiologique des comportements. Il nous a donc semblé intéressant d'étudier l'activation de zones plus profondes du cerveau par l'application, chez l'animal vigile, d'odeurs véhiculant des messages biologiquement signifiants.

Les travaux sur le traitement profond des odeurs chez l'animal ayant jusque-là fait appel essentiellement à des odeurs mono-moléculaires ne véhiculant aucune signification particulière, nul ne sait aujourd'hui clairement si des messages olfactifs différents véhiculés par des odeurs naturelles activent des régions cérébrales distinctes. Par conséquent, il reste un long chemin à parcourir pour comprendre, chez l'Homme, le fondement neuroanatomique et neurophysiologique des activations cérébrales induites par des odeurs perçues comme plaisantes ou déplaisantes (Rolls *et al.*, 2003).

Dans ce travail, nous avons abordé la question de l'activation cérébrale par des odeurs signifiantes au moyen de l'imagerie par résonance magnétique fonctionnelle (IRMf). La méthode de référence basée sur le contraste « blood oxygen level dependent » (BOLD), présente chez l'animal des difficultés particulières (que nous détaillons plus loin) qui nous ont conduits à l'écarter et à nous porter plutôt vers l'IRMf utilisant un agent de contraste fonctionnel, le manganèse (« Manganese-enhanced magnetic resonance imaging», MEMRI). Cette technique a été surtout utilisée pour tracer des voies neuronales, mais relativement peu pour explorer des fonctions sensorielles. C'est pourquoi nous avons conduit deux études visant l'une à définir les conditions d'application du manganèse et l'autre à optimiser le traitement des images MEMRI, avant d'aborder la question biologique proprement dite.

Chapitre I

Revue de littérature

1. Rappels historiques

Le survol historique qui suit résulte notamment de la consultation de l'ouvrage de Cloquet (1821) pour les études antérieures au premier quart du 19ème siècle, du chapitre d'ouvrage de Doty (2003), de l'article de Gordon Shepherd (Shepherd *et al.*, 2011) à propos de la première image des connexions neuronales intrabulbaires et de l'article de Philpott *et al.* (2008).

La première intuition géniale du mécanisme de la perception olfactive est celle de Démocrite (env. - 460 – env. - 360) qui pensait que nous sentions des « atomes » de formes et de tailles différentes émis par les objets. Il faudra attendre la fin du 19ème siècle et la révolution de la chimie organique (synthèse de la coumarine par Sir William H. Perkin) pour la mise en évidence de ces « atomes » et 1991 avec les travaux de Buck et Axel (Buck et Axel, 1991) pour la démonstration du mode de perception. Dans l'intervalle, l'évolution historique des concepts liés à l'olfaction est, jusqu'à la mise en évidence des neurones par Golgi et Cajal, surtout une affaire d'anatomie. Galien (env. 129 – env. 201) pensait que les

Figure 2 : Neuroanatomie du bulbe olfactif de chien. Imprégnation par les sels d'argent. Observation au microscope et dessin réalisé par Golgi. [De Shepherd *et al.*, 2011]

bulbes olfactifs sont des appendices du cerveau par lesquels les vapeurs lui arrivent tandis que les humeurs s'en échappent. Il leur refuse donc la qualification de « nerfs ». Les successeurs de Galien, n'ayant trouvé chez l'animal que deux grosses éminences emplissant les fosses ethmoïdales, dont la cavité interne communique avec les ventricules cérébraux, leur ont attribué divers noms (processus mammilares, apophyses, *processus olfactorii*…).

Pendant près de 600 ans, la médecine étant exclusivement fondée sur l'analyse et l'interprétation du dogme de Galien, aucun concept nouveau n'émerge. Ce n'est que vers 800 qu'un moine grec nommé Protospatharios écrit dans un traité d'anatomie humaine que ces organes sont des nerfs qui servent à l'odorat. Ce concept restera cependant ignoré jusqu'au 16ème siècle, où Vésale, sur la base des nombreuses dissections qu'il réalise, affirme que les bulbes olfactifs sont bien des nerfs et que Galien commet une erreur en prétendant qu'ils servent de canaux à un liquide. En 1536, Massa identifie les prolongements des bulbes olfactifs à l'intérieur des fosses nasales. Il est ainsi le premier à mettre en évidence les véritables nerfs olfactifs. La bataille n'est pourtant pas gagnée pour autant car avant Cloquet (1821) les très nombreux investigateurs s'opposent encore sur l'implication du bulbe olfactif dans l'odorat. L'ignorance que les neurones sont le support de la communication nerveuse est évidemment la cause des nombreuses controverses sur l'anatomie et le rôle des bulbes olfactifs. Linné en avait eu l'intuition dès 1752 dans son ouvrage « *Odores Medicamentorum* » en écrivant que « si nous comprenions mieux la théorie de la fonction nerveuse, alors nous comprendrions plus facilement les bases de l'odorat ».

Grâce à l'évolution des techniques, notamment celles de la microscopie et des colorations des tissus, les descriptions anatomiques s'enrichissent des apports de l'histologie. Les neurones sont mis en évidence et leurs relations à l'intérieur et à l'extérieur d'une même structure sont décrites. Les réseaux qu'ils dessinent constituent désormais des bases neuroanatomiques solides de la transmission des sensations. Golgi (1875, Figure 2) produit ainsi les premières images de neurones : ceux du bulbe olfactif. Avec Ramon y Cajal, ils vont décrire l'organisation anatomique du bulbe olfactif et des régions qu'il innerve : hippocampe, cortex olfactif primaire, *etc*. Les « nerfs » olfactifs s'appellent désormais les bulbes. Les vrais nerfs olfactifs ont été identifiés.

Au début du 20ème siècle, il semble acquis (en dépit de la controverse entre Golgi et Cajal eux-mêmes) que les neurones sont des entités anatomiquement indépendantes et non un continuum réticulé. Cependant, le mode de transmission des informations demeure inconnu. En ce qui concerne l'olfaction, des liens entre structure et fonction avaient bien été établis dès

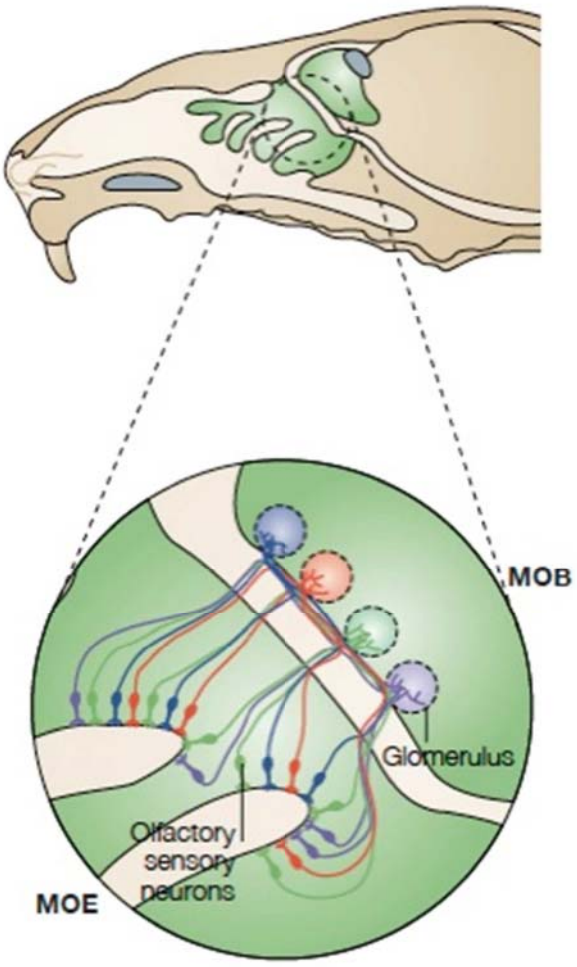

Figure 3 : Projection des neurones de l'épithélium olfactif sur le bulbe olfactif. Les neurones sensoriels olfactifs (olfactory sensory neurons) qui expriment le même récepteur projettent leurs axones sur le même glomérule (glomerulus). MOE : épithélium olfactif principal ; MOB : bulbe olfactif principal. [De Mombaerts, 2004]

le 16ème siècle en observant *post mortem* l'absence de bulbes olfactifs chez des individus anosmiques, mais les connaissances demeuraient très grossières. Sherrington (1857-1952), en découvrant le point de connexion entre neurones et en inventant le mot synapse, ouvre le champ de l'électrophysiologie dont l'olfaction sera un des premiers terrains d'étude. Sherrington partagera en 1932 le prix Nobel avec Adrian pour leurs découvertes sur les fonctions des neurones. Adrian lui-même montrera en 1942 la modification du signal électrophysiologique dans le bulbe olfactif du hérisson sous l'effet d'odeurs (Adrian, 1942). Une autre étape importante sera franchie par Ottoson en 1955 qui montrera que les odeurs ont des effets sur les propriétés électriques de la muqueuse olfactive, révélant ainsi que le premier maillon de la communication olfactive nerveuse se situe dans la muqueuse olfactive (Ottoson, 1955). La dernière percée majeure est celle de la découverte des récepteurs olfactifs par Buck et Axel (1991) qui sera la clé de la compréhension de la perception olfactive dans l'épithélium olfactif. Le codage spatio-temporel des odeurs dans l'épithélium et dans le bulbe deviendra un axe essentiel de recherche (Lledo *et al.*, 2005). Pour autant, il semble maintenant reconnu que l'analyse des odeurs par les centres plus profonds du cortex olfactif primaire ne repose pas sur un tel codage et l'élucidation de l'intersection entre olfaction et autres fonctions cérébrales est une nouvelle frontière.

2. Anatomie et physiologie du cortex olfactif primaire

Ce travail de thèse ayant été principalement consacré au traitement des odeurs par le cortex olfactif primaire, cette revue de la littérature est dévolue à cet ensemble de structures. En conséquence, nous n'évoquerons que rapidement le premier étage qu'est la muqueuse olfactive et le second, le bulbe olfactif. D'autre part, nous ne traiterons pas des phéromones et du système olfactif accessoire.

Les sens chimiques (goût, odorat et chimioréception viscérale) constituent des modalités sensorielles particulières dans la mesure où le stimulus n'est pas un signal analogique reposant sur un apport d'énergie d'intensité variable mais un signal discret reposant sur un grand nombre de molécules odorantes. Pour l'olfaction, chez les mammifères, le capteur

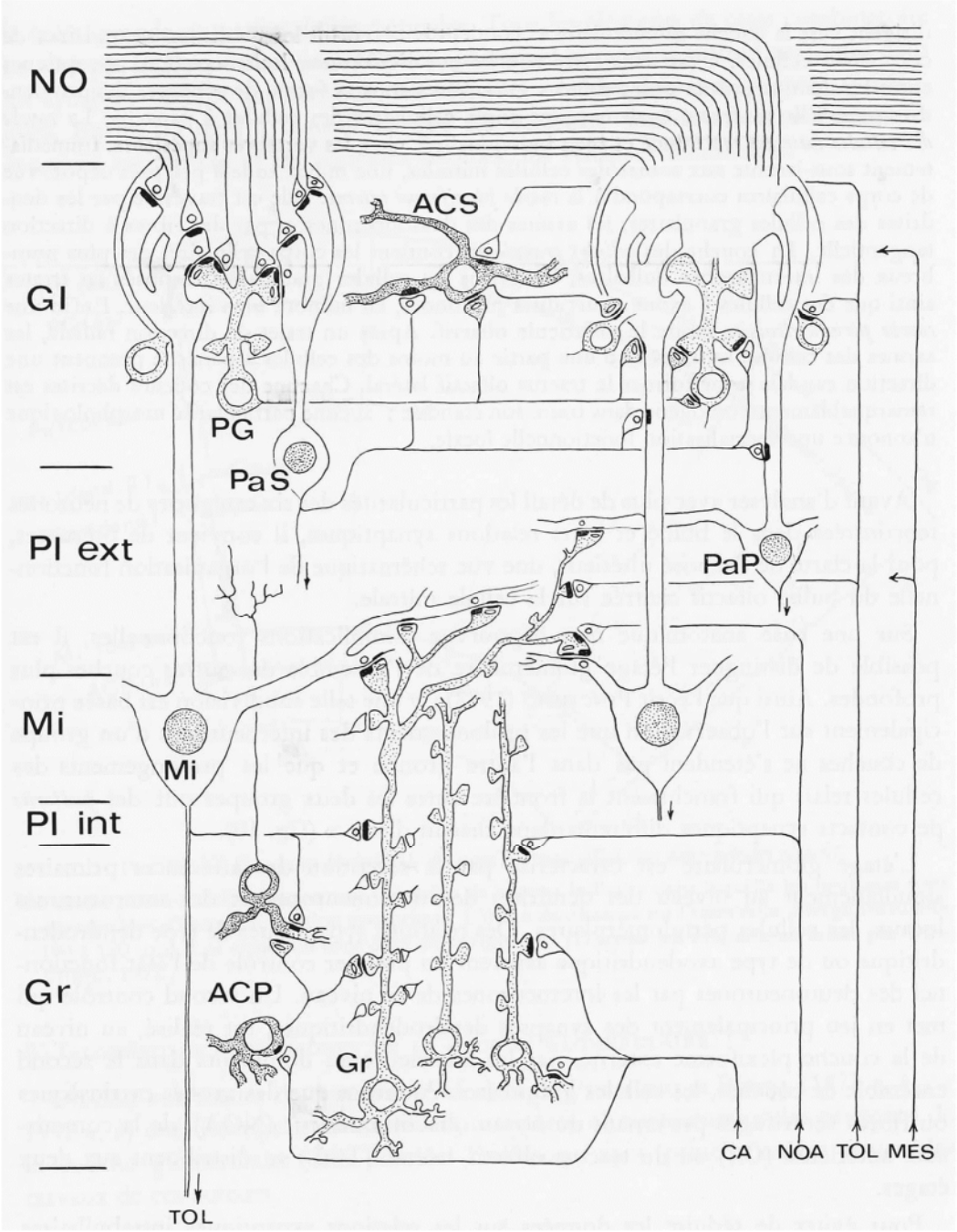

Figure 4 : Organisation des connexions intrabulbaires. Les couches cellulaires sont indiquées en colonne, à gauche. NO : couche du nerf olfactif ; Gl : couche glomérulaire ; Pl ext : couche plexiforme externe ; Mi : couche des cellules mitrales ; Pl int : couche plexiforme interne ; Gr : couche des cellules granulaires ; Mi : cellules mitrales ; PaS : cellules à panache superficielles ; PG : cellules périglomérulaires ; ACP : cellules à axones courts profondes ; ACS : cellules à axones courts superficielles ; PaP : cellules à panache profondes ; Gr : cellules granulaires ; TOL : tractus olfactif latéral ; CA : commissure antérieure ; NOA : noyau olfactif antérieur ; MES : mésencéphale. [De Holley et Mac Leod, 1977]

périphérique est l'épithélium olfactif situé au fond des fosses nasales, sous la lame criblée de l'os ethmoïde. L'épithélium olfactif baigne dans un mucus qui contient les corps cellulaires et les dendrites des neurones sensoriels. Ces neurones projettent leurs axones à travers la lame criblée, vers la première structure cérébrale, le bulbe olfactif qui lui-même envoie des projections vers le cortex olfactif primaire (Shipley et Adamek, 1984). Ainsi, l'olfaction se distingue encore des autres modalités sensorielles puisque les informations ne sont pas relayées par le thalamus avant d'atteindre le cortex. Dans l'épithélium olfactif, les composants chimiques des odeurs se fixent sur les dendrites des neurones récepteurs dont chacun n'exprime qu'un seul parmi le millier de récepteurs olfactifs existants (Buck et Axel, 1991). Les axones des neurones exprimant le même récepteur se réunissent en faisceau, franchissent la lame criblée et se terminent dans le bulbe olfactif sur deux glomérules symétriques (Figure 3).

Dans ces glomérules, les axones de ces neurones récepteurs olfactifs font synapse avec les dendrites des cellules mitrales et en panache (Mombaerts, 2004; Ressler *et al.*, 1994; Vassar *et al.*, 1994). Différentes odeurs activent des combinaisons uniques et spatialement invariantes de glomérules (Ressler *et al.*, 1994; Vassar *et al.*, 1994). Chaque glomérule reçoit les dendrites de 20 à 50 cellules mitrales ou en panache (Haberly et Price, 1977). Mais si un glomérule est innervé par plusieurs cellules, une cellule n'innerve qu'un seul glomérule. A l'intérieur du bulbe olfactif, deux catégories de cellules inhibitrices, les cellules périglomérulaires et les cellules granulaires connectent les glomérules et, par ces connexions inhibitrices, augmentent le rapport signal/bruit en faveur des messages saillants (Figure 4).

Les axones des cellules mitrales et en panache forment le faisceau olfactif principal qui innerve le cortex olfactif primaire dont les neurones cibles intègrent l'information en provenance de plusieurs glomérules pour distinguer des odeurs chimiquement différentes (Apicella *et al.*, 2010; Lei *et al.*, 2006; Stettler et Axel, 2009). La manière dont ce transcodage s'opère est encore mystérieuse, car la cartographie corticale des informations glomérulaires relayées par les cellules mitrales et en panache n'est pas connue.

L'absence de cartes sensorielles est une autre différence entre l'olfaction et les autres modalités sensorielles. Les cartes sensorielles sont des projections de l'organisation spatiale de récepteurs périphériques, de stimuli ou du monde extérieur sur des cibles cérébrales. Ainsi, la représentation de l'environnement visuel sur la rétine est elle conservée dans le thalamus (Sanderson, 1971) et le cortex visuel primaire (Tusa *et al.*, 1978). Il en va de même de l'organisation somatotopique dans le cortex somatosensoriel (Whitsel *et al.*, 1978) et de

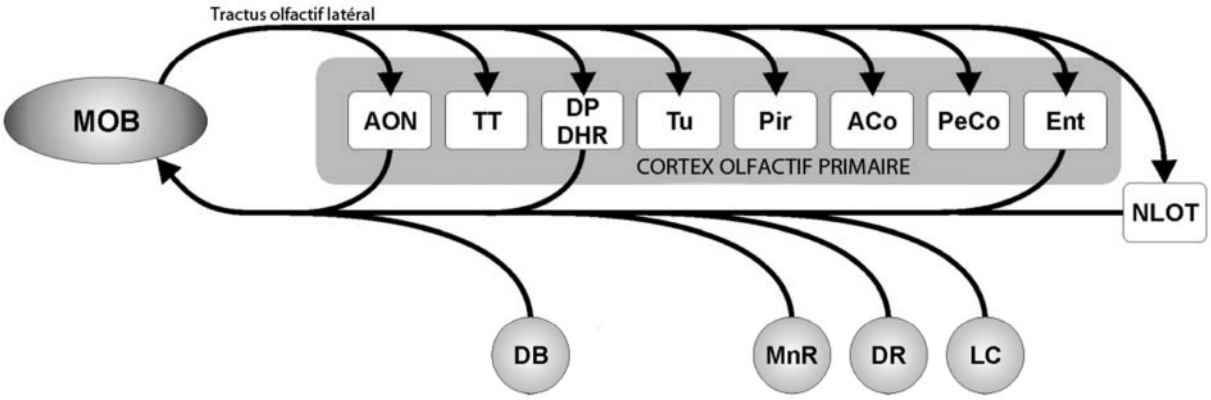

Figure 5 : Afférences et efférences du bulbe olfactif. MOB : bulbe olfactif ; AON : noyau olfactif antérieur ; TT : tenia tecta ; DP-DHR : cortex pédonculaire dorsal, rudiment hippocampique ; Tu : tubercule olfactif ; Pir : cortex piriforme ; ACo : noyau amygdalien cortical antérieur ; PeCo : cortex périamygdalien ; Ent : cortex entorhinal ; DB : bande diagonale de Broca ; MnR : noyau médian du raphe ; DR : noyau dorsal du raphe ; LC : locus coeruleus ; NLOT : noyau du tractus olfactif latéral. [De Shipley *et al.*, 2004]

l'organisation tonotopique dans le cortex auditif primaire (Merzenich *et al.*, 1975). Ces cartes topographiques sont quelquefois maintenues, bien que de manière moins précise, au delà des structures corticales. Il en est ainsi des projections topographiques du cortex sur le *striatum* (Alexander et Crutcher, 1990) et des projections striatales sur la substance noire (Deniau *et al.*, 1996; Maurin *et al.*, 1999). L'olfaction semble constituer une exception à ce modèle. Les cellules mitrales ou en panache innervent de vastes régions du cortex olfactif primaire alors que des zones restreintes de ce cortex sont afférentées par de larges ensembles de cellules mitrales et en panache (Buonviso *et al.*, 1991; Luskin et Price, 1982).

Le cortex olfactif primaire, ainsi nommé pour la première fois par De Olmos (De Olmos *et al.*, 1978), est constitué d'un ensemble de structures innervées par le tractus olfactif latéral (Figure 5).

La première est le noyau olfactif antérieur, dans la partie externe duquel la carte spatiale du bulbe est partiellement conservée (Ghosh *et al.*, 2011). La seconde est la *tenia tecta* qui compose, avec l'*indusium griseum*, le rudiment hippocampique, et reçoit des afférences du bulbe olfactif (Shipley et Adamek, 1984), mais aussi du cortex entorhinal (Wyss, 1981) et de l'hippocampe (Ino *et al.*, 1987). L'hippocampe, qui est également une voie de passage des informations olfactives vers le cortex entorhinal (Biella et De Curtis, 2000), est donc une structure où se croisent des informations olfactives ascendantes et descendantes. Compte tenu de son rôle dans la mémoire (Eichenbaum *et al.*, 1996), cette organisation anatomique est le support du lien entre olfaction et mémoire (Gottfried *et al.*, 2004; Staubli *et al.*, 1987; Wilson et Stevenson, 2003).

Le tubercule olfactif fait partie du cortex olfactif primaire, bien qu'il soit plutôt, de par sa localisation (sous le noyau accumbens), ses neuromédiateurs et sa structure cellulaire, une structure du striatum ventral (Ikemoto, 2007; Voorn *et al.*, 2004). Il n'envoie pas de projections vers le bulbe mais vers le noyau olfactif antérieur (Newman et Winans, 1980) et le pallidum ventral (Newman et Winans, 1980; van Dongen *et al.*, 2005). Il en reçoit des cortex piriforme, entorhinal, orbitaire et insulaire, du noyau olfactif antérieur, de l'amygdale et de l'aire tegmentale ventrale (Newman et Winans, 1980), ainsi que du noyau médian dorsal du thalamus (Price et Slotnick, 1983). Il est associé chez l'animal au circuit de la récompense (Ikemoto, 2007). Chez l'Homme, il interviendrait dans la différenciation entre odeurs pures ou à composante trigéminale (Zelano *et al.*, 2007). Comme élément du striatum ventral, il pourrait relier l'olfaction aux mécanismes de la récompense et aux circuits moteurs du striatum dorsal. A l'appui de ce rôle intégratif, il a été montré que ses neurones répondent

simultanément à des stimulations olfactives et tactiles (West et Michael, 1990) ou auditives (Wesson et Wilson, 2010).

Le cortex piriforme est un paléocortex à 3 couches (Shipley *et al.*, 2004) qui, chez les rongeurs, est, juste après le bulbe, la structure olfactive ayant la plus grande extension. Il envoie des projections rostralement vers le cortex préfrontal (Datiche et Cattarelli, 1996; Haberly, 2001), vers le tubercule olfactif et le bulbe olfactif (Powell *et al.*, 1963) et caudalement vers le cortex entorhinal, l'hypothalamus, l'amygdale (Powell *et al.*, 1963) et le noyau habénulaire du thalamus (Powell *et al.*, 1963; Price et Slotnick, 1983). Le cortex piriforme a été le support de plusieurs études électrophysiologiques chez l'animal (Litaudon *et al.*, 2003; Nemitz et Goldberg, 1983; Rennaker *et al.*, 2007; Schoenbaum et Eichenbaum, 1995; Wilson, 1997) qui montrent que ses neurones ont une activité spontanée faible, voire nulle, en absence de stimulation et que les réponses induites par des odorants mono-moléculaires sont courtes et spécifiques. Les cartes d'activation de l'épithélium et du bulbe olfactif n'y ont pas été retrouvées (Sosulski *et al.*, 2011), puisque des grands ensembles de neurones sont activés dans le cortex piriforme par des odeurs mono-moléculaires appliquées seules ou en combinaison (Darquie *et al.*, 2001; Ghosh *et al.*, 2011; Illig et Haberly, 2003; Stettler et Axel, 2009) ou par des odeurs signifiantes telles que triméthyl-thiazoline (TMT, extraite des fèces de renard) ou litière souillée par des rattes en œstrus (Fendt *et al.*, 2003; Kippin *et al.*, 2003). D'une manière plus générale, il apparaît que le cortex piriforme est impliqué dans le traitement d'odeurs sexuelles ou induisant la peur. Chez l'Homme, son implication dans l'analyse de la valence des odeurs a été montrée (Rolls *et al.*, 2003; Zelano *et al.*, 2007).

Les noyaux amygdaliens sont un ensemble très complexe de petits groupes cellulaires très intriqués qui ont des connexions réciproques avec de nombreuses structures olfactives, notamment le bulbe olfactif et le cortex piriforme et envoient des projections sur la *tenia tecta*, le tubercule olfactif et le cortex entorhinal (De Olmos *et al.*, 2004). En dehors des structures olfactives, les noyaux amygdaliens ont des connexions réciproques avec l'hypothalamus et l'hippocampe et reçoivent des afférences thalamiques (De Olmos *et al.*, 2004). L'amygdale est ainsi impliquée dans les circuits de la peur et de l'aversion (Blanchard *et al.*, 2005; Butler *et al.*, 2011; Chen *et al.*, 2007; Dielenberg et McGregor, 2001; LeDoux, 2003), de la mémoire (Ehrlich *et al.*, 2009; Inui-Yamamoto *et al.*, 2010), de la reproduction (Kang *et al.*, 2009; Kelliher *et al.*, 1999; Kippin *et al.*, 2003), de la récompense (Ambroggi *et al.*, 2008; Cador *et al.*, 1989; Everitt *et al.*, 1989). Chez l'Homme, l'amygdale interviendrait dans le traitement de l'intensité des odeurs (Anderson *et al.*, 2003).

Le cortex entorhinal a fait l'objet de moins d'attention que les structures situées plus en amont. Il fait partie, avec les cortex périrhinal et postrhinal, du cortex parahippocampique. Il établit des connexions réciproques avec la quasi totalité des structures olfactives, mais ses connexions les plus importantes sont avec l'hippocampe (Haberly et Price, 1978; Wyss, 1981). Il intervient ainsi dans les processus mémoriels mais également dans des fonctions complexes comme l'identification d'objets, l'orientation spatiale et bien sûr l'olfaction (Murray et Richmond, 2001) puisque, en supplément aux afférences olfactives directes, il reçoit des afférences indirectes du bulbe olfactif via l'hippocampe (Biella et De Curtis, 2000). Il exercerait un contrôle inhibiteur sur le bulbe olfactif, le cortex piriforme, l'amygdale et l'hippocampe (Bernabeu *et al.*, 2006) et participerait ainsi à un rétrocontrôle sur les voies olfactives dans la mesure où sa propre activité est modifiée par des stimulations olfactives (Mouly *et al.*, 2001; Mouly et Di, 2006).

Il apparaît, au travers de ce survol bibliographique, que l'information olfactive se distribue sur un vaste ensemble de structures interconnectées qui composent le cortex olfactif primaire. Dans ce système, l'information est sujette à de nombreux transferts. Elle peut aussi atteindre les structures distales du cortex olfactif primaire par des voies indirectes (comme l'hippocampe), ce qui assure la communication entre les processus olfactifs et d'autres fonctions cérébrales, notamment la mémoire. Le cortex olfactif primaire émet enfin des projections centrifuges vers des structures non directement olfactives (thalamus, cortex préfrontal, striatum ventral, aire tegmentale…), ce qui étend encore le spectre d'interactions de l'olfaction.

Les mécanismes fondamentaux qui sous-tendent ces interactions sont loin d'être compris. Les investigations fonctionnelles chez l'Homme font une très large part aux processus cognitifs (valence, hédonicité, souvenirs…) et il est permis de penser que ce ne sont pas elles qui jetteront un éclairage sans ambiguïté sur ceux-là. Un enjeu important est aujourd'hui de faire le lien entre les connaissances parcellaires issues des approches essentiellement cellulaires conduites chez l'animal et celles, globales, issues de l'imagerie cérébrale. C'est l'objet du présent travail.

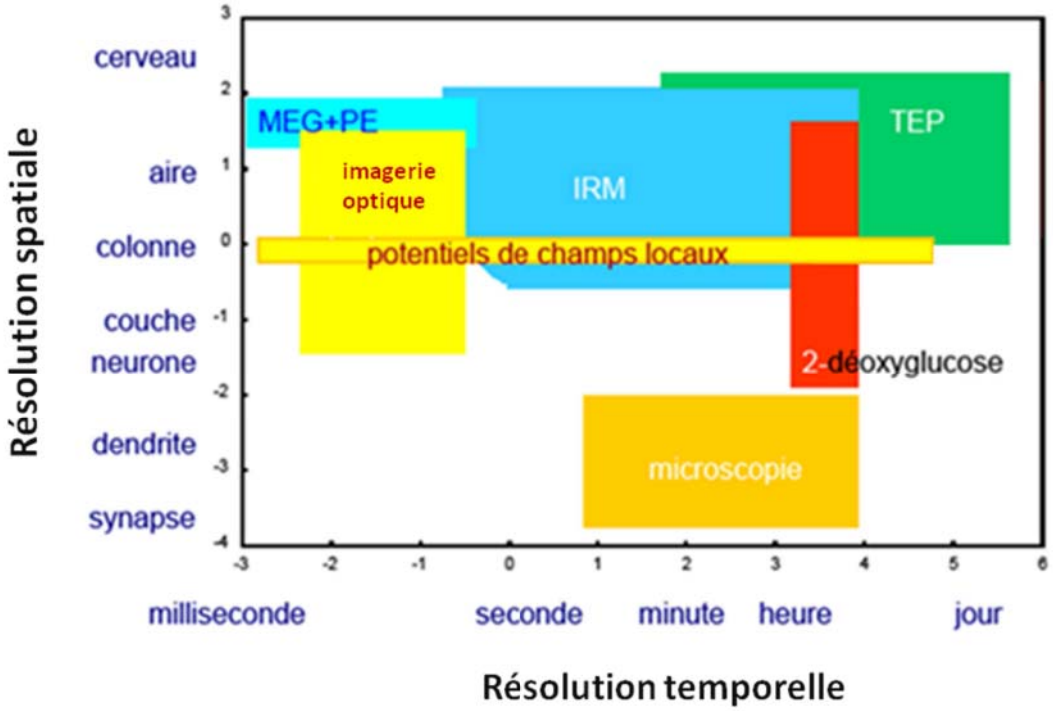

Figure 6 : Synthèse des méthodes d'imagerie. [Adapté d'après Garnero, 2001]

3. L'imagerie fonctionnelle

3.1. Vue d'ensemble

L'imagerie fonctionnelle cérébrale a pour but de localiser les régions répondant à une stimulation. Les différentes méthodes d'imagerie fonctionnelle sont toutes fondées sur un principe couplant le signal recueilli sous forme d'image à l'activité des neurones. Seule l'électroencéphalographie (EEG) repose sur la mesure directe de l'activité électrique mais la résolution spatiale de cette technique est limitée (cm). La mesure directe par IRM de l'activité électrique des neurones a bien été envisagée (Petridou *et al.*, 2006), mais aucune validation expérimentale n'a encore pu être réalisée (Cassara *et al.*, 2008). Le signal image des principales autres méthodes d'imagerie fonctionnelle est indirectement lié à l'activité des neurones et reflète donc imparfaitement les modulations de l'activité neuronale, que ce soit dans le temps ou dans l'espace. Dans la synthèse proposée par Garnero (Figure 6, 2001), on constate que chacune de ces méthodes se caractérise par un compromis entre résolution spatiale et temporelle.

La tomographie par émission de positons (TEP) cartographie les variations du débit sanguin au moyen d'un traceur radioactif injecté par voie intraveineuse. Les premières études cognitives ont été réalisées chez l'Homme avec cette technique et en particulier celles sur l'olfaction (Royet *et al.*, 2000; Savic et Gulyas, 2000; Zald et Pardo, 1997; Zatorre *et al.*, 1992). Etant à la fois moins résolutive spatialement (cm) et temporellement (min-h) que l'IRM fonctionnelle, la technique TEP a, aujourd'hui, été supplantée par cette dernière.

Même si l'IRM de diffusion peut fournir des informations fonctionnelles (Darquie *et al.*, 2001), le terme IRMf fait le plus souvent référence au contraste BOLD (Bandettini *et al.*, 1992; Kwong *et al.*, 1992; Ogawa et Lee, 1990). Son principe consiste à sensibiliser le signal IRM aux variations de l'oxygénation du sang. Lors de l'activation d'un groupe de neurones, il se produit simultanément une augmentation du débit sanguin cérébral, une vasodilatation et une surconsommation d'oxygène par les neurones. Ces trois phénomènes provoquent, selon un décours temporel complexe (Buxton *et al.*, 1998), une modulation de l'oxygénation du sang détectable par IRM (Figure 7). En pratique, une expérience BOLD consiste à acquérir rapidement des images du cerveau en alternant les phases de repos et d'activation. Les régions

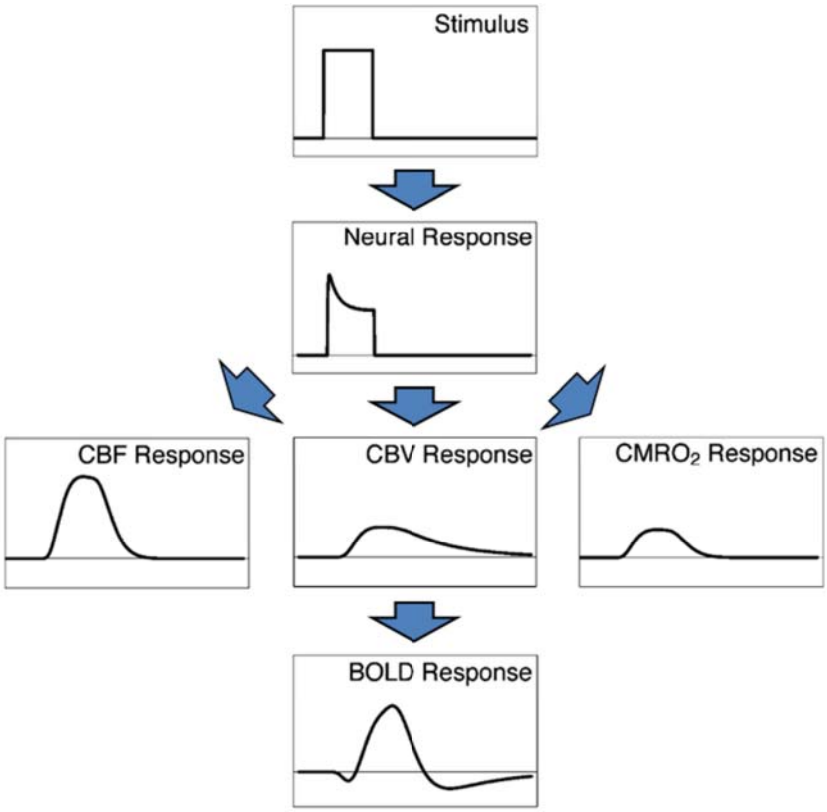

Figure 7 : Principes de l'IRMf BOLD. Une stimulation entraine l'activation d'un groupe de neurones qui induit simultanément une augmentation du débit sanguin cérébral, une vasodilatation et une surconsommation d'oxygène par les neurones. Ces trois phénomènes provoquent, selon un décours temporel complexe, une modulation de l'oxygénation du sang détectable par IRM. CBV : cerebral blood volume ; CBF : cerebral blood flow ; $CMRO_2$: cerebral metabolic rate of oxygen [Adapté d'après Buxton, 2004]

activées sont détectées *a posteriori* en recherchant les meilleures corrélations entre le signal image et le paradigme de stimulation. L'IRMf BOLD s'est imposée pour trois raisons essentielles. Tout d'abord, elle n'est pas invasive car basée sur la détection d'un produit de contraste endogène, le sang. Ensuite, la variation de signal provoquée par le stimulus ne dure que quelques secondes, on peut donc répéter les phases successives d'activation et de repos pour augmenter la sensibilité de détection de cette variation. Une seule expérience suffit donc pour mesurer les niveaux de repos et d'activation dans toutes les régions cérébrales. Le sujet étant son propre contrôle, une cartographie des régions activées chez un individu particulier est donc possible (analyse individuelle). Enfin, on peut recueillir des images fonctionnelles ainsi que des images de l'anatomie cérébrale du sujet pendant la même expérience. Ceci facilite le recalage des données fonctionnelles dans un espace de référence (normalisation spatiale), espace dans lequel sont référencés la plupart des atlas anatomiques qui permettent d'identifier les régions cérébrales activées.

Si l'IRMf BOLD s'est affirmée comme une approche fonctionnelle de référence (près de 13000 références sur ScienceDirect à ce jour), elle n'en présente pas moins certains inconvénients. Le premier est une faible sensibilité puisque la variation de signal provoquée par le stimulus n'est que de quelques pourcents. D'autre part, la dynamique du signal fonctionnel étant influencée par celle de la perfusion sanguine, la résolution temporelle du signal BOLD est faible par rapport aux variations temporelles de l'activité électrique des neurones. Enfin, la perfusion sanguine étant en excès, l'extension des territoires détectés par IRMf BOLD est supérieure à celle des neurones activés. L'effet négatif de ces trois paramètres diminue lorsque le champ statique de l'aimant augmente, ce qui explique le développement des imageurs à très haut champ pour étudier les fonctions cérébrales.

La magnétoencéphalographie (MEG) est une méthode d'imagerie fonctionnelle applicable à l'Homme. Fondée sur les variations de champ magnétique induites par l'activité électrique des neurones, elle est très résolutive temporellement. La difficulté réside essentiellement dans la localisation des foyers d'activations dans le cerveau à partir des réponses mesurées à la surface du crâne. Ce problème mathématique explique, en partie, le faible nombre d'applications pratiques de la MEG.

Les techniques d'imagerie citées précédemment sont utilisables chez l'Homme et l'animal. D'autres méthodes d'imagerie fonctionnelles existent, comme l'autoradiographie du 2-deoxyglucose, l'immunodétection de la protéine c-Fos ou encore MEMRI, mais sont utilisables uniquement chez l'animal car invasives. Le but de cette vue d'ensemble des méthodes d'imagerie fonctionnelle n'étant pas d'être exhaustif, nous nous focaliserons sur

MEMRI qui est la principale méthode d'imagerie utilisée dans cette thèse, et Fos, ce dernier étant considéré par beaucoup comme une technique de référence. Le gène c-fos, codant la protéine du même nom, fait partie de la famille des gènes d'expression précoce immédiate. La protéine c-Fos a très fréquemment été utilisée comme marqueur d'activité neuronale (Bullitt, 1990; Datiche *et al.*, 2001; Dielenberg *et al.*, 2001; Kelliher *et al.*, 1999; Morgan *et al.*, 1987; Sallaz et Jourdan, 1993; Tronel et Sara, 2002). La transcription du gène c-fos débute entre 5 et 10 min après la stimulation cellulaire, et la quantité d'ARNm est maximale après 30 à 40 min. Le pic d'expression de la protéine c-Fos est atteint après environ 90 min (Muller *et al.*, 1984). La stimulation capable d'induire l'expression de c-Fos doit donc être très forte et assez longue. La détection de la protéine, et donc des neurones activés, est révélée *ex vivo* par immunohistochimie. Fos présente une très bonne résolution spatiale (neurone) mais une faible résolution temporelle (min-h). Bien que Fos permette une localisation précise des cellules marquées, il présente une limite majeure du fait qu'il n'est pas strictement quantitatif car tous les neurones activés n'expriment pas Fos (Deurveilher et Semba, 2006). D'autre part, la révélation des neurones activés est très sensible à de faibles variations des conditions dans lesquelles l'immunodétection a été effectuée. Pour finir, la mise en évidence des neurones activés par immunohistochimie est très lourde et s'effectue sur des coupes de cerveau de quelques µm d'épaisseur. Ces spécificités limitent l'utilisation de cette méthode d'imagerie fonctionnelle à l'étude de régions cérébrales choisies *a priori*.

Puisqu'il s'agit de notre technique d'élection, les principes de MEMRI sont décrits en détails dans le paragraphe suivant.

3.2. Imagerie fonctionnelle de l'agent de contraste manganèse (« Manganese-enhanced magnetic resonance imaging », MEMRI)

MEMRI est basé sur les étapes suivantes : (i) le système nerveux central de l'animal est d'abord imprégné de manganese (Mn) (ii) l'ion Mn^{2+}, analogue calcique, est mobilisé par les régions cérébrales activées, mais il n'est pas métabolisé (iii) Mn^{2+} étant paramagnétique, il est détectable par IRM.

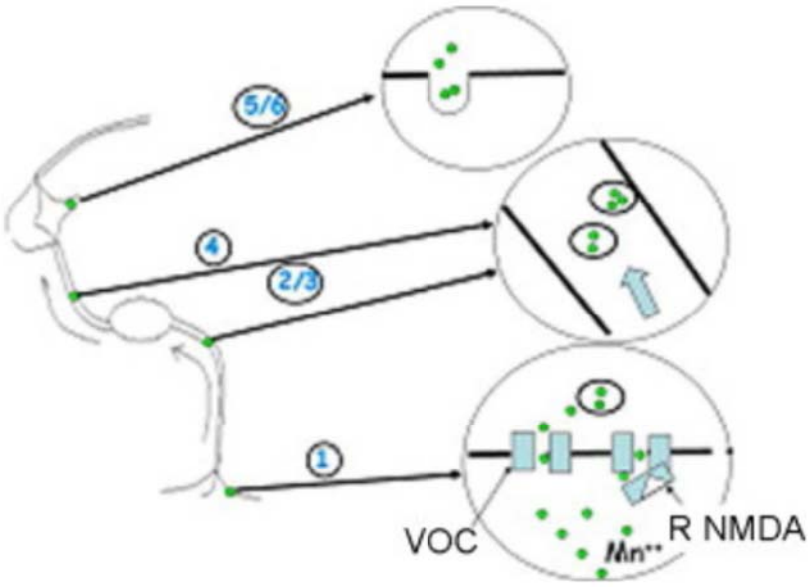

Figure 8 : Schéma du transport de manganèse dans un neurone. 1. Entrée par les canaux de Ca^{2+} de type L (et éventuellement par les canaux VOC et NMDA). 2/3. Séquestration dans le réticulum endoplasmique et cumul pour le transport. 4. Transport dans l'axone le long des microtubules. 5/6. Libération dans les synapses et recapture par les autres neurones. [De Gillet *et al.*, 2010]

Le Mn, au contraire d'autres agents de contraste IRM comme par exemple le gadolinium, est un agent de contraste fonctionnel. En effet, les ions Mn^{2+}, analogues du calcium, pénètrent dans les neurones activés lors de l'ouverture des canaux calciques voltage-dépendants (Silva *et al.*, 2004). La quantité de Mn^{2+} capté par un neurone est proportionnelle à l'activité des neurones (Lin et Koretsky, 1997). Une fois entré dans le neurone, le Mn^{2+} est séquestré dans le réticulum endoplasmique (Van der Linden *et al.*, 2007) et transporté relativement lentement (quelques mm/h) le long des microtubules (Sloot et Gramsbergen, 1994) jusqu'à la fente synaptique où il est libéré. Il est alors éventuellement capté par un autre neurone activé (Pautler *et al.*, 2003). La libération synaptique ne suffisant pas à éliminer le pool intracellulaire du Mn^{2+}, sa présence dans les neurones qui ont été activés peut être détectée pendant une longue période (Silva *et al.*, 2004). En effet, la demi-vie du Mn^{2+} dans le cerveau est d'environ dix jours (Chuang *et al.*, 2009a). La Figure 8 synthétise les différentes étapes d'entrée, de transport et de sortie du Mn.

L'ion Mn^{2+} est connu pour réduire les temps de relaxation T_1 et T_2, faisant de lui un excellent agent de contraste détectable en IRM (Mendonca-Dias *et al.*, 1983). L'imagerie couramment utilisée pour révéler le Mn^{2+} est celle fondée sur le contraste T_1 car elle permet de créer une variation du signal positive avec l'augmentation de la concentration de Mn^{2+}, au contraire du contraste basé sur le T_2. D'autre part, lorsque le Mn^{2+} pénètre dans le compartiment intracellulaire, il se complexifie avec des protéines intracellulaires ce qui se traduit par une forte modification de la relaxivité des protons intracellulaires (Nordhoy *et al.*, 2004). Cette modification de la relaxivité induite par le Mn^{2+} intracellulaire est huit fois supérieure à celle mesurée *in vitro* (Nordhoy *et al.*, 2004). Par conséquent, c'est le Mn^{2+} intracellulaire qui est principalement détecté par IRM. En résumé, le Mn peut être considéré comme un agent de contraste fonctionnel, intracellulaire et rémanent.

Pour refléter l'activité neuronale de l'ensemble du cerveau, le Mn doit être disponible *ad libitum* dans l'espace extracellulaire des structures étudiées. Injecté par voie systémique, il ne passe pas au travers de la barrière hémato-encéphalique (BHE) et s'accumule lentement dans le cerveau via les plexus choroïdes situés au niveau des ventricules (Aoki *et al.*, 2004b). Pour que le Mn présent dans le sang atteigne rapidement le cerveau, une solution est de perméabiliser temporairement la BHE (Lin et Koretsky, 1997). Le Mn est alors disponible dans la majorité des régions cérébrales. Les Figures 9 et 10 illustrent respectivement l'accumulation de Mn dans les régions cérébrales après son injection systémique sans/avec

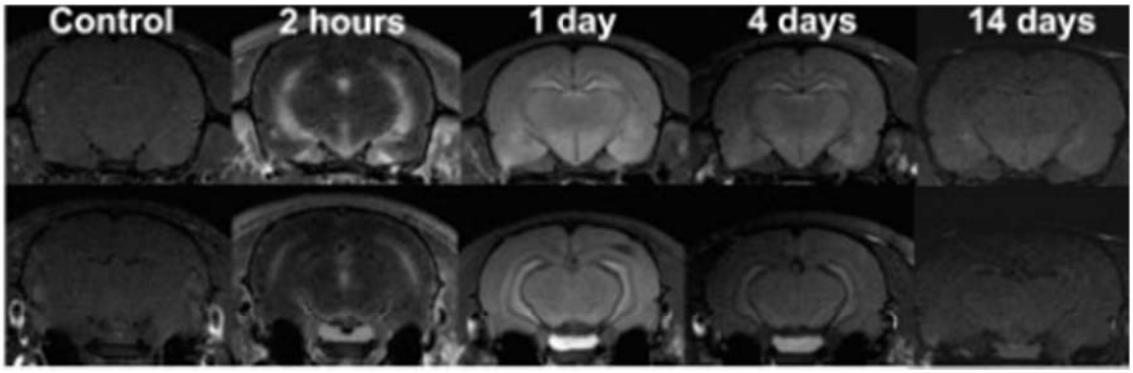

Figure 9 : Images pondérées T_1 acquises à différents temps après injection systémique de Mn. Les images proviennent de différents animaux avant (control), 2h, 1 jour, 4 jours et 14 jours après l'injection de Mn. L'augmentation du contraste dans le cerveau est la plus homogène 1 jour après l'injection du Mn. [De Aoki *et al.*, 2004b]

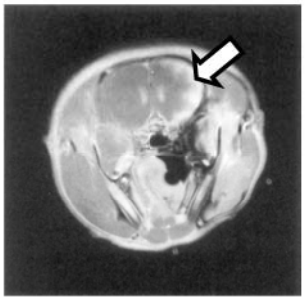

Figure 10 : Image pondérée T_1 après injection systémique de Mn et rupture de la barrière hémato-encéphalique. Une augmentation du contraste dans le cortex est clairement visible du coté où la barrière hémato-encéphalique a été rompue. [De Lin et Koretsky, 1997]

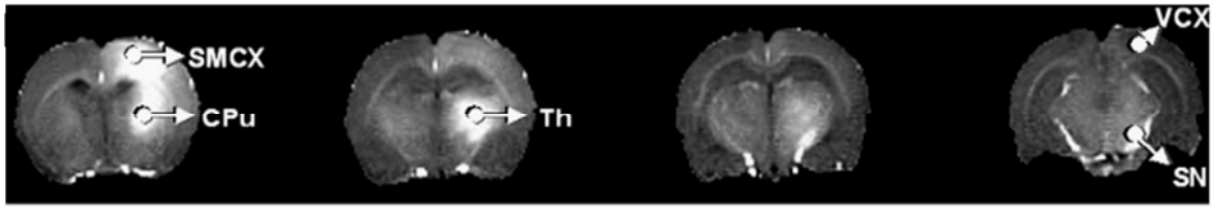

Figure 11 : Cartographie R1 (=1/T_1) réalisée 2 jours après injection de Mn dans le cortex sensorimoteur d'un rat sain. L'augmentation de contraste est notable dans le cortex sensorimoteur (SMCX), le caudé putamen (CPu), le thalamus (Th), la substance noire (SN) et plus faible dans le cortex visuel (VCX). [De Van der Zijden *et al.*, 2007]

rupture de la BHE. Une alternative est d'injecter le Mn intra-cérébralement au voisinage des structures d'intérêts (Chuang et Koretsky, 2006). Pour l'étude de fonctions sensorielles comme la vision (Thuen *et al.*, 2005) ou l'olfaction (Pautler *et al.*, 1998), le Mn peut être injecté directement à l'entrée du système sensoriel. La mise à disposition locale du Mn a des conséquences sur les informations que MEMRI peut fournir. En effet, la détection du Mn sera, dans ce cas, limitée principalement aux régions proches du lieu d'injection. Le transport transsynaptique du Mn permettra également de mettre en évidence les voies neuronales qui sont activées et fonctionnellement connectées à ces régions comme l'illustre la Figure 11 (van der Zijden *et al.*, 2007). Dans ce cas, le Mn ne sera pas disponible *ad libitum* pour les structures éloignées du site d'injection. Le signal MEMRI d'une structure éloignée du site d'injection ne reflètera pas directement l'activité neuronale mais représentera un bilan entre la quantité de Mn disponible dans la synapse et l'activité de cette structure. La toxicité du Mn (Henriksson et Tjalve, 2000) limite cependant la quantité maximale de Mn injectable sans conséquences directes sur le fonctionnement cérébral (Canals *et al.*, 2008) et sur les systèmes périphériques (Eschenko *et al.*, 2010b). Un pré-requis avant l'utilisation de MEMRI pour toute étude fonctionnelle est de trouver un compromis entre les effets toxiques du Mn et le signal détectable par IRM dans les régions d'intérêt (Silva *et al.*, 2004).

Quel que soit le mode d'administration du Mn, celui-ci persiste dans les neurones activés. La détection par IRM peut donc être effectuée *a posteriori*, la stimulation étant appliquée à l'animal vigile, dans les conditions les plus proches de la perception naturelle. Les images sont acquises, sous anesthésie, pendant un temps long afin d'augmenter le rapport signal sur bruit (RSB), et donc la résolution spatiale. La résolution temporelle de MEMRI est faible car les images révèlent l'accumulation du Mn intracellulaire pendant toute la période comprise entre l'administration du Mn et l'acquisition des images. Enfin, la rémanence du Mn dans les neurones empêche d'utiliser l'animal comme son propre témoin au cours d'une seule expérience MEMRI. Pour révéler les régions activées, il faut comparer les images d'un animal stimulé à celles issues d'un animal témoin. Cette comparaison doit être étendue à des groupes d'animaux pour conférer un poids statistique significatif à l'accumulation fonctionnelle du Mn.

Une revue des applications de MEMRI a été rédigée par Silva et Bock (2008). Il est à noter que, pour des raisons essentiellement pratiques, MEMRI a surtout été utilisé pour mettre en évidence des différences d'activité chronique dans certaines régions cérébrales, par exemple

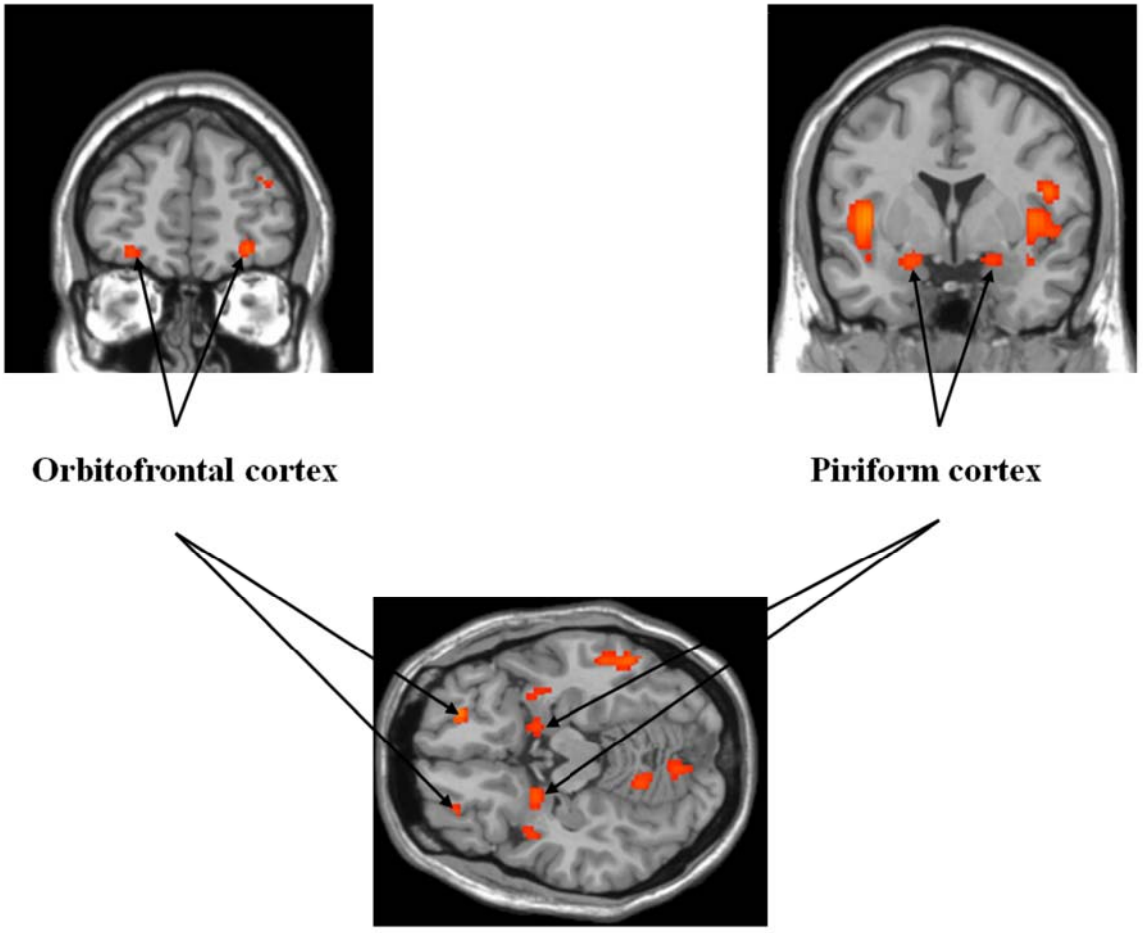

Figure 12 : Activations mises en évidence par IRMf BOLD dans différentes régions cérébrales suite à une stimulation olfactive chez l'Homme. Ces images représentent les résultats d'une analyse de groupe de 60 sujets et montrent, notamment, une activation du cortex orbitofrontal et du cortex piriforme. [Données non publiées]

suite à un régime alimentaire particulier (Zeeni *et al.*, 2010) ou d'une maladie (Dodd *et al.*, 2005). MEMRI a été utilisé avec succès dans quelques études pour cartographier les régions activées par des stimulations aigües, notamment auditives (Yu *et al.*, 2005) et olfactives (Chen *et al.*, 2007; Chuang *et al.*, 2009b; Pautler et Koretsky, 2002).

3.3. Imagerie fonctionnelle de l'olfaction

a. Chez l'Homme

Depuis une vingtaine d'années, l'olfaction humaine est étudiée par imagerie fonctionelle. Les études menées sur l'Homme présentent un certain nombre d'avantages dont le premier est que le meilleur sujet pour étudier l'olfaction humaine est l'Homme lui-même. En effet, les résultats obtenus sur d'autres modèles posent inévitablement le problème de leur transposition à l'Homme. De plus, le sujet étudié est coopératif et il est possible d'accéder à des fonctions cognitives complexes. Pour finir, l'Homme est capable grâce au langage d'exprimer les émotions ressenties au cours de l'expérimentation, expressions qui peuvent être utilisées pour comprendre les mécanismes étudiés.

L'olfaction humaine a été essentiellement étudiée en utilisant soit la TEP, soit l'IRMf BOLD. Chez l'Homme, l'information olfactive semble être traitée à la fois par des processus parallèlement et hiérarchiquement distribués (Savic *et al.*, 2000) dont la complexité et l'organisation ne sont pas encore totalement connues. Des activations fonctionnelles ont été ainsi détectées dans les cortex piriforme et orbitofrontal, mais aussi dans d'autres régions cérébrales telles que l'insula ou l'amygdale (Sobel *et al.*, 1998a; Sobel *et al.*, 1999; Zald et Pardo, 1997; Zatorre *et al.*, 1992). La Figure 12 illustre l'activation du cortex piriforme et orbitofrontal détectée par IRMf BOLD. Suite à une stimulation olfactive, certaines études ont montré que des réponses cérébrales étaient détectables dans des régions en dehors des circuits olfactifs traditionnellement connus. C'est le cas, par exemple, du cortex cingulaire (Levy *et al.*, 1997; Yousem *et al.*, 1997), ou encore du cervelet (Small *et al.*, 1997; Sobel *et al.*, 1998b). Cependant, l'implication de ces régions dans les fonctions olfactives reste méconnue.

D'après les revues de Zald et Pardo (2000) et de Gottfried (2006), un consensus semble émerger, entre les études d'IRMf de l'olfaction humaine, sur les rôles respectifs du cortex

piriforme, de l'amygdale et du cortex orbitofrontal. Le cortex piriforme ne serait pas qu'un simple relais vers des structures plus profondes mais participerait à l'apprentissage et à la mémoire olfactive. Cependant, ses réponses sont transitoires et sujettes à une rapide habituation. L'amygdale, quant à elle, encoderait l'émotion associée à un stimulus olfactif. Elle interviendrait aussi dans le traitement de l'intensité des odeurs (Anderson *et al.*, 2003). Il est intéressant de noter que l'amygdale est activée lors d'une simple détection passive d'odorants. L'activation immédiate de l'amygdale ainsi que ses fortes connections avec l'hippocampe et le cortex orbitofrontal pourraient, en partie, expliquer la force de la valence émotionnelle présente dans la mémoire des odeurs ainsi que sa rétention à long terme (Savic *et al.*, 2000). Le cortex orbitofrontal, principale cible néocorticale du cortex olfactif primaire, est le lieu de nombreux processus de plus haut niveau reliés par exemple à l'intégration multi-sensorielle ou encore à l'apprentissage associatif.

Alors que plusieurs études ont montré que la détection simple d'odorants était traitée de manière symétrique dans le cerveau, l'identification d'une odeur mettrait en jeu des processus cognitifs latéralisés (Zatorre *et al.*, 1992). Cependant ces résultats sont controversés car de nombreux paramètres comme par exemple la valence hédonique peuvent influencer le traitement latéralisé d'une odeur (Brand *et al.*, 2001). Cette valence hédonique, qu'un individu associe à une odeur, fluctue en fonction de nombreux paramètres contextuels (par exemple, l'âge, l'état de satiété, l'histoire sensorielle…). Par ailleurs, l'intensité d'activation de certaines zones cérébrales dans le traitement d'une odeur peut varier en fonction de la nature du stimulus (Yousem *et al.*, 1997), de la tâche effectuée (Zald *et al.*, 1998) ou encore du sexe des sujets (Levy *et al.*, 1997; Yousem *et al.*, 1999). Une nouvelle fois, certains résultats comme par exemple l'influence du sexe sur l'intensité d'activation dans le cortex piriforme, sont contestés par d'autres études (Bengtsson *et al.*, 2001).

L'étude de l'olfaction chez l'Homme présente un certain nombre de limites dont la principale est la forte variabilité inter individuelle. Les résultats obtenus par imagerie fonctionnelle sont souvent contradictoires car ils pourraient être, en partie, dépendants des cohortes étudiées. Ils convergent finalement sur le fait que de nombreux paramètres influent sur le traitement cérébral d'une odeur et que ceux-ci peuvent varier aussi bien entre individus (âge, sexe…) qu'au sein d'un individu donné (valence hédonique d'une odeur, habituation…). Enfin, l'Homme étant un animal aux fonctions cognitives très développées, les mécanismes de base de la réponse cérébrale à une odeur sont difficilement directement accessibles. Il n'est

probablement pas, à l'heure actuelle, le meilleur modèle pour étudier le traitement cérébral de la perception olfactive par imagerie fonctionnelle.

b. Chez l'animal

Bien que l'objet ultime de toute étude biologique soit l'Homme, celui-ci n'est pas toujours le sujet d'étude le plus approprié. Nous avons vu plus haut quelques obstacles que l'Homme présente à l'exploration fonctionnelle de l'olfaction. Pour aborder les mécanismes fondamentaux du traitement cérébral de la perception odorante, le recours à des modèles animaux peut ainsi s'avérer plus efficace. Leurs populations sont génétiquement contrôlées, phénotypiquement homogènes et leur histoire sensorielle est contrôlable depuis la naissance. Cette homogénéité permet la répétition des expériences et donc la production de données statistiquement robustes. Enfin, il est possible de mettre en œuvre des paradigmes interdits chez l'Homme et de recourir à des méthodes invasives. Enfin, le développement des fonctions cognitives chez l'Homme peut contribuer à masquer les mécanismes fondamentaux, plus facilement accessibles chez l'animal. Finalement, il existe chez l'animal des odeurs naturelles véhiculant des messages particulièrement forts. C'est le cas, par exemple, pour les lapereaux qui sont guidés par une phéromone mammaire pour s'alimenter (Schaal *et al.*, 2003) ou pour le rat qui manifeste des comportements de peur en présence d'une odeur de prédateur (Vernet-Maury, 1980).

L'olfaction a tout d'abord été étudiée, chez le petit animal, par des méthodes invasives comme l'autoradiographie du 2-deoxyglucose ou la détection de l'activation du proto-oncogène c-fos. Les différentes études se sont d'abord focalisées sur la compréhension de l'organisation fonctionnelle dans le bulbe olfactif (Guthrie et Gall, 1995; Sallaz et Jourdan, 1993; Stewart *et al.*, 1979). Actuellement, les recherches sont principalement tournées vers l'intégration du message olfactif dans les régions cérébrales plus profondes comme par exemple le cortex piriforme (Illig et Haberly, 2003) ou encore l'amygdale (Martel et Baum, 2009; Tronel et Sara, 2002). Il a par exemple été montré qu'une odeur de prédateur active plus fortement de nombreuses régions cérébrales situées dans le bulbe olfactif, l'amygdale et l'hypothalamus (Dielenberg *et al.*, 2001; Dielenberg et McGregor, 2001).

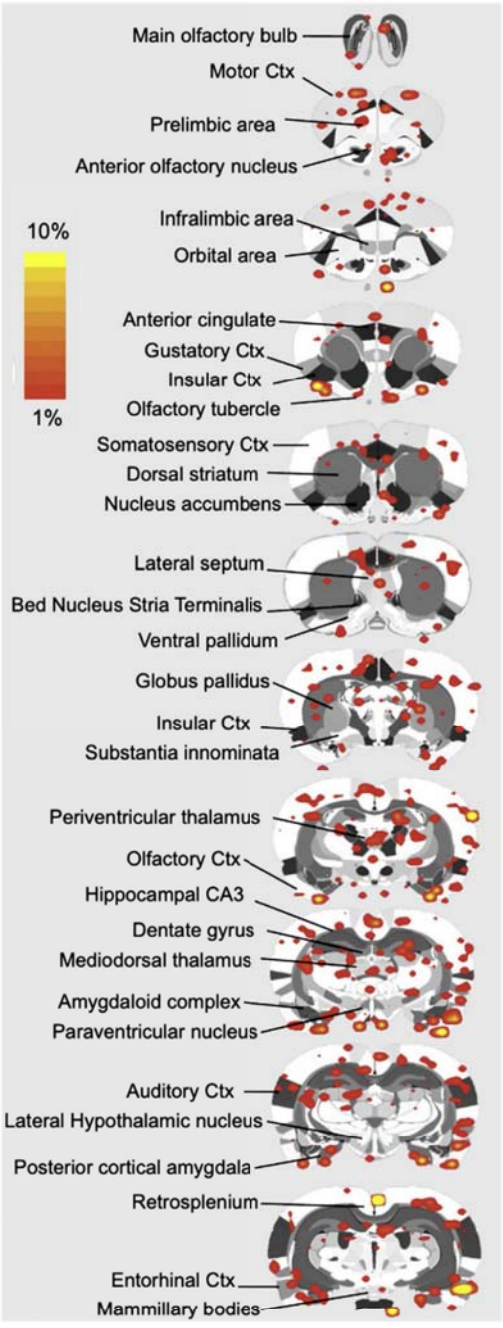

Figure 13 : Activations mises en évidence par IRMf BOLD en réponse à la TMT chez le rat vigile. Ces images montrent des activations constellées dans l'ensemble du cerveau. Cortx : cortex [Adapté d'après Febo *et al.*, 2009]

L'étude de l'olfaction par IRMf sur le petit animal a été, dans un premier temps, menée en BOLD. Ce contraste fournit un signal détectable durant quelques secondes après la stimulation. Il impose donc que la stimulation soit appliquée pendant l'acquisition des images. Or, au contraire de l'Homme, les animaux ne sont pas coopératifs. Ils doivent être soit anesthésiés et donc non conscients pendant la stimulation, soit conscients pendant la stimulation mais acclimatés à demeurer restreints dans l'aimant. Dans la première situation expérimentale, il faut prendre en compte l'éventuel effet de l'anesthésie sur la réponse cérébrale à la stimulation. D'une part, l'activité de base du cerveau diminue avec l'intensité de l'anesthésie. D'autre part, les fonctions cérébrales sont affectées (Massimini *et al.*, 2005; Shulman *et al.*, 1999) et l'état inconscient provoqué par une anesthésie semble être caractérisé par une incapacité à intégrer les signaux sensoriels dans les régions profondes (Alkire *et al.*, 2008). A ce jour, l'IRMf BOLD sur animal anesthésié a mis en évidence des variations fonctionnelles en réponse à des stimulations olfactives uniquement dans le bulbe olfactif (Kida *et al.*, 2002; Martin *et al.*, 2007; Xu *et al.*, 2003; Xu *et al.*, 2005). Pour s'affranchir de l'anesthésie, un protocole a été proposé afin d'acclimater les animaux à rester contraints et conscients dans l'aimant (Ferris *et al.*, 2006), ce qui a permis notamment d'étudier l'olfaction. Des variations dans le traitement cérébral d'odeurs de prédateurs ont alors été mises en évidence dans les régions olfactives et dans les régions associatives (Chen *et al.*, 2009; Febo *et al.*, 2009; Febo et Pira, 2011; Huang *et al.*, 2011). Les cartes obtenues, et en particulier celles induites par l'odeur de TMT (figure 13), montrent des activations très constellées. Il est difficile de distinguer celles spécifiques à l'odeur de celles dues aux multiples conséquences possibles de la contention en état vigile (Martin, 2007), comme par exemple le stress, la douleur ou encore les mouvements. MEMRI est une alternative pour étudier l'olfaction dans les conditions les plus proches de la perception naturelle.

MEMRI a tout d'abord été utilisé pour tracer les voies olfactives (Figure 14) montrant notamment une accumulation de Mn dans le tractus olfactif, le tubercule olfactif mais aussi l'amygdale (Cross *et al.*, 2004). Il a également été utilisé pour montrer l'effet de l'âge, de lésions ou de maladies sur le transport axonal dans le cortex olfactif primaire (Cross *et al.*, 2006; Cross *et al.*, 2008; Kivity *et al.*, 2010; Smith *et al.*, 2007). Peu d'études ont, à ce jour, cartographié par MEMRI les réponses cérébrales à une odeur. A notre connaissance, une seule a ciblé les zones cérébrales profondes (Chen *et al.*, 2007). Après injection systémique du Mn, et rupture de la BHE, Chen *et al.* (2007) ont montré une activation de l'amygdale et de l'hypothalamus plus forte lorsqu'un animal est stimulé par une odeur de prédateur que par d'autres odeurs, corroborant les résultats obtenus avec Fos (Dielenberg *et al.*, 2001;

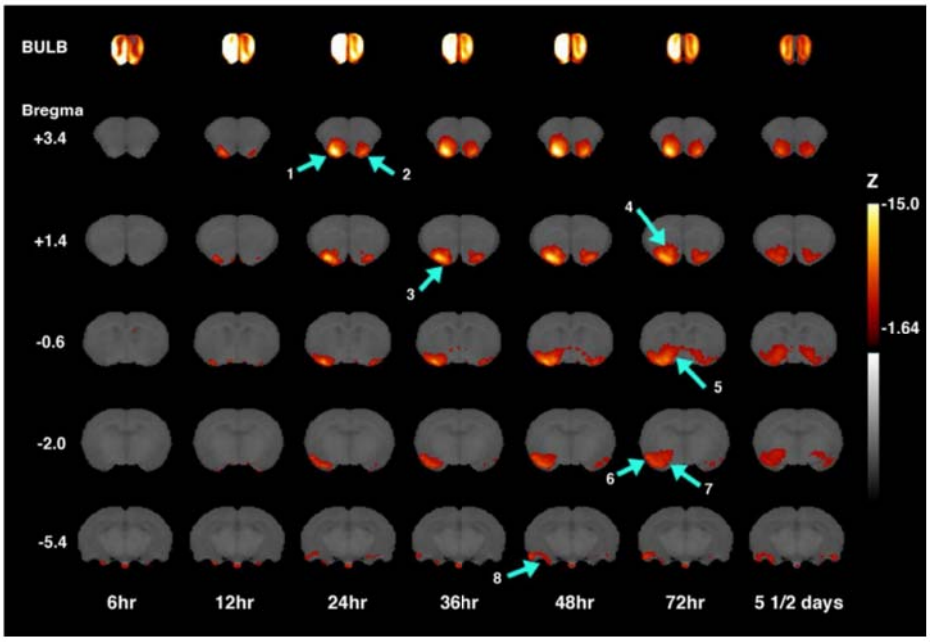

Figure 14 : Traçage des voies olfactives après injection de Mn dans une narine de rats. Les cartes statistiques Z montrent l'accumulation significative du Mn 6, 12, 24, 48, 72h et 5.5 jours après l'injection de Mn. Les flèches représentent approximativement les structures suivantes: (1) tractus olfactif ipsilatéral (2) tractus olfactif contralatéral (3) tubercule ipsilatéral (4) commissure antérieur ipsilatérale (5) pallidum ventral ipsilatéral (6) cortex piriforme ipsilatéral (7) amygdale ipsilatérale (8) zone de transition entre l'amygdale et le piriforme. [De Cross *et al.*, 2004]

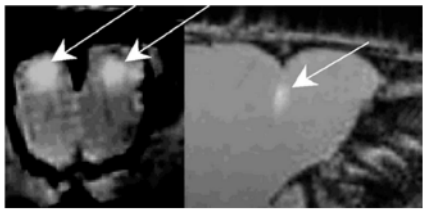

Figure 15 : Images pondérées T1 montrant l'accumulation de Mn dans le bulbe olfactif accessoire suite à l'exposition d'une souris à des phéromones. La vue de gauche est une coupe coronale, celle de droite une coupe sagittale. [De Pautler et Koretsky, 2002]

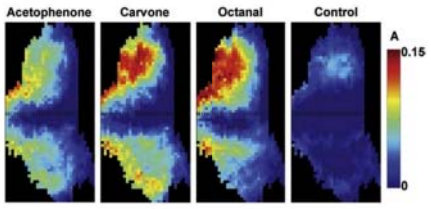

Figure 16 : Cartographies de l'accumulation de Mn dans la couche glomérulaire suite à l'exposition de rats à différentes odeurs. [De Chuang *et al.*, 2009b]

Dielenberg et McGregor, 2001). Cependant, ce protocole expérimental requiert une chirurgie lourde. De plus, la rupture de la BHE peut entrainer des dysfonctionnements cérébraux précoces (Aoki *et al.*, 2004a). Toutes les autres études utilisent un mode d'administration moins invasif, en injectant le Mn dans les narines de l'animal. Dans ces conditions, les résultats fonctionnels ont été rapportés uniquement dans le bulbe olfactif (Chuang *et al.*, 2009b; Pautler et Koretsky, 2002). L'activation du bulbe olfactif accessoire a été mise en évidence par Pautler et Koretsky (2002) suite à l'exposition de souris mâles à de l'urine d'un congénère (Figure 15). Chuang *et al.* (2009b) ont montré des accumulations différentes de Mn dans la couche glomérulaire pour différentes stimulations olfactives mono-moléculaires (Figure 16).

A l'heure actuelle, l'olfaction n'a jamais pu être étudiée chez l'animal dans l'ensemble des régions cérébrales dans les conditions les plus proches de la perception naturelle. Sauf à s'intéresser spécifiquement à l'animal en lui-même (ce qui présente un intérêt notamment à l'INRA), sa principale limite lorsqu'il est utilisé comme modèle de l'Homme est que l'analogie n'est pas parfaite. Le modèle animal permet cependant d'étudier des mécanismes olfactifs communs à tous les mammifères.

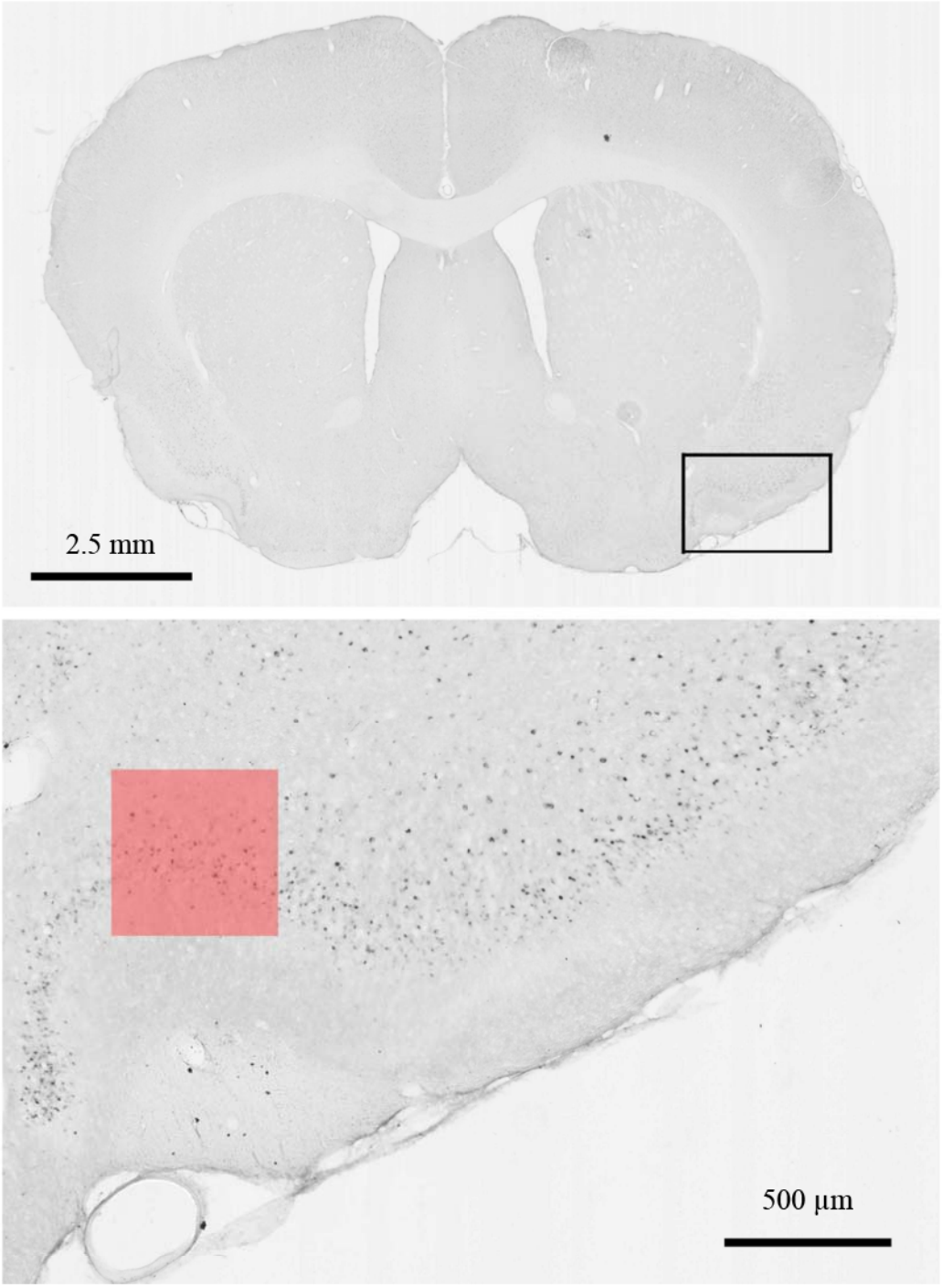

Figure 17 : Coupe coronale dans la partie médiane du cortex piriforme antérieur illustrant la résolution spatiale des études MEMRI. L'image du bas est un zoom de la région située dans le carré noir sur l'image du haut. Le carré rouge est de la même taille qu'un voxel acquis dans nos expériences MEMRI.

Chapitre II

Travail personnel

1. Objectifs de la thèse

L'objectif de ce travail est d'utiliser la technique MEMRI pour révéler un traitement cérébral différentiel d'odeurs véhiculant des informations différentes.

Comme nous l'indiquions dans la revue de littérature, la technique MEMRI révèle des informations de deux ordres : géographique et quantitatif. L'information géographique reflète la distribution dans le cerveau des neurones ayant capté du Mn. Toutes les expériences de ce travail ont été réalisées avec le même aimant de 4.7 T à une résolution isotrope de 500 μm^3, un voxel englobe par conséquent quelques milliers de neurones comme l'illustre la Figure 17. L'information d'intensité traduit, quant à elle, l'accumulation intra-neuronale de Mn. Cette accumulation reflète, au moment de l'imagerie, le bilan de l'entrée de Mn par les canaux calciques voltage-dépendants et de sa sortie par les terminaisons synaptiques. L'ouverture des canaux calciques dépend de l'activité des neurones, de même que le flux axonal (Chuang *et al.*, 2009b). L'activité des neurones conditionne également la libération conjointe par les terminaisons axonales de neuromédiateurs et de Mn (Van der Linden *et al.*, 2007). L'entrée

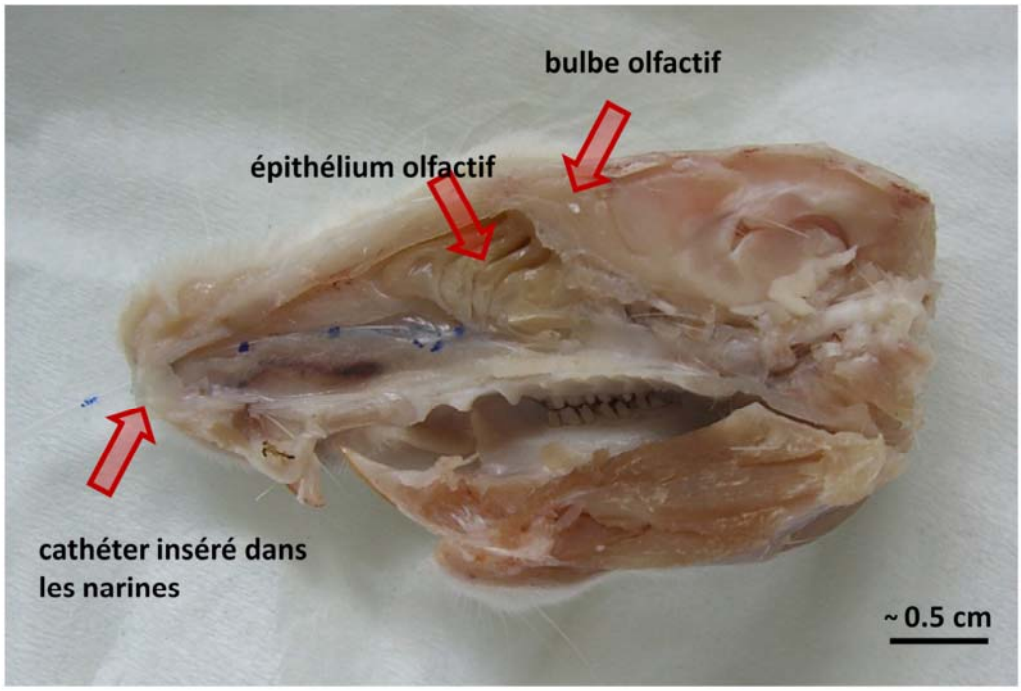

Figure 18 : Coupe parasagittale d'une tête de rat révélant l'anatomie de la fosse nasale. L'accès par les narines à l'épithélium olfactif est direct. La distance entre l'épithélium olfactif et le bulbe olfactif est de quelques mm.

du Mn dans les cellules par les canaux calciques voltage-dépendants est plus efficiente que sa sortie (Nordhoy *et al.*, 2004), ce qui conduit à son accumulation dans les neurones et est sans doute à l'origine de sa toxicité. En revanche cette accumulation assure la rémanence du signal Mn dont la technique tire parti.

Le signal MEMRI étant lié au degré d'activation des neurones, la technique est donc propice à la détection de différences d'activité. MEMRI se prête donc bien à l'investigation fonctionnelle des effets de stimulations sensorielles chez l'animal. Le Mn pourra être administré à l'animal qui sera ensuite stimulé à l'état vigile. La distribution cérébrale du Mn sera ensuite révélée sous anesthésie par IRM. Cependant, le Mn ne traverse pas la BHE. S'il est administré par voie sanguine, on le retrouve rapidement (après ~2h) en forte concentration dans les ventricules cérébraux, mais sa concentration dans le parenchyme cérébral est très faible (Aoki *et al.*, 2004b). Il existe bien sûr une diffusion passive (Aoki *et al.*, 2004b) mais la lenteur du processus est incompatible avec des stimulations sensorielles aigües. Il est possible de contourner cet obstacle de deux manières : soit l'injection intracérébrale directe (Chuang et Koretsky, 2006), soit la rupture temporaire de la BHE (Lin et Koretsky, 1997). La première approche est lourde (anesthésie, stéréotaxie, micro-injection). La seconde repose le plus souvent sur l'administration d'agents hyper-osmotiques dont le plus utilisé est le mannitol, nécessitant également une chirurgie. De plus, la rupture de la BHE n'est pas sans conséquence sur le fonctionnement cérébral pendant la période où les stimulations doivent être appliquées.

Dans la mesure où nos expériences portaient sur l'olfaction, nous avons tiré parti de l'organisation anatomique particulière de cette modalité sensorielle pour déposer directement le Mn sur l'épithélium olfactif situé à quelques millimètres des bulbes olfactifs (Figure 18). Le premier avantage est que cette voie d'administration est très peu invasive. Le second est que le Mn entre dans le système nerveux par des neurones périphériques qui pénètrent directement dans le cerveau. Ce marquage est ainsi immédiatement spécifique des voies olfactives (Cross *et al.*, 2004), auxquelles il est fortement probable que les effets toxiques seront limités. Le principal inconvénient est que le Mn n'est pas disponible *ad libitum* dans l'ensemble du cerveau. Le marquage des régions activées sera ainsi conditionné par son transport à partir de l'épithélium olfactif.

Personne n'a encore, à notre connaissance, comparé chez l'animal les traitements cérébraux réservés à des odeurs biologiquement signifiantes véhiculant des messages de natures différentes. Nous avons choisi d'étudier l'effet d'odeurs contrastées dont la signification touche des fonctions essentielles : la survie et la prise alimentaire. Pour la première, il s'agit de l'odeur des fèces de renard mâle, prédateur naturel du rat, qui induit chez

ce dernier un comportement inné de fuite (Vernet-Maury, 1980). Pour la seconde, il s'agit de l'odeur de céréales chocolatées (Chocapic™, Nestlé) dont l'association à une friandise est rapidement acquise par les rats.

La recherche sur la compréhension des mécanismes cérébraux participant au traitement d'odeurs signifiantes est d'intérêt pour plusieurs thématiques de l'INRA. Une première thématique de l'INRA concerne l'alimentation humaine. Les modes de vie des sociétés développées changent et, avec eux, l'alimentation. Nous constatons une augmentation significative de la prévalence de l'obésité qui traduit l'inadaptation des habitudes alimentaires. Une piste pour remédier à cette situation pourrait consister par exemple à utiliser les odeurs pour orienter les comportements alimentaires, en d'autres termes de maîtriser la valence hédonique des odeurs. Une seconde thématique de l'INRA est la conduite des élevages. Une préoccupation essentielle des éleveurs est la maîtrise de la reproduction et la détection des chaleurs dans plusieurs espèces, dont la vache et le cheval. Cependant, certaines femelles ne présentent pas de signes évidents de chaleurs lors de la période d'œstrus. La détection de l'œstrus peut néanmoins se faire par le biais de moyens techniques relativement coûteux ou difficiles à mettre en place (par exemple : échographie, étalon souffleur…). Comme le suggère l'étude de Rampin *et al.* (2006), l'utilisation des odeurs de fèces d'animaux pourrait permettre de discriminer les périodes du cycle ovarien de ces espèces.

Dans les deux cas que nous venons d'évoquer, une connaissance des mécanismes cérébraux sous-jacents serait évidemment un apport essentiel au développement de stratégies *ad hoc*. Bien que notre étude ne concerne pas les odeurs d'*œstrus*, elle constitue un premier pas dans la compréhension de ces mécanismes que nous espérons pouvoir explorer plus avant dans des études futures.

Présentation de l'article #1

Comme indiqué dans l'introduction bibliographique, MEMRI est une technique qui a fait ses preuves pour étudier le système olfactif chez le petit animal (Chen *et al.*, 2007; Chuang *et al.*, 2009b; Cross *et al.*, 2004; Cross *et al.*, 2006; Cross *et al.*, 2008; De Groof *et al.*, 2010; Kim *et al.*, 2011; Smith *et al.*, 2007). Cependant, quoiqu'étant un élément indispensable au fonctionnement normal d'un grand nombre de processus physiologiques, le Mn est reconnu comme neurotoxique depuis le XIXème siècle (Couper, 1837). De récentes études ont rapporté des effets toxiques du Mn, dans le cadre d'expériences MEMRI, suite à son injection par voie systémique (Eschenko *et al.*, 2010b), intracérébrale (Canals *et al.*, 2008) ou intravitréenne (Thuen *et al.*, 2008). Ces études ont montré que l'injection de doses élevées de Mn entraine des conséquences directes sur le fonctionnement des neurones, et qu'elles peuvent provoquer aussi des effets néfastes sur les systèmes périphériques.

Un pré-requis avant l'utilisation de MEMRI pour toute étude fonctionnelle est donc de trouver une dose de Mn présentant le meilleur compromis entre les effets toxiques induits par l'administration du Mn et le signal détectable par IRM dans les régions d'intérêt (Silva *et al.*, 2004). Les effets de l'administration de Mn par voie nasale étant inconnus, l'objectif de ce premier article est de trouver une dose de Mn qui d'une part, préserve la perception olfactive, et d'autre part, conduit à un marquage MEMRI détectable et reproductible dans le cortex olfactif primaire.

Pour cela, nous avons injecté dans les narines de rats des doses croissantes de Mn (1-8 µmol) et analysé leurs effets (i) sur l'activité motrice spontanée des rats ainsi que sur celle induite par des odeurs et (ii) sur le marquage détectable en IRM.

L'étude comportementale a montré que l'activité motrice spontanée n'était pas affectée par l'injection du Mn dans les narines, alors que les comportements induits par les odeurs diminuaient en fonction de la dose. Les expériences MEMRI ont montré, quant à elles, que la relation entre la dose de Mn injectée et le marquage détectable en IRM n'était pas linéaire dans la gamme de doses étudiée. La combinaison des études comportementales et MEMRI a permis de définir une dose de Mn préservant certains comportements induits par des odeurs tout en assurant un contraste détectable et reproductible par IRM dans le cortex olfactif primaire.

Ce travail a été accepté pour publication en 2011 dans la revue *Magnetic Resonance Imaging*.

2. Effet du manganèse injecté dans les narines de rat : implications pour les études fonctionnelles *in vivo* de l'olfaction utilisant MEMRI.

Effects of manganese injected into rat nostrils: implications for *in vivo* functional study of olfaction using MEMRI.

Benoist Lehallier [1], Gérard Coureaud [2], Yves Maurin [3], Jean-Marie Bonny [1*]

(1) UR370 QuaPA, INRA, F-63122 Saint-Genès-Champanelle, France

(2) CSGA, UMR 6265 CNRS, 1324 INRA, Université de Bourgogne, Agrosup Dijon, Dijon, France.

(3) UR 1197 NOeMI, INRA, F-78350 Jouy-en-Josas, France

* Corresponding author

Phone number: (33) 4 73 62 41 52

Fax number: (33) 4 73 62 40 89

E-mail address: bonny@clermont.inra.fr

Abstract

Manganese-enhanced MRI (MEMRI) is a powerful tool for visualizing neuronal pathways and mapping brain activity modulation. A potential drawback of MEMRI lies in the toxic effects of manganese (Mn), which also depend on its administration route. The aim of this study was to analyze the effects of Mn doses injected into the nostrils of rats on both olfactory perception and MRI contrast enhancement. For this purpose, doses in the range 0–8 μmol MnCl2 were tested. Behavioral items were quantified with and without odor stimulation during the first 2 h following Mn injection. The MRI study was performed after 16 h of intermittent olfactory stimulations. Behavioral results showed that, during the early period following Mn administration, spontaneous motor activity was not affected, while odor-related behaviors were dose-dependently reduced. MRI results showed that, in the primary olfactory cortex, contrast was rapidly enhanced for Mn doses up to 0.3 μmol and very slowly above. This dose of 0.3 μmol Mn can thus be taken as the optimal dose for injection into rat nostrils to ensure a reproducible contrast in MRI studies while sparing olfactory perception.

Keywords: MEMRI, manganese, dose, toxicity, olfaction, behavior, rat

Table 1.1: Bibliographic survey of Mn doses injected into nostrils in previous MEMRI experiments.

Reference	Year	Volume per nostril (µL)	Concentration (M)	Dose (µmol)	Species
Pautler *et al.* [2]	1998	0.5-4	0.004-3.9	0.002-15.6	Mice
Pautler and Koretsky [11]	2002	Not available	1.5	Not available	Mice
Cross *et al.* [3]	2004	10	1	10	Rat
Cross *et al.* [12]	2006	5-10	1	5-10	Rat
Drobyshevsky *et al.* [13]	2006	50	0.05	2.5	Rabbit
Smith *et al.* [14]	2007	4	3.7	14.8	Mice
Cross *et al.* [15]	2008	8-10	1	8-10	Rat
Serrano *et al.* [16]	2008	2	3.8	7.6	Mice
Chuang *et al.* [17]	2009	7	0.01	0.07	Mice
Chuang and Koretstky [18]	2009	20	0.5	10	Rat
Kivity *et al.* [19]	2010	4	0.5	2	Mice
De Groof *et al.* [20]	2010	10	0.04	0.4	Bird
Massad *et al.* [21]	2010	2	3.7	7.4	Mice
Peethumnongsin *et al.* [22]	2010	2	3.7	7.4	Mice
Sharma *et al.* [23]	2010	4	3.7	14.8	Mice
Kim *et al.* [24]	2011	4	0.16	0.64	Mice

1. Introduction

Since its initial development [1, 2], manganese-enhanced MRI (MEMRI) has proved a valuable method for visualizing neuronal pathways [3] and mapping brain activity modulation [4]. However, the main drawback of using manganese (Mn) as a contrast agent is its toxicity [5], which can bias results of MEMRI studies. Mn doses as low as possible should thus be administered to avoid confounding factors, as Mn can modify the function being studied and/or indirectly impact the stimulation paradigm. Yet Mn concentration in the extracellular space must be high enough for its uptake by activated neurons and its detection by MRI [6].

Mn is neurotoxic [7]. Moreover, its toxicity strongly depends on its administration route [8-10]. This helps to explain the wide range of Mn doses used in previous MEMRI studies. Thus, a prerequisite for any functional MEMRI experiment is to determine the best compromise between MRI contrast and maintenance of the biological functions being analyzed. Several studies have shown the relevance of the nasal route to study odor processing in the olfactory bulb [11], trace olfactory tracts [3] and highlight the impact of age, lesion or disease on axonal transport [12-15]. A wide range of doses was used in these studies, as shown in Table 1. In addition, the effects of Mn dose on animal behavior have seldom been researched.

In order to use MEMRI for mapping deep brain regions activated by odors in conscious rats, one prerequisite is therefore the optimization of the Mn dose. The dose-dependent effects of intranasally injected Mn were thus assessed on (i) spontaneous motor activity and response to olfactory stimulation and (ii) T_1-weighted signal enhancement in the primary olfactory cortex using *in vivo* multi-subject MRI exploration. Our results show that a particular dose of Mn ensures a detectable contrast in the primary olfactory cortex, while sparing olfactory perception.

2. Methods

2.1. Mn injection

Adult male Wistar rats weighing 240 ± 24 g (Charles River labs, France) were housed individually under a reversed 12 h light / 12 h dark cycle (light on at 20:00). Experiments were performed in compliance with European legislative, administrative and statutory provisions for the protection of animals used for experimental or other scientific purposes (86/609/EEC). The rats were anaesthetized with 4% isoflurane and placed in the supine

position. Mn was injected into both nostrils through a polyethylene catheter (PE 10 tubing) attached to a Hamilton syringe. When they woke (approximately 1-2 min after Mn administration), the rats were put into clean, empty cages with free access to water. As pointed out by Silva *et al.* [25], the osmolarity of a 100 mM Mn solution is required to be compatible with that of body fluids. Indeed, a non-isotonic solution can induce epithelial changes [26] and reduce Mn uptake [27]. In our dose-effect experiments, the concentration of the Mn solution was therefore kept constant and the injected volume was adjusted to reach the desired dose. Volumes of 1, 3, 10, 30 and 80 µL of a 100 mM MnCl2.4H2O solution (Sigma-Aldrich Co, France) were administered.

2.2. Olfactory stimulation

During the week preceding olfactory stimulation, the rat diet was supplemented with 6 g/day of chocolate-flavored cereals (Chocapic ™, Nestlé, Switzerland) to confer a positive value to the stimulus. On the day of the experiment, the odor released by these cereals was used as the olfactory stimulus.

A custom-made device delivered a reproducible, constant flow of deodorized air into the rat cage through a sniffing port. During a total period of 2 h (for behavioral observations) or 16 h (for MEMRI experiments), the air was enriched for 5 min every 30 min with the stimulation odor. This intermittent paradigm was chosen to prevent habituation of the rat to the odor [28].

2.3. Behavioral assessment

It was carried out in two conditions; the first to quantify the effect of Mn on some behaviors usually displayed by rats in their cages, in the absence of any experimental stimulation, and the second to quantify behaviors induced by the experimentally controlled olfactory stimulation. In both conditions, four groups of three rats fasted for 48 h received different doses of Mn in their nostrils, i.e. 0.3, 1, 3, and 8 µmol. For each condition, three other rats formed a solution-free (and so Mn-free) control group.

The behavior of each rat was video-recorded using a camera placed above the cage, starting 25 min after the Mn injection and running for 120 min. Four sequences of 5 min spaced 25 min apart (sequence 1 started at the beginning of the recording) were extracted from each video recording, and then visually analyzed. These sequences matched the times of odor stimulation (when applied). General locomotion of each rat was first analyzed by

dividing the cage area into four equal-sized zones on the monitor. The first experimental variable was the number of crossings between zones. Total durations of two other behavioral items displayed during the successive periods were also measured: (i) olfactory exploration of the surroundings displayed by the rat when it stopped, stood on its hind legs, and sniffed; and (ii) active sniffing at the port through which the odor was delivered.

2.4. MEMRI

Five groups of satiated rats received different doses of Mn in each nostril (n = 3 for 0.1 µmol, n = 4 for 0.3 µmol, n = 3 for 1 µmol, n = 3 for 3 µmol, n = 1 for 8 µmol). A single rat was used as a Mn-free control. At 25 min after Mn injection, the familiar food odor was intermittently delivered for 16 h. This prolonged period of odor stimulation was chosen for a significant progression of Mn into the primary olfactory cortex.

Images were acquired on a Bruker (Bruker, GmbH, Ettlingen, Germany) 4.7 T / 40 cm horizontal magnet equipped with a 12 cm gradient coil and interfaced to an AVANCE III console. A 9 cm-diameter linearly-polarized birdcage resonator was used for emission and reception. Rats were anesthetized with 1–1.5% isoflurane in a 0.3/0.7 mixture of O2/air. Animals were placed in a rat-tailored bed equipped with a three-points fixation system (tooth-bar and ear-plug) and a temperature-controlled warming blanket. Physiological conditions were monitored using breathing and temperature probes.

T_1-weighted images covering the whole brain were acquired using a 3D rapid acquisition with a relaxation enhancement sequence (RARE, acceleration factor = 4). With a TR/TE of 500 ms/7.4 ms, a 64 × 64 × 64 matrix with an isotropic voxel size of 500 µm was obtained every 8.5 min. Acquisitions were repeated for 136 min, corresponding to a time-series of 16 volumetric images for each rat. After MRI acquisition, the rats were sacrificed by sodium pentobarbital injection (200 mg/kg). In summary, MRI acquisitions sampled Mn progression under anesthesia 16 h after Mn administration into nostrils and after several short periods of odor stimulation.

Each rat's image series was first motion-corrected via rigid registration under automated image registration software [29]. All the series were then segmented and normalized using our iterative algorithm for spatial and intensity normalization of MEMRI images [30, 31]. The reference signal used for the intensity normalization was measured in the tongue. A 3D Gaussian linear filter (full-width at half-maximum = 0.5 mm) was applied on each normalized image to increase its signal-to-noise ratio and smooth the inter-animal misregistrations. T_1-

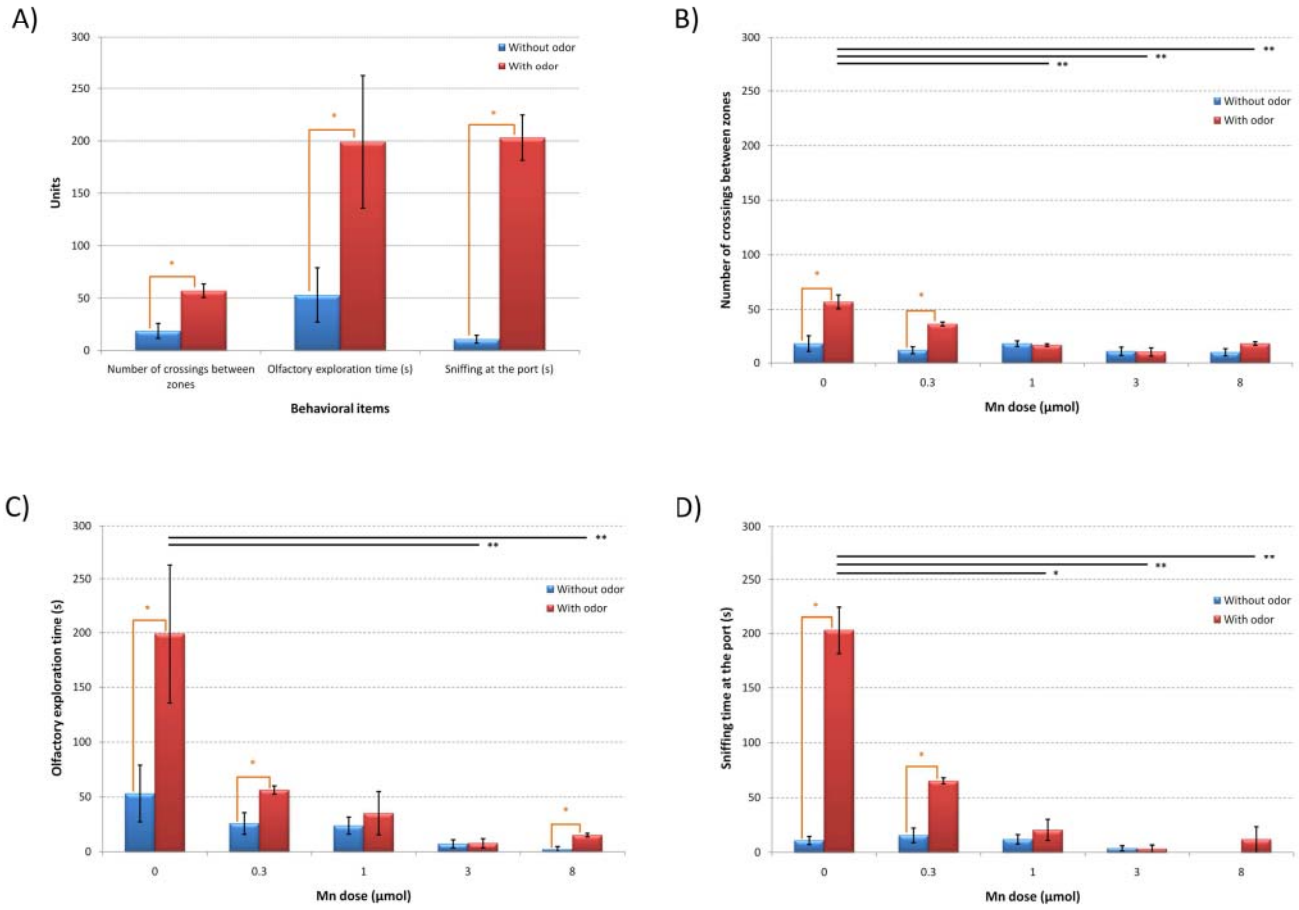

Figure 1.1: Behavioral effects of odor stimulation on Mn-free and Mn-impregnated rats. Bars represent means ± SEM of behavioral parameters within a group of 3 rats. (A) Effects of odor stimulation on the three chosen behavioral items in Mn-free rats. (B, C, D) Effects of Mn dose on these three items: the number of crossings between regions of the cage (B), the olfactory exploration time (C) and the time spends sniffing at the port (D). p-values <0.05 (*) and <0.01 (**) were considered as statistically significant and highly significant, respectively.

weighted 3D-RARE is not prone to signal drift. However it remained possible that Mn concentration changed under anesthesia [11], thus yielding different images along the 16 repetitions acquired on each rat. Consequently, we have analyzed the repetitions using independent component analysis for group inferences [32] under FSL software [33]. Since no temporal signal evolution was detected, the 16 volumetric images of each rat were averaged.

Signal was measured in 2 olfactory ROIs manually delineated in the olfactory bulbs and the primary olfactory cortex. Signal enhancements due to Mn were calculated by normalizing signal values in these ROIs by those of homologous regions in the Mn-free animal. Assuming that Mn concentration in any impregnated tract linearly follows the injected dose, it is possible to theoretically extrapolate the MR enhancement for every dose. The only constraint is to impose to this theoretical curve that it intercepts a single experimental value. We chose to intercept MR enhancements measured at the lowest dose (0.1 µmol) to compare experimental and theoretical enhancements for higher Mn doses. Theoretical enhancement was obtained using the expression S/M_0 (dose)=1-exp[-TR.(R_1,0+k.c.dose)], where R_1,0 is the Mn-free longitudinal relaxation rate considered constant in both ROIs and equal to 0.66 s-1 (according to Kettunen *et al.* [34]), where k is the intra-cellular relaxivity of Mn measured in rat brain and equal to 5.15 mM-1.s-1 (according to Tambalo *et al.* [35]), and where c is a constant linking injected dose of Mn to local concentration. In each ROI, the constant c was adjusted to have the same theoretical and measured enhancements at the dose of 0.1 µmol.

2.5. Statistical comparisons

For all comparisons between groups, normality of the distributions and equality of variances were tested using a Shapiro-Wilk and a Bartlett test respectively. Since the two conditions were never simultaneously met, statistical comparisons of behavioral scores were made using non-parametric tests.

Effect of odors on behavioral scores was analyzed using a Wilcoxon test. Effects of Mn doses on behavioral parameters and on MEMRI were assessed using a Kruskal-Wallis test. When there were significant differences, pairwise comparisons were performed according to Siegel and Castellan [36].

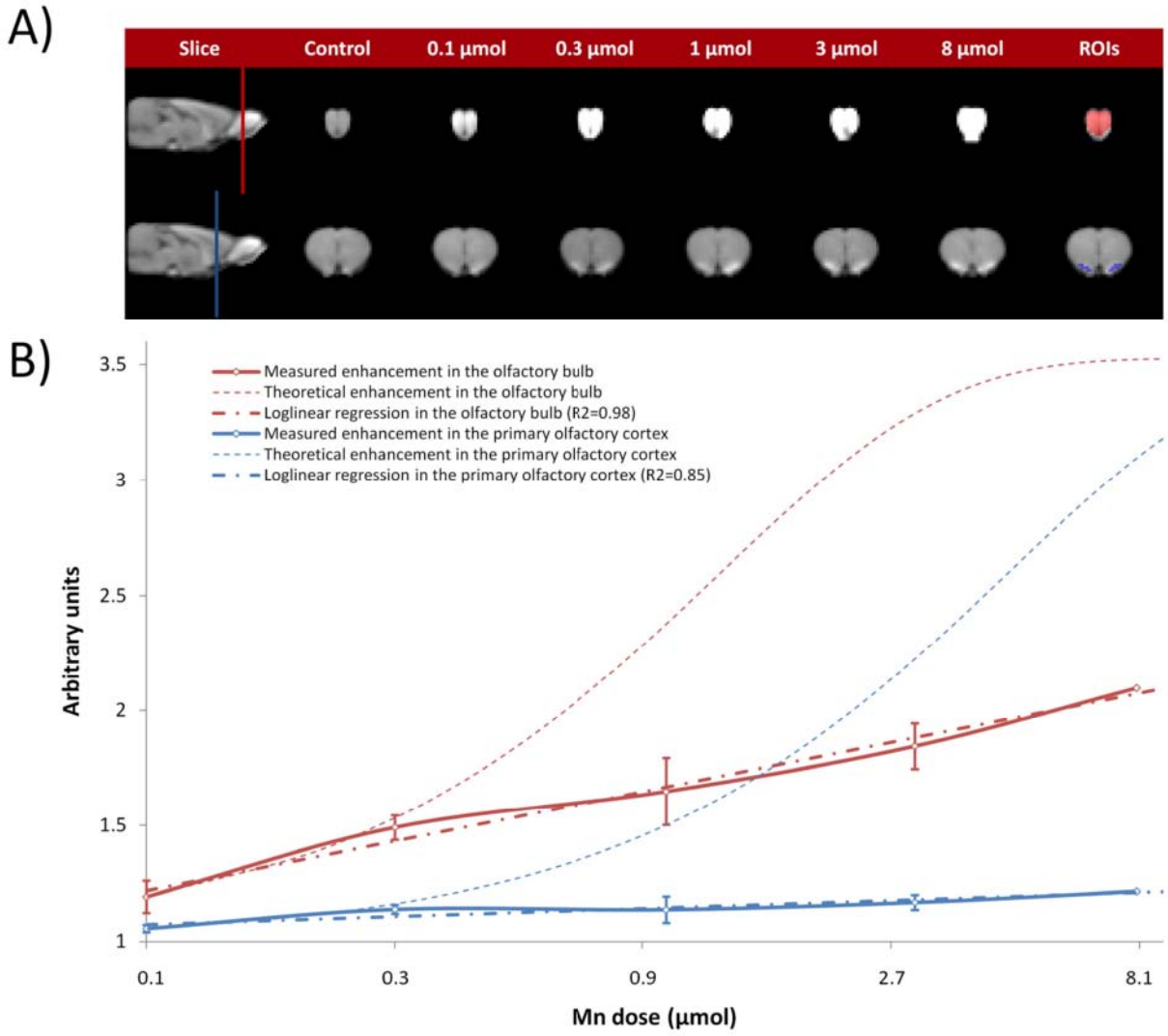

Figure 1.2: Effects of Mn dose on MR enhancements in the olfactory bulb and the primary olfactory cortex. (A) Group-averaged images as a function of Mn dose in two coronal slices through the olfactory bulb (upper row) and the primary olfactory cortex (lower row). (B) Group-averaged enhancements as a function of Mn dose measured in the two ROIs shown in (A). Each enhancement (mean ± SEM) was normalized by the signal of the Mn-free animal. Linear regressions were performed between log3-transformed dose and MR enhancement.

3. Results

3.1. Behavioral assessment

Behavioral parameters have been quantified 25, 55, 85 and 115 minutes after Mn administration. Parameter values recorded 25 minutes after Mn administration did not change thereafter ($p > 0.05$). Consequently, behavioral measures were not recorded beyond the first 2 hours following Mn administration. Values at the different time points were cumulated for each rat. Group averaged results are presented in Figure 1. Figure 1A shows the different behavioral parameters measured in the Mn-free group with and without olfactory stimulation. Upon olfactory stimulation, rats displayed increased motor activity, olfactory exploration and sniffing at the port ($p < 0.05$). This suggests that responsiveness to odors can be evaluated using our behavioral parameters.

Figures 1B, 1C and 1D show the dose-effect relationships of Mn on rat behavior with and without odorous stimulation. Without stimulation, spontaneous motor activity remained low and did not change markedly with dose (Fig 1B, $p > 0.05$). Comparable results were observed for cumulated time spent in exploration and sniffing at the port (Fig 1C-D, $p > 0.05$). With odor stimulation, these behavioral scores decreased significantly with the Mn dose (Fig 1B-C-D, $p < 0.05$). Doses of 1, 3 and 8 µmol Mn abolished the increase in motor activity induced by the olfactory stimulation (Fig 1B, $p > 0.05$). By contrast, a dose of 0.3 µmol of Mn did not significantly alter the effect of olfactory stimulation (Fig 1B, $p < 0.05$). Similar effects were observed on olfactory exploration and sniffing at the port (Fig 1C-D).

3.2. MEMRI analysis

Figure 2A presents group-averaged images in two coronal slices located in the primary olfactory cortex as a function of the Mn dose injected into the nostrils. Visually, a signal enhancement due to Mn was observed in both olfactory bulbs and primary olfactory cortex whatever the injected dose. Figure 2A also depicts ROIs drawn in these two regions in which the mean signal of T_1-weighted images was measured. Figure 2B shows that the mean signal moderately increased in both regions in the 0.1 – 8 µmol Mn dose range. It also highlights marked deviations between experimental and theoretical enhancements for Mn doses beyond ~0.3 µmol in both brain regions, and shows that the relationship between log-transformed Mn dose and MR enhancement was linear, as previously observed by Thuen *et al.* [37]. The slope of a linear regression performed between log3-transformed doses and MR enhancement was ~

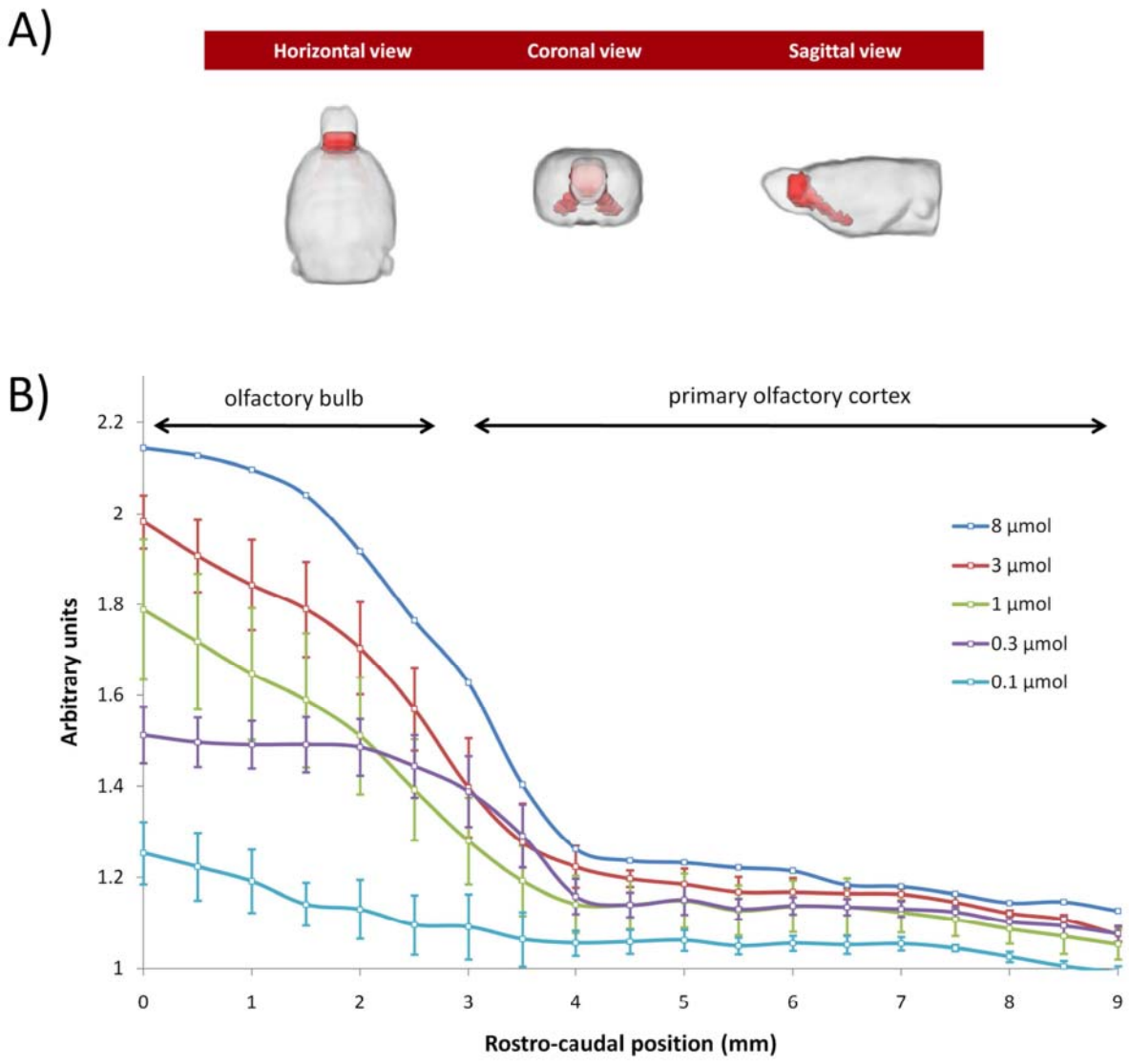

Figure 1.3: Group-averaged contrast enhancement along the olfactory pathway for different Mn doses. (A) ROIs delimiting the olfactory pathway in 19 coronal contiguous slices. ROI boundaries were manually outlined on the images obtained with the maximal 8 µmol Mn dose. (B) Group-averaged enhancements in the ROIs shown on (A) as a function of the rostro-caudal position in the olfactory pathway. Each enhancement (mean ± SEM) was normalized using the signal in the Mn-free animal.

0.2 in the olfactory bulb and approximately 10 times lower in the primary olfactory cortex. To compare MR enhancements between Mn doses along the olfactory pathway, 19 other ROIs were manually drawn in coronal contiguous slices from the middle of the olfactory bulb to the primary olfactory cortex (Figure 3A). Figure 3B depicts the group-averaged enhancements measured in these ROIs along a rostro-caudal axis for the five increasing Mn doses i.e. 0.1 to 8 µmol. It shows that the Mn enhancement in the olfactory pathways decreased with the distance to the injection site. Increase in Mn dose induced significant differences ($p < 0.05$) of enhancements from 0 (middle of the olfactory bulb) to 2.5 mm (end of the olfactory bulb), when signal differences between groups became non significant in deeper regions of the primary olfactory cortex ($p > 0.05$).

4. Discussion

Manganese is a powerful contrast agent for MR imaging of brain function, and particularly olfaction since the primary olfactory cortex can be readily reached via the nasal route. It has however been shown that Mn affects brain function [5] and motor activity [38]. It remained unknown whether administration of Mn through the nostrils alters olfactory perception and to what extent motor defects might contribute to any apparent decreased odor-related behaviors. Prior to MEMRI mapping of brain regions recruited by olfactory stimulation, it was therefore of crucial importance to find a satisfactory compromise between the deleterious effects of Mn and its contrast-enhancing properties in functional brain MR imaging.

Our results show that Mn (in the range 0.3–8 µmol) did not significantly affect spontaneous motor activity (i.e. that of olfactory unstimulated rats) 2 h after injection into nostrils. This argues against a possible effect of Mn mediated by a discomfort caused by the presence of a liquid in the nasal cavity. As a matter of fact, in this case one would expect behavioral alterations in rats both stimulated or not, while alterations appeared only in stimulated animals. Moreover, behavioral alterations in stimulated rats were observed with a volume of Mn solution of 10 µL, which represents only 4% of the nasal cavity volume of adult rats [39]. If discomfort induced by Mn injection was the cause of behavioral alterations, one would also expect an increase in these alterations with the injected volume; it was not observed. Thus, behavioral effects of Mn injection are most likely due to intrinsic properties of Mn than to intranasal injection. The fact that Mn did not significantly affect spontaneous motor activity also contrasts with the results obtained by Eschenko *et al.* [40], who reported a dose-dependent decrease in motor performance 3 h after intraperitoneal injection of Mn.

However, experimental conditions may account for this discrepancy. Indeed, systemic administration of Mn, besides long recognized peripheral effects [41], has been shown to affect brain structures involved in motor functions [42]. In the present study, the lack of significant motor effects after intranasal injection suggests that this mode of administration restricts Mn diffusion to olfactory structures. It also suggests that the fraction of nasally injected Mn that leaks into the respiratory and/or gastric systems, and indirectly reaches motor brain structures, has weak behavioral effects.

Although Mn has been administered by the intranasal route in a number of studies (see Table 1), in none of these was a behavioral effect of Mn ever visually noticed, even at doses higher than those used in the present experiments. Although some of these studies were concerned with tracing of olfactory pathways (for which functional toxicity is of lesser importance), others were focused on the functional exploration of olfaction [3, 11, 17]. Our data suggest that mere visual control of behavior is not sufficient to detect the effects of Mn upon odor-induced behaviors. This is why we carried out quantitative measures during the first 2 h of olfactory stimulation. The effect of Mn dose on olfactory perception may admittedly change over time, but we verified that olfactory stimulation, 13 h after Mn administration, still elicited locomotor and olfactory-related behavioral responses (data not shown).

In addition, *in vivo* multi-subject MRI experiments provide information on the dose-effect relationship between the quantity of intranasally injected Mn and T_1-weighted signal enhancement. A model was fitted, based upon a linear relationship between the dose of Mn administered into the nostrils and intra-neuronal Mn concentration. Our results indicate that Mn concentration in the olfactory pathway increases more slowly than predicted by the model for doses above 0.3 µmol. Two hypotheses may contribute to explain this discrepancy. Firstly, we can reasonably assume that the whole olfactory epithelium will be covered by a certain volume of solution. This puts a ceiling on the dose of Mn that can be made available on the olfactory epithelium. Beyond this amount, Mn may leak outside the olfactory epithelium to the nasopharynx and even into the respiratory and/or gastric systems [26]. Secondly, because Mn toxicity increases with its intra-neuronal concentration [43], neuronal uptake of Mn from the olfactory epithelium is likely limited. Hence, in the primary olfactory cortex, the observed slow increase of contrast enhancement with Mn dose may simply reflect toxic effects of Mn. This hypothesis is supported by the observation that the Mn dose above which curves of experimental and theoretical contrast enhancement diverge is also the dose above which noticeable toxic effects on behavior are noticed.

A key to the successful use of MEMRI is a good compromise between the dose-dependent toxic effects of Mn on the function studied and the quantity available to detect a significant MR enhancement in the brain region of interest [44]. In our experimental conditions, 16 h after Mn injection into nostrils, a dose of 0.1 µmol produced an enhancement of ~20% of the MR signal in the olfactory bulb. This signal decreased to ~5% at the beginning of the primary olfactory cortex, and vanished rapidly. This progression (roughly estimated at ~1 mm/h) is consistent with the relatively slow Mn transport rate previously reported (i.e. ~1-6 mm/h according to references [45-47]). Longer diffusion time is then required to transport Mn further into deeper brain regions, such as the primary olfactory cortex (e.g. ~24 h for the piriform cortex according to Cross [3]). However, 0.1 µmol Mn requires injecting a small quantity of solution into the nostrils. In this condition, we noted that MR enhancements were not symmetrical for all the animals in the olfactory tract (data not shown). A dose of ~ 0.3 µmol seems thus preferable to induce reproducible, bilateral Mn enhancements in the olfactory tract and still preserve olfactory perception in rats.

In conclusion, (i) olfactory perception is altered by high doses of Mn early after injection into rat nostrils (ii) MR enhancements in the olfactory pathway no longer increase linearly with dose beyond 0.3 µmol. In our experimental conditions, 0.3 µmol seems therefore optimal to achieve a detectable contrast in olfactory pathways while preserving olfactory perception. The duration of Mn progression is an experimental degree of freedom that must be chosen according to the brain regions targeted.

Acknowledgments

The authors are indebted to Dr Olivier Rampin and Dr Benoist Schaal for helpful suggestions during the course of this study. This work has been partly funded by the French Research Agency (ANR). The MRI experiments were performed at the MR of biological systems platform at the INRA research center in Clermont-Ferrand, France (www.clermont.inra.fr/rmsb/).

References

1. Lin YJ, Koretsky AP. Manganese ion enhances T-1-weighted MRI during brain activation: An approach to direct imaging of brain function. Magnetic Resonance in Medicine 1997;38(3):378-388.

2. Pautler RG, Silva AC, Koretsky AP. In vivo neuronal tract tracing using manganese-enhanced magnetic resonance imaging. Magnetic Resonance in Medicine 1998;40(5):740-748.

3. Cross DJ, Minoshima S, Anzai Y, Flexman JA, Keogh BP, Kim Y, Maravilla KR. Statistical mapping of functional olfactory connections of the rat brain in vivo. Neuroimage 2004;23(4):1326-1335.

4. Weng JC, Chen JH, Yang PF, Tseng WYI. Functional mapping of rat barrel activation following whisker stimulation using activity-induced manganese-dependent contrast. NeuroImage 2007;36(4):1179-1188.

5. Crossgrove J, Zheng W. Manganese toxicity upon overexposure. NMR Biomed 2004;17(8):544-553.

6. Koretsky AP. New Developments in Magnetic Resonance Imaging of the Brain. NeuroRX 2004;1(1):155-164.

7. Hazell AS. Astrocytes and manganese neurotoxicity. Neurochem Int 2002;41(4):271-277.

8. Eschenko O, Canals S, Simanova I, Logothetis NK. Behavioral, electrophysiological and histopathological consequences of systemic manganese administration in MEMRI. Magn Reson Imaging 2010;28(8):1165-1174.

9. Canals S, Beyerlein M, Keller AL, Murayama Y, Logothetis NK. Magnetic resonance imaging of cortical connectivity in vivo. NeuroImage 2008;40(2):458-472.

10. Thuen M, Berry M, Pedersen TB, Goa PE, Summerfield M, Haraldseth O, Sandvig A, Brekken C. Manganese-enhanced MRI of the rat visual pathway: acute neural toxicity, contrast enhancement, axon resolution, axonal transport, and clearance of Mn(2+). J Magn Reson Imaging 2008;28(4):855-865.

11. Pautler RG, Koretsky AP. Tracing Odor-Induced Activation in the Olfactory Bulbs of Mice Using Manganese-Enhanced Magnetic Resonance Imaging. NeuroImage 2002;16(2):441-448.

12. Cross DJ, Flexman JA, Anzai Y, Morrow TJ, Maravilla KR, Minoshima S. In vivo imaging of functional disruption, recovery and alteration in rat olfactory circuitry after lesion. Neuroimage 2006;32(3):1265-1272.

13. Drobyshevsky A, Robinson AM, Derrick M, Wyrwicz AM, Ji XH, Englof I, Tan S. Sensory deficits and olfactory system injury detected by novel application of MEMRI in newborn rabbit after antenatal hypoxia-ischemia. NeuroImage 2006;32(3):1106-1112.

14. Smith KD, Kallhoff V, Zheng H, Pautler RG. In vivo axonal transport rates decrease in a mouse model of Alzheimer's disease. Neuroimage 2007;35(4):1401-1408.

15. Cross DJ, Flexman JA, Anzai Y, Maravilla KR, Minoshima S. Age-related decrease in axonal transport measured by MR imaging in vivo. Neuroimage 2008;39(3):915-926.

16. Serrano F, Deshazer M, Smith KD, Ananta JS, Wilson LJ, Pautler RG. Assessing transneuronal dysfunction utilizing manganese-enhanced MRI (MEMRI). Magn Reson Med 2008;60(1):169-175.

17. Chuang KH, Lee JH, Silva AC, Belluscio L, Koretsky AP. Manganese enhanced MRI reveals functional circuitry in response to odorant stimuli. NeuroImage 2009;44(2):363-372.

18. Chuang KH, Koretsky AP. Accounting for nonspecific enhancement in neuronal tract tracing using manganese enhanced magnetic resonance imaging. Magn Reson Imaging 2009;27(5):594-600.

19. Kivity S, Tsarfaty G, gmon-Levin N, Blank M, Manor D, Konen E, Chapman J, Reichlin M, Wasson C, Shoenfeld Y, Kushnir T. Abnormal olfactory function demonstrated by manganese-enhanced MRI in mice with experimental neuropsychiatric lupus. Ann N Y Acad Sci 2010;1193:70-77.

20. De Groof G, Gwinner H, Steiger S, Kempenaers B, Van der Linden A. Neural correlates of behavioural olfactory sensitivity changes seasonally in European starlings. PLoS One 2010;5(12):e14337.

21. Massaad CA, Amin SK, Hu L, Mei Y, Klann E, Pautler RG. Mitochondrial superoxide contributes to blood flow and axonal transport deficits in the Tg2576 mouse model of Alzheimer's disease. PLoS One 2010;5(5):e10561.

22. Peethumnongsin E, Yang L, Kallhoff-Munoz V, Hu L, Takashima A, Pautler RG, Zheng H. Convergence of presenilin- and tau-mediated pathways on axonal trafficking and neuronal function. J Neurosci 2010;30(40):13409-13418.

23. Sharma R, Buras E, Terashima T, Serrano F, Massaad CA, Hu L, Bitner B, Inoue T, Chan L, Pautler RG. Hyperglycemia induces oxidative stress and impairs axonal transport rates in mice. PLoS One 2010;5(10):e13463.

24. Kim J, Choi IY, Michaelis ML, Lee P. Quantitative in vivo measurement of early axonal transport deficits in a triple transgenic mouse model of Alzheimer's disease using manganese-enhanced MRI. Neuroimage 2011.

25. Silva AC, Lee JH, Aoki I, Koretsky AP. Manganese-enhanced magnetic resonance imaging (MEMRI): methodological and practical considerations. NMR Biomed 2004;17(8):532-543.

26. Dhuria SV, Hanson LR, Frey WH. Intranasal delivery to the central nervous system: mechanisms and experimental considerations. J Pharm Sci 2010;99(4):1654-1673.

27. Dufes C, Olivier JC, Gaillard F, Gaillard A, Couet W, Muller JM. Brain delivery of vasoactive intestinal peptide (VIP) following nasal administration to rats. Int J Pharm 2003;255(1-2):87-97.

28. Poellinger A, Thomas R, Lio P, Lee A, Makris N, Rosen BR, Kwong KK. Activation and habituation in olfaction--an fMRI study. Neuroimage 2001;13(4):547-560.

29. Woods RP, Grafton ST, Holmes CJ, Cherry SR, Mazziotta JC. Automated image registration: I. General methods and intrasubject, intramodality validation. Journal of Computer Assisted Tomography 1998;22(1):139-152.

30. Lehallier B, Andrey P, Burguet J, Maurin Y, Bonny JM. Methods for groupwise analysis of functional MEMRI data. Book of abstracts: 17th triennual ISMAR Conference, Firenze - Italy 2010;289.

31. Lehallier B, Andrey P, Maurin Y, Bonny JM. Iterative algorithm for spatial and intensity normalization of MEMRI images. Application to tract-tracing of rat olfactory pathways. Magn Reson Imaging 2011; In press.

32. Beckmann CF, Smith SM. Probabilistic independent component analysis for functional magnetic resonance imaging. IEEE Trans Med Imaging 2004;23(2):137-152.

33. Smith SM, Jenkinson M, Woolrich MW, Beckmann CF, Behrens TE, Johansen-Berg H, Bannister PR, De LM, Drobnjak I, Flitney DE, Niazy RK, Saunders J, Vickers J, Zhang Y, De SN, Brady JM, Matthews PM. Advances in functional and structural MR image analysis and implementation as FSL. Neuroimage 2004;23 Suppl 1:S208-S219.

34. Kettunen MI, Grohn OH, Lukkarinen JA, Vainio P, Silvennoinen MJ, Kauppinen RA. Interrelations of T(1) and diffusion of water in acute cerebral ischemia of the rat. Magn Reson Med 2000;44(6):833-839.

35. Tambalo S, Daducci A, Fiorini S, Boschi F, Mariani M, Marinone M, Sbarbati A, Marzola P. Experimental Protocol for Activation-Induced Manganese-Enhanced MRI (AIM-MRI) Based on Quantitative Determination of Mn Content in Rat Brain by Fast T-1 Mapping. Magnetic Resonance in Medicine 2009;62(4):1080-1084.

36. Siegel S, Castellan NJ. Non parametric statistics for the behavioural sciences. New York: 1988. 213 p.

37. Thuen M, Singstad TE, Pedersen TB, Haraldseth O, Berry M, Sandvig A, Brekken C. Manganese-enhanced MRI of the optic visual pathway and optic nerve injury in adult rats. J Magn Reson Imaging 2005;22(4):492-500.

38. Cersosimo MG, Koller WC. The diagnosis of manganese-induced parkinsonism. Neurotoxicology 2006;27(3):340-346.

39. Gross EA, Swenberg JA, Fields S, Popp JA. Comparative morphometry of the nasal cavity in rats and mice. J Anat 1982;135(Pt 1):83-88.

40. Eschenko O, Canals S, Simanova I, Beyerlein M, Murayama Y, Logothetis NK. Mapping of functional brain activity in freely behaving rats during voluntary running

using manganese-enhanced MRI: implication for longitudinal studies. Neuroimage 2010;49(3):2544-2555.

41. Wolf GL, Baum L. Cardiovascular toxicity and tissue proton T1 response to manganese injection in the dog and rabbit. AJR Am J Roentgenol 1983;141(1):193-197.

42. Baek SY, Cho JH, Kim ES, Kim HJ, Yoon S, Kim BS, Kim JB, Lee CR, Yoo C, Lee JH, Lee H, Park J, Kim JW, Kim Y. CDNA array analysis of gene expression profiles in brain of mice exposed to manganese. Ind Health 2004;42(3):315-320.

43. Henriksson J, Tjalve H. Manganese taken up into the CNS via the olfactory pathway in rats affects astrocytes. Toxicol Sci 2000;55(2):392-398.

44. Silva AC, Bock NA. Manganese-enhanced MRI: An exceptional tool in translational neuroimaging. Schizophrenia Bulletin 2008;34(4):595-604.

45. Leergaard TB, Bjaalie JG, Devor A, Wald LL, Dale AM. In vivo tracing of major rat brain pathways using manganese-enhanced magnetic resonance imaging and three-dimensional digital atlasing. Neuroimage 2003;20(3):1591-1600.

46. Saleem KS, Pauls JM, Augath M, Trinath T, Prause BA, Hashikawa T, Logothetis NK. Magnetic Resonance Imaging of Neuronal Connections in the Macaque Monkey. Neuron 2002;34(5):685-700.

47. Watanabe T, Michaelis T, Frahm J. Mapping of retinal projections in the living rat using high-resolution 3D gradient-echo MRI with Mn2+-induced contrast. Magn Reson Med 2001;46(3):424-429.

Présentation de l'article #2

Nous avons souligné, dans la première étude, la nécessité d'injecter de faibles doses de Mn dans les narines de rats pour limiter ses effets toxiques sur la perception olfactive. Nous avons montré qu'une dose de 0.3 µmol de Mn permet à la fois de préserver la perception olfactive et d'assurer un contraste détectable et reproductible par IRM dans le cortex olfactif primaire.

MEMRI tire profit de la rémanence du Mn dans les neurones activés. Il est possible de stimuler olfactivement des animaux vigiles puis de révéler l'accumulation du Mn dans le cerveau par IRM *a posteriori*. Cependant, la rémanence du Mn empêche l'animal d'être son propre témoin, comme en IRMf BOLD. De faibles variations de concentration de Mn n'étant pas détectables par un simple examen visuel des images, la mise en place de stratégies sophistiquées d'analyse de groupes ayant subis des stimulations olfactives différentes s'impose afin de détecter des variations fonctionnelles d'accumulation de Mn (Cross *et al.*, 2004; Yu *et al.*, 2008).

Cette comparaison de groupes n'est pertinente que si les différences entre les images obtenues sur plusieurs animaux ne sont dues qu'aux variations de concentration de Mn. Deux facteurs de variations, inhérents à une expérience multi-sujets, doivent par conséquent être corrigés par traitement des images. Le premier concerne une constante multiplicative globale qui, dans le cas d'images pondérées, varie entre les sujets. Elle est liée au gain variable du système d'acquisition et nécessite donc une normalisation en intensité. Le second concerne l'absence de correspondance spatiale entre les images obtenues sur les différents sujets. Elle est due à des différences intrinsèques (variabilités anatomiques) et extrinsèques (variabilité du repère image), et doit donc être corrigée par normalisation spatiale. Bien que des algorithmes de normalisation spatiale aient été proposés et optimisés pour l'analyse de groupe chez l'Homme (Klein *et al.*, 2009), ces derniers ne sont pas directement transposables chez l'animal en raison des nombreuses différences (par exemple les contrastes utilisés, la résolution spatiale, l'anatomie du cerveau…). Dans le cadre MEMRI, des stratégies de normalisation *ad hoc* ont été utilisées. Par exemple, la normalisation spatiale a été effectuée en utilisant aussi bien des algorithmes linéaires que non linéaires. De même, le signal utilisé pour la normalisation en intensité a été mesuré dans des références soit externes, soit internes au cerveau. Sans remettre en cause la pertinence de ces stratégies, celles-ci sont souvent insuffisamment décrites ou justifiées pour pouvoir être génériques. L'objectif de ce second travail est de proposer un algorithme itératif pour normaliser, spatialement et en intensité, les

images MEMRI. L'efficacité de cet algorithme pour révéler l'accumulation de Mn a été testée sur une expérience de traçage des voies olfactives du rat. Il a permis de révéler le traçage des voies olfactives, 48h après l'injection de Mn, depuis le bulbe olfactif jusqu'aux cortex entorhinal postérieur.

Nous avons optimisé chacune des deux étapes de normalisation (i) en comparant les différents algorithmes de recalage spatial et (ii) en analysant l'effet du choix de la région de référence sur la détection des marquages Mn. Les étapes de normalisation spatiale et en intensité ont été intégrées dans un même processus itératif, dont elles tirent toutes les deux profit. L'étape de normalisation spatiale améliore la reproductibilité de localisation de la région dans laquelle le signal de référence, servant pour la normalisation en intensité, est mesuré. Réciproquement, une meilleure normalisation en intensité permet d'estimer plus précisément l'image moyenne qui sert de cible de recalage aux images MEMRI, et améliore donc la normalisation spatiale.

Pour améliorer l'efficacité de la normalisation spatiale, la segmentation du cerveau des tissus périphériques est un pré-requis (Hajnal *et al.*, 1995). Cependant, plusieurs heures sont nécessaires pour segmenter manuellement des images 3D comme celles acquises dans nos expériences MEMRI. Une méthode de segmentation rapide (2-3 min) du cerveau a donc été développée pour accélérer cette étape.

Ce travail a été accepté pour publication en 2011 dans la revue *Magnetic Resonance Imaging*.

3. Algorithme itératif pour la normalisation spatiale et en intensité des images MEMRI. Application au traçage des voies olfactives chez le rat.

Iterative algorithm for spatial and intensity normalization of MEMRI images. Application to tract-tracing of rat olfactory pathways

Benoist Lehallier [1], Philippe Andrey [2,3], Yves Maurin [2], Jean-Marie Bonny [1*]

(1) UR370 QuaPA, INRA, F-63122 Saint-Genès-Champanelle, France

(2) UR 1197 NOeMI, INRA, F-78350 Jouy-en-Josas, France

(3) UPMC Université de Paris 06, France

* Corresponding author

Phone number: (33) 4 73 62 41 52

Fax number: (33) 4 73 62 40 89

E-mail address: bonny@clermont.inra.fr

Abstract

Manganese-enhanced MRI (MEMRI) is an emerging technique for visualizing neuronal pathways and mapping brain activity modulation in animal models. Spatial and intensity normalization of MEMRI images acquired from different subjects are crucial steps as they can influence the results of group-wise analysis. However, no commonly accepted procedure has yet emerged. Here, a normalization method is proposed which performs both spatial and intensity normalizations in a single iterative process without the arbitrary choice of a reference image. Spatial and intensity normalizations benefit from this iterative process. On one hand, spatial normalization increases the accuracy of ROI positioning for intensity normalization. On the other hand, improving the intensity normalization of the different MEMRI images leads to a better averaged target on which the images are spatially registered. After automatic fast brain segmentation and optimization of the normalization process, this algorithm revealed the presence of manganese (Mn) up to the posterior entorhinal cortex in a tract-tracing experiment on rat olfactory pathways. Quantitative comparison of registration algorithms showed that a rigid model with anisotropic scaling is the best deformation model for intersubject registration of 3D MEMRI images. Furthermore, intensity normalization errors may occur if the ROI chosen for intensity normalization intersects regions where Mn concentration differs between experimental groups. Our study suggests that cross-comparing Mn-injected animals against a Mn-free group may provide a control to avoid bias introduced by intensity normalization quality. It is essential to optimize spatial and intensity normalization as the detectability of local between-group variations in Mn concentration is directly tied to normalization quality.

Keywords: Intensity normalization, spatial normalization, segmentation, MEMRI, tract-tracing, olfaction, rat

1. Introduction

Since its initial development [1, 2], manganese-enhanced MRI (MEMRI) has proven a valuable method for visualizing neuronal pathways [3] and mapping brain activity modulation [4]. Manganese ions (Mn2+) are calcium ion analogs that are recruited by activated neurons through voltage-dependent calcium channels, released into the synaptic cleft and taken up by following neurons [5, 6]. At variance with calcium, the slow extrusion of Mn [7] induces its persistence in activated neurons that is detectable in MRI by a strong T1 contrast increase [8]. Image contrast therefore reflects neuronal activity throughout the stimulation period [9]. Because a major trait of this method is the long-lasting intracellular remanence of Mn, the variation in Mn content cannot be revealed in a single MRI experiment. Consequently, Mn accumulation in a particular brain region can only be demonstrated by comparing the results of at least two experiments. Since images derived from only two individuals cannot yield biologically consistent conclusions because of experimental and biological variability, MEMRI images must be acquired through multi-subject studies and spatial variation of Mn concentration assessed by statistical image comparison [3]. This comparison will only yield relevant data if images are not biased by factors unrelated to Mn concentration. The purpose of normalization is to clear the MEMRI images of these contaminating factors. Since the advent of MEMRI, *ad hoc* normalization strategies have been used. As a rule, although they yield relevant results in their particular application domain, these normalization strategies are insufficiently described to be transposable to new experimental situations or insufficiently justified to viably evaluate their efficiency. This would be only a minor concern if unspecific signals were small, yet as highlighted by Aoki *et al.* [10] separating Mn enhancement due to specific stimulation from nonspecific effects remains a challenging issue. The aim of this paper is to propose an iterative algorithm for spatial and intensity normalization of MEMRI images in order to compare brain scans from subjects experiencing different injection paradigms (e.g. Mn *vs* control for tract-tracing) or stimulation paradigms (e.g. stimulation *vs* control for functional mapping).

Intensity normalization of MRI acquisitions is essential to suppress signal variations due to intersubject differences unrelated to Mn concentration changes. This can be done through T1 mapping [11], since T1 relaxation rate (i.e. 1/T1) of tissue water is linearly linked to Mn concentration. T1 mapping requires voxelwise non-linear fitting of a T1-dependent model with at best two degrees-of-freedom onto several MR acquisitions obtained at different T1 weightings (e.g. Look and Locker sequence). This approach suffers a deficit of the signal-to-noise ratio (SNR) compared to the strategy consisting in averaging multiple acquisitions

obtained at the same T1 weighting. Moreover, it is prone to possible inter-individual variations in basal brain T1 values obtained without Mn. Thus, the large majority of MEMRI studies are based on the acquisition of T1-weighted (T1W) images. However, T1W imaging has two major drawbacks: i) the non-linear relationship between signal and Mn concentration [12], and ii) experimental variability caused by the global multiplying factor, due to variable gain introduced by the acquisition system. This experimental variability implies an intensity normalization step based on the measurement of a reference signal (i.e. devoid of any Mn contribution). Methods for intensity normalization of T1W images rely on manually outlining a region of interest (ROI) where the reference signal is averaged. It has been proposed to use an external reference [13-15] or an internal reference taken from either brain tissue [16-21] or non-brain tissue [4, 22-25]. Even if the reference ROI is outlined by an expert, it remains subject to operator bias [26], in addition to being labor-intensive and time-consuming.

Besides intensity normalization, images derived from different animals also have to be spatially normalized using intersubject registration algorithms to place them in some common space and reduce anatomical variability [27]. This mandatory step for drawing statistical inferences about group data at voxel scale is also required for multi-subject BOLD studies [28] and voxel-based analysis [29]. Previous studies comparing intersubject registration algorithms for MRI images on phantoms [30] and humans [27, 31] suggest that performances are dependent on image contrast, deformation model, and the cost function minimized during the process. Spatial normalization of MEMRI images has been performed using either linear [19, 32-36] or non-linear transformations [4, 16, 37, 38]. The way this geometric transformation is performed is seldom fully justified, and normalization accuracy is seldom quantified. A prerequisite to spatial normalization is the segmentation of brain from non-brain tissues (e.g. skull, eyes). Suppressing these tissues-of-no-interest increases the accuracy and robustness of intersubject image registration [39, 40]. Challenges in the segmentation of T1W MEMRI data are mainly related to the low contrast and spatial resolution of acquired images, which both lead to artefactual incomplete separation between brain and neighboring tissues. In this context, automated or semi-automated approaches [41-45] have limited effectiveness. Alternatively, manual outlining is prohibitively time-consuming for 3D brain images, taking several hours per subject for a 643 image. Despite the fact that segmentation is an important step before spatial normalization, it is sometimes ignored in MEMRI studies.

No consensus procedure has yet emerged for spatial or intensity normalization of MEMRI images. Here, a normalization method is proposed which performs both spatial and intensity normalization in a single iterative process without the arbitrary choice of a reference image. In

addition, using *in vivo* rat MEMRI T1W images, we have developed a brain segmentation method, which is a prerequisite to spatial normalization; we have optimized our registration algorithm and assessed the incidence of the choice of anatomical region used for intensity normalization. The efficiency of this new normalization method was evaluated in a tract-tracing experiment on rat olfactory pathways.

2. Methods

2.1. Acquisition of 3D brain datasets

3D brain datasets are needed for (i) constructing an average brain model, (ii) optimizing intersubject registration, and (iii) testing our iterative normalization algorithm by tracing olfactory pathways in rats using MEMRI.

Experiments were carried out on male Brown Norway rats (9 weeks old). The study was performed in compliance with European legislative, administrative and statutory provisions for the protection of animals used for experimental or other scientific purposes (86/609/EEC). Twenty animals were used to construct the average brain model for the brain segmentation method, and 8 of these 20 animals were randomly selected and used for optimization of the intersubject registration. These 20 3D brain datasets were acquired using the same imaging protocol as that detailed for the tract-tracing experiment.

To trace olfactory pathways, 3 µl of a 100 mM aqueous solution of MnCl2.4H2O (Sigma-Aldrich, France) were injected into both nostrils of 8 rats. Rats were anaesthetized with 4% isoflurane, placed in the supine position and Mn was then injected in a single bolus through a polyethylene catheter (PE 10 tubing attached to a Hamilton syringe) inserted 1.5 cm into the nostril. The catheter length was chosen so as to reach the olfactory epithelium, as previously determined ex vivo on a separate set of rats. Immediately after Mn injection, rats were put back (always in supine position) into clean, empty cages where they awoke in approximately 2 min. They were left in these cages for the next 48 hours, with free access to water. Another set of 8 rats composed the Mn-free control group. MRI scans were acquired 48 h after Mn administration to allow for its progression inside deep brain regions.

Images were acquired on a Bruker (Bruker, GmbH, Ettlingen, Germany) 4.7 T / 40 cm horizontal magnet equipped with a 12-cm gradient coil and interfaced to an Avance III console driven by Paravision 4.0. A 9-cm-diameter linearly polarized birdcage resonator was used for emission and reception. Animals were placed in a rat-tailored bed equipped with a three point-fixation system (tooth-bar and ear-plug) and a temperature-controlled warming

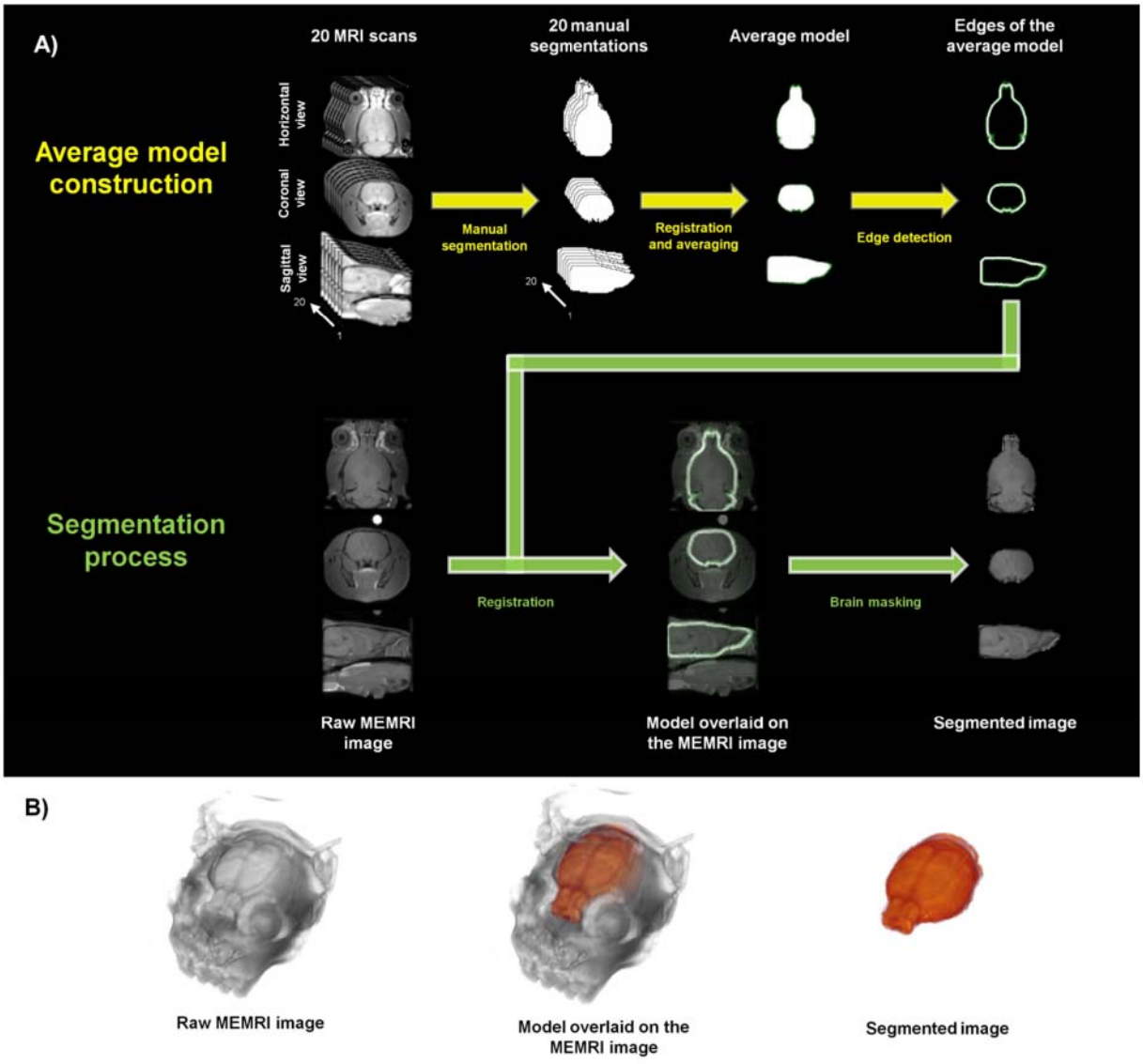

Figure 2.1: (A) Automatic segmentation strategy. An average model of the brain was constructed from 20 manual outlines. All segmented masks were co-registered and averaged to obtain a 3D rat brain model. This model was subsequently used to automatically segment brain from non-interest-tissues for each new MEMRI acquisition by registering its outer edges with the T1W images. (B) 3D views of fast automatic segmentation steps.

blanket. To avoid the use of odorized anesthetic gas, anesthesia was maintained during image acquisitions using urethane (1.3g/kg). Physiological conditions were monitored using breathing and temperature probes.

T1-weighted images covering the whole brain were acquired by 3D rapid acquisition with a relaxation enhancement sequence. Centric encoding was used to keep echo time short (5.5 ms). With a repetition time of 500 ms, a 64^3 matrix with an isotropic voxel size of 500 µm was obtained every 7 min 30 s. Acquisitions were continuously repeated for 2 h 30 min, corresponding to 20 volumetric images in each rat. The MRI volume series of each rat was corrected for motion during scanning sessions via rigid registration [46]. After MRI acquisition, animals were sacrificed by sodium pentobarbital injection (200 mg/kg).

2.2. Fast automatic brain segmentation

The objective of brain segmentation is to suppress tissues-of-no-interest in order to increase the accuracy and robustness of intersubject image registration. Automatic precise segmentation is difficult for MEMRI T1W images of the rat brain, while manual outlining is excessively time-consuming. Mn concentration variation at voxel scale in all brain structures can be satisfactorily quantified by a coarse segmentation, as (i) keeping a minority of non-brain tissues will have little influence on the spatial normalization result, and (ii) segmented volumes are not designed for size quantification and comparison. Because brain shape is very similar in different rats of the same strain and approximately the same age, model-based segmentation looks to be an effective approach for achieving this coarse segmentation.

To construct a 3D brain model, manual outlines were drawn by the same expert on MR T1W brain images (see acquisition parameters below) of 20 different rats (mean weight = 260g, sd = 26g) under MRIcron software [47], then transformed into 3D binary masks (Fig. 1A). Assuming that brains from different rats differ only by global scaling, each segmentation was co-registered under automated image registration (AIR) 5.2.6 [46, 48] to the segmentation corresponding to the median brain volume using a 7-parameter linear deformation model with global scaling. Then, all segmented masks were averaged to obtain a 3D rat brain model on which the outer edges of the brain were enhanced by computing the gradient norm (Fig. 1A).

Registering, using the 7-parameter linear deformation model which takes into account global brain size variations, this image of the outer edges of the average brain on each subsequent MEMRI T1W acquisition provided an automatic brain delineation (Fig. 1A and

B). This registration step quickly converged when these edges overlaped the hyposignal target region surrounding the brain in the T1W images (i.e. cerebrospinal fluid and skull). Each segmentation was inspected, and manual corrections such as rotations and translations of the 3D model were performed *a posteriori* by the operator if necessary.

The accuracy of this segmentation method was evaluated by comparing manual segmentations used to build the 3D brain model and their corresponding automatically segmented images with two complementary indexes: Jaccard similarity coefficient (JS) and relative volume error (RV). JS is a spatial coincidence measure in the range [0, 1], where 1 corresponds to an ideal match between each automatically segmented image (A) and its corresponding manually segmented image (M). The JS index is defined in Eq (1):

$$JS = \frac{|A \cap M|}{|A \cup M|} \quad (1)$$

The optimal JS value is 1. RV was also calculated to check that segmentation prevents brain cropping, as shown in Eq. (2):

$$RV = 2.\frac{|A| - |M|}{|A| + |M|} \quad (2)$$

RV quantifies the volume error between manual and automatic segmentations; the optimal RV value is 0, whereas a positive (resp. negative) value indicates coarse by excess (resp. default) segmentation.

2.3. Iterative algorithm for spatial and intensity normalization

For statistical analysis of between-group variations in Mn concentration, images have to be normalized for shape and intensity fluctuations. The spatial normalization step is generally performed onto an arbitrary target, which introduces bias [49] into the registration results. Woods *et al.* [48] proposed an atlasing algorithm for multi-subject registration that removes the sensitivity to an arbitrary target. It consists in creating an atlas image derived from several acquisitions obtained on different subjects. For this end, one image is randomly selected and all images are registered to this target. The images are averaged to create the first atlas image. This process is repeated iteratively, using current atlas image as the target for the spatial normalization, until idempotency. However, this atlasing algorithm cannot be applied directly to MEMRI acquisitions obtained from different rats because the images, averaged at each iteration, are biased by a multiplicative constant due to variable gain introduced by the acquisition system. To perform intensity normalization, a ROI has to be precisely placed on

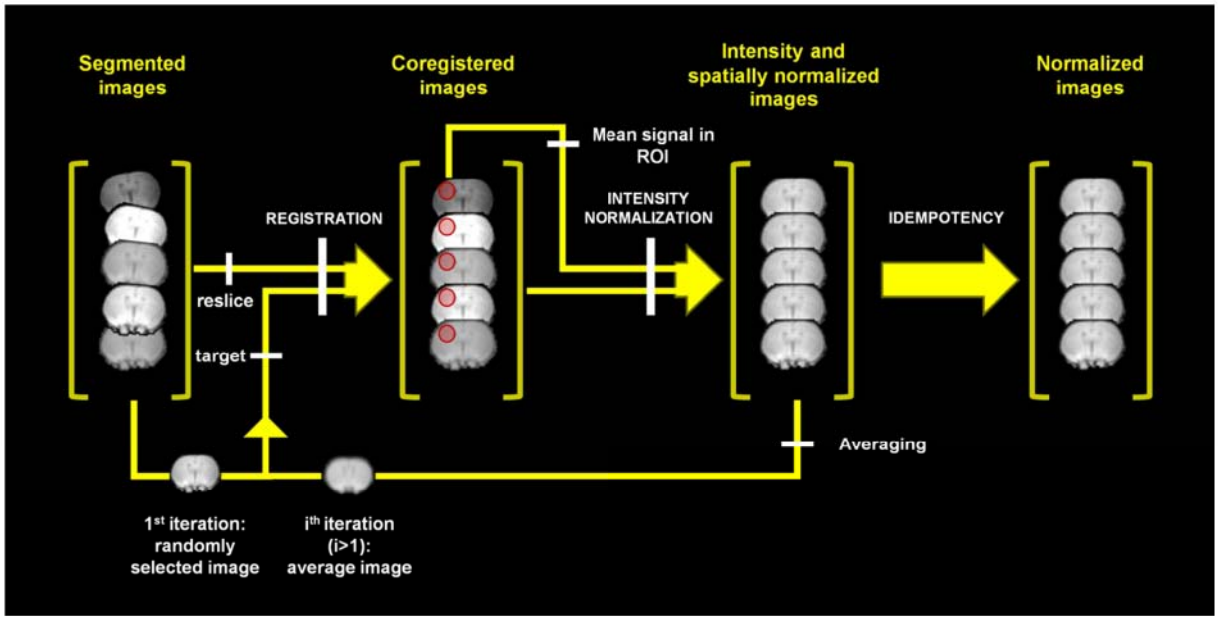

Figure 2.2: Flowchart of the iterative spatial and intensity normalization algorithm. All images were registered to a randomly selected image. The ROI was positioned, and image intensities of each subject were normalized by the mean intensity of the subject's own ROI. Images were averaged and used to create the first average image. This entire process was repeated iteratively, using the current average image as the target for spatial normalization, until reaching idempotency.

each MRI image, but this step is time-consuming and subject to operator bias. To optimize this, we nested the intensity normalization in the iterative atlasing algorithm for spatial normalization proposed by Woods *et al.* [48]. The ROI was initially delineated on the randomly selected target. Thanks to the registration process, it was then automatically placed, at each iteration, on all other ones and the signal over the ROI was averaged in each image. This reference value was used to normalize the intensity of each image.

Fig. 2 schematizes the algorithm flowchart. The iterative process benefits both spatial and intensity normalizations, as proposed by Ashburner *et al.* [50] for segmenting human brain MR images. ROI positioning accuracy thus increases with spatial normalization, the same anatomical regions being intercepted by this ROI in different images. Furthermore, ROI positioning consistency improves the intensity normalization of the different images, leading to a better-averaged target for spatially registering images at the next iteration. These steps converge into both spatial and intensity normalization in a joint iterative process without arbitrary choice of a target image. The algorithm is generic, as it operates with any cost function and deformation model, which are nevertheless optimized for our application in the following paragraph.

2.4. Optimization of intersubject registration algorithm configuration using anatomic landmarks

To optimize the spatial normalization step, we compared different configurations for pairwise registration under the AIR package [46, 48]. This package was chosen because it allows many degrees-of-freedom and can perform both linear and non-linear deformations [30, 31]. It is also widely used [19, 37, 51, 52] and available to the research community free of charge (http://bishopw.loni.ucla.edu/air5/). To quantitatively compare efficiency between registration configurations, we used anatomical landmarks to first estimate the error of intersubject registration and then to determine the best deformation model for registering T1W brain images of rats.

The algorithms available in the AIR 5.2.6 package differ from deformation models and cost functions, which are minimized during the registration process. Different relevant combinations were compared. For linear registration, two cost functions were compared: standard deviation of ratio image (SDRI) and least squares with intensity rescaling (LSIR). Five 3D linear deformation models were compared, i.e. 6, 7, 9, 12 and 15-parameter models corresponding to rigid deformation, rigid deformation and isotropic scaling, rigid deformation

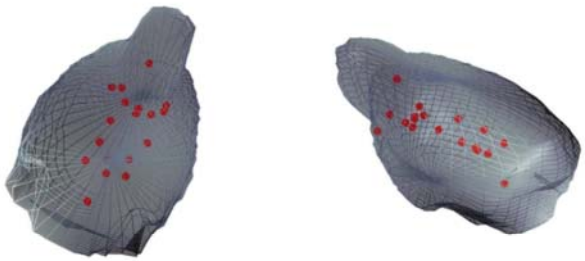

Figure 2.3: 3D views of the 18 anatomical landmarks distributed throughout the brain. Landmarks were located on eight animals to quantitatively compare the accuracy of linear and non-linear spatial normalization algorithms bundled with the AIR 5.2.6 package.

and anistropic scaling, affine deformation, and perspective deformation, respectively. In addition, non-rigid 3D deformation models were compared: 30, 60 105 and 168-parameter models corresponding to polynomial deformation models of increasing complexity. This resulted in a total of 14 different deformation model plus cost function configurations, which were compared after testing on the same data.

For this quantitative comparison, 18 landmarks on each of 8 segmented image volumes were manually identified by a neuroanatomist. These landmarks were distributed throughout the brain, as shown in Fig. 3. Following landmark selection, the 8 volumes were registered using each tested registration configuration. However, the registration step requires choosing one of the 8 volumes as a target volume. This arbitrary selection introduces bias [49]. To avoid this bias, each volume was registered on the 7 others. As registration between two images is asymmetric (i.e. being dependent of the target), this gives a total of 56 registrations for each tested configuration.

We chose two quality criteria to quantify the effectiveness of each intersubject registration configuration: (i) a mean registration error, which is an average of the Euclidean distances between the 18 homologous landmarks, and (ii) a sum of rank calculated as follows: for each landmark, configuration were ranked by mean registration error, and ranks of the 18 landmarks algorithm were summed. Mean registration error estimates the magnitude of the intersubject registration error for each algorithm, and the sum of rank enables landmark normalization of this error to determine the relative best deformation model.

2.5. Effect of ROI selection on tracing olfactory pathways using MEMRI

After optimization of the registration algorithm, choice of ROI position is the only degree-of-freedom of our normalization procedure. The objective is to find a region where the average signal between scans differs only by a constant ratio due to variable gain introduced by the acquisition system. For MEMRI studies, this ROI was located in different regions: outside the brain, such as in a muscle [24], in an external reference [13], in the background [53]; or inside various brain regions [16, 17, 19, 21]. We analyzed the effect of ROI selection for tracing olfactory pathways on the detectability of local between-groups variations in Mn concentration by decreasing potential bias due to normalization.

The sample (here the rat), the receiver coil and electronics all contribute to background noise intensity, making them possible sources of intersubject variation. In our current hardware configuration, dedicated to 3D MRI of the rat brain using high magnetic-field

Table 2.1: Results of landmark-based comparison of the spatial normalization algorithms bundled with the AIR 5.2.6 package. Six-, 7-, 9-, 12- and 15-parameter linear models corresponded to rigid deformation, rigid deformation and isotropic scaling, rigid deformation and anisotropic scaling, affine deformation and perspective models, respectively. Thirty, 60, 105 and 130 correspond to polynomial deformation models of increasing complexity.

Number of parameters for the linear registration model	Cost function for the linear registration model	Number of parameters for the non-linear registration model	Mean of registration error (mm)	Min of registration error (mm)	Max of registration error (mm)	Sum of ranks
ø	ø	ø	0.97	0.00	2.12	1076
9	LSIR	ø	0.56	0.02	1.39	66
15	LSIR	ø	0.56	0.04	1.25	86
12	SDRI	ø	0.57	0.04	1.50	102
9	SDRI	ø	0.57	0.00	1.34	103
15	SDRI	ø	0.58	0.05	1.66	108
12	LSIR	ø	0.58	0.04	1.36	108
6	LSIR	ø	0.58	0.06	1.35	120
7	LSIR	ø	0.59	0.03	1.33	133
7	SDRI	ø	0.59	0.04	1.45	128
ø	ø	30	0.61	0.08	1.39	164
6	SDRI	ø	0.62	0.04	1.46	192
ø	ø	60	0.63	0.08	1.59	185
ø	ø	105	0.63	0.08	1.59	190
ø	ø	168	0.63	0.08	1.59	208

strength and a volume coil, the rat is the dominant source of noise. Since the signal measured in the background is not linked exclusively to the constant ratio due to variable gain introduced by the acquisition system, this ROI is ruled out from the intensity normalization. The use of an external reference requires substances that are chemically stable over time and a perfect repositioning of the reference within the coil. Moreover, the T1W NMR signal produced by the reference should be close to that of the brain in order to avoid large attenuation of brain intensity or low signal-to-noise ratio of the reference signal. For these reasons, we also ruled out normalization by an external standard.

To compare the effect ROI of location choice on intensity normalization and its impact on the detection of Mn concentration variations, 5 normalization regions were tested: the pituitary region, as suggested by Chuang and Koretsky [18], two regions outside the brain (the temporal muscle and the tongue) and two brain regions (sensorimotor and motor/cingulate cortices) expected to remain Mn-free following administration of a small Mn amount into the nostrils.

The normalization algorithm described above allows selection of ROI outside the brain, as each spatial transformation performed on a segmented image is also applied to the corresponding non-segmented image.

2.6. Spatial smoothing and statistical analysis

Once normalized, 3D Gaussian spatial smoothing was applied on each MEMRI image to increase the signal-to-noise ratio. The full-width at half-maximum of the smoothing filter was set at 0.5 mm according to the mean error of registration for the best deformation model.

Voxel-wise two-tailed Student's t-tests ($p<0.01$) were performed to detect differences in brain Mn distribution between groups of Mn-injected animals and a Mn-free control group. 3D statistical t-maps were reconstructed by assigning the resulting t-value from each voxel-wise t-test to the corresponding voxel of the 3D image.

3. Results

3.1. Fast automatic brain segmentation

The result of a single representative subject is illustrated in Fig. 1 for visual evaluation. Segmentations were quantitatively evaluated by comparing the 20 manual segmentations used to build the 3D brain model and their corresponding automatic segmentation using JS and RV

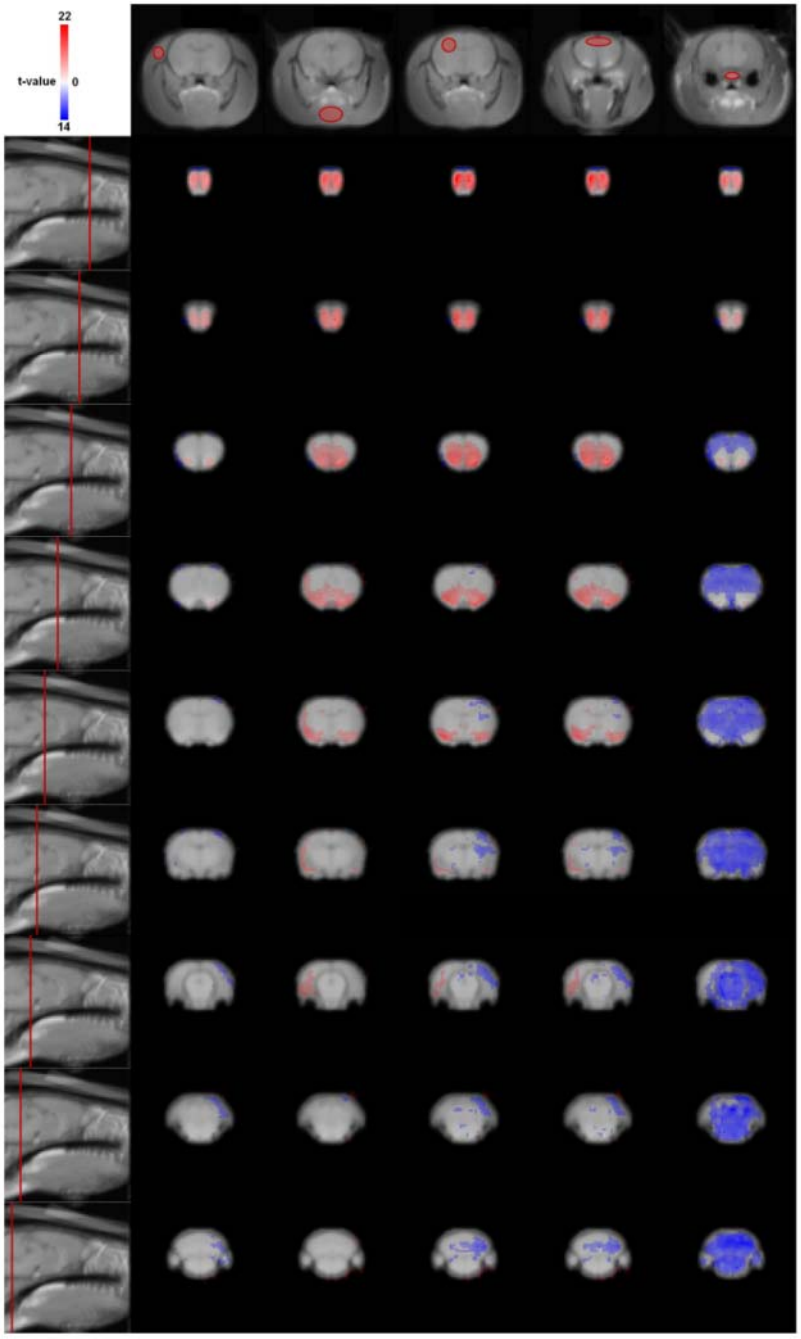

Figure 2.4: Effect of the choice of the ROI used for intensity normalization upon activation maps. Statistical t-maps overlaid on T1W MEMRI images showing Mn enhancement and normalization-related artifacts. Each image in the first column shows the position of the coronal slice represented in the corresponding row in a sagittal view. The first row of each column represents the ROI used for the intensity normalization, i.e. temporal muscle, tongue, motor and cingulate cortices, sensorimotor cortex, and pituitary, respectively. t-values in red represent voxels whose mean intensity of MnG, is higher than mean intensity of CtG ($p<0.01$). Red patterns correspond to significant Mn signal increase due to Mn enhancement. t-values in blue represent the opposite case and correspond to false-positive voxels caused by incorrect normalization.

indexes. The JS calculated between manual and automatic segmentations was 0.85 ± 0.02 (mean ± SD), indicating a good spatial overlap. RV was 0.06 ± 0.02, indicating a small difference between manually and automatic segmented volumes. The volume of segmentations achieved with our method was on average 6% higher than when performed manually, indicating that this method produced coarse brain segmentations, as expected.

3.2. Optimization of intersubject registration algorithm configuration using anatomic landmarks

Results of the quantitative comparison of dispersion before and after registration of 18 homologous landmarks in 8 animals are reported in Table 1. Before registration, the initial mean distance between homologous landmarks was 0.96 ± 0.40 mm, which corresponds to ~2 ± 1 voxel size. This relatively small initial mean distance was the result of careful positioning i) of animals in the MR imager and ii) of the acquisition matrix with respect to scout images of the rat head. Table 1 shows that all registration algorithms decreased this initial mean distance. It also shows that the best deformation model was a linear 9-parameter model (i.e. translations, rotations, and independent scaling in the three directions) combined with LSIR cost function. This algorithm roughly halved the distances between homologous landmarks and decreased the mean error of registration to 0.55 ± 0.20 mm. Moreover, halving registration error for each landmark (data not shown) indicated that this improvement was well distributed over the different landmarks. Finally, the rank sum criterion confirmed that combining a 9-parameter deformation model and the LSIR cost function was the best algorithm for intersubject registration of MEMRI images.

Registration of 3D non-segmented brain images with this algorithm decreased mean error of registration to 0.80 ± 0.40 mm. Segmentation prior to registration also enabled a four-fold decrease in registration duration. These findings confirmed the importance of performing brain segmentation before spatial normalization.

3.3. Effect of ROI selection on tracing olfactory pathways using MEMRI

As shown in Fig. 4, statistical maps resulting from group wise comparison between the Mn group (MnG) and the control group (CtG) differed depending on the ROI chosen for intensity normalization. When this ROI was taken outside the brain (i.e. temporal muscle or tongue, columns 1 and 2, respectively), only a few image voxels of Mn-injected animals displayed a lower intensity than the corresponding voxels in control animals (see rows 6-9 in columns 1

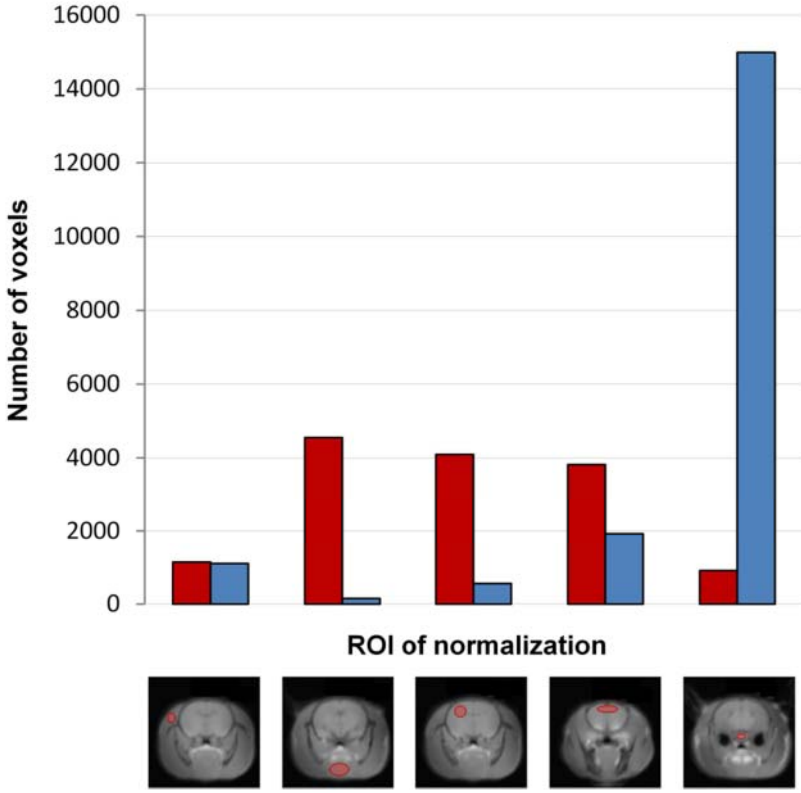

Figure 2.5: Effect of the choice of the ROI used for intensity normalization on the number of statistically significant voxels (t-test, $p<0.01$). Normalization regions were temporal muscle, tongue, motor and cingulate cortices, sensorimotor cortex, and pituitary. Bars in red represent number of Mn-enhanced voxels. Bars in blue represent the number of false-positive voxels.

& 2). When the ROI was taken inside the brain (i.e. sensorimotor cortex, column 3, and motor and cingulate cortices, column 4), many more voxels of Mn-injected animals had a lower intensity than the corresponding voxels in control animals (see rows 5-9 in columns 3 & 4). This paradoxical observation most likely resulted from an intensity normalization ROI that was not devoid of Mn in the Mn-injected animals. These voxels could be considered as false-positive voxels, since the increase in Mn concentration only leads to T1W enhancement (influences of proton-density and T2 weightings were considered negligible). This is supported by the results shown in column 5, in which the ROI was placed in the pituitary, which is known to accumulate Mn after nasal administration [18]. Most of the control voxels in column 5 showed a higher intensity than the corresponding voxels in Mn-injected animals. Thus, the best ROI for intensity normalization is the one that yields the smallest number of control voxels with a higher intensity than the corresponding voxels in Mn-injected animals (and consequently, the largest distribution of Mn in Mn-injected animals). In the present setting, as illustrated in Fig. 5, the best ROI appeared to be the ROI placed over the tongue (column 2), which revealed presence of Mn up to the posterior entorhinal cortex (see Fig. 4).

4. Discussion

The purpose of the present study was to design an algorithm for normalizing (both spatially and in intensity) MEMRI images, so as to compare intensities of different data sets at the highest possible spatial resolution.

Manganese was used as a contrast agent that provides a reproducible contrast enhancement in olfactory pathways. It was administered intranasally under conditions emphasized by Dhuria and coworkers [54]. Manganese being a potent neurotoxic, we have, in a parallel study [55], determined the Mn dose ensuring the best possible compromise between deleterious effects and contrast enhancement. This dose (0.3 µmol) was used in the present study to validate our algorithm. A possible bias lies in image variability resulting from changes of coil responses. These changes are essentially due to the variation of animal positioning with respect to coil(s). We have taken this general issue of MEMRI studies into account by putting the anaesthetized rat in a stereotaxic head-holder and always positioning the coil in the same manner with respect to this device.

4.1. Fast automatic brain segmentation

The brain segmentation method proposed in this study is based on the deformation of the

outer edges of an average 3D brain model on each T1W MEMRI image. Our method allowed 3D extraction of the brain in approximately 2-3 minutes, where manual segmentation requires a few hours per subject. The time spent in segmentation covered two steps: (i) efficient registration of the average brain model on each MEMRI image, which was achieved automatically within a few seconds, and (ii) if required, correction of small segmentation errors by the operator, which took up to 2 minutes, and where simple geometric transformations could be applied manually. Thus, entire cohorts of animals could be segmented in 3D within just a few hours. Although our method was less accurate than manual segmentation, it was designed conservatively so as to preserve all brain tissues. Our results are also consistent with previous studies [39, 40] reporting an increased accuracy and computational speed in the spatial normalization of segmented *vs.* non-segmented brain. One way to further optimize this method could be to modulate the thickness of the edges of the 3D brain model to match it to the target area, which is the hyposignal region between brain and scalp.

4.2. Iterative spatial and intensity algorithm for Mn detection in the olfactory pathway

The iterative process proposed for normalizing MEMRI images benefited both spatial and intensity normalizations. Spatial normalization is independent of an a priori-chosen target, unlike pairwise registration approaches [34, 35], while the accuracy of ROI positioning is increased by nesting this step in the algorithm. Optimizing the normalization of MEMRI images made it possible to improve the detectability of local between-group variations in Mn concentration by decreasing bias due to normalization.

Our results differ from those obtained by Cross *et al.* [3] who performed longitudinal tract-tracing of the olfactory pathway using MEMRI. In our study, Mn distribution was highlighted in deep brain areas such as the posterior entorhinal cortex. Several reasons may explain the differences. Firstly, Cross *et al.* [3] did not normalize MEMRI image intensity by the signal measured in a ROI. They calculated the normalization factor by averaging voxel intensities across the whole brain, intensities being thresholded in order to render this average insensitive to differences in Mn distributions. Although they used this preventive threshold to render the normalization insensitive to maxima caused by Mn, there must be regions below this threshold that contain Mn, thus biasing the calculation of the normalization factor. As our study showed, biased intensity normalization reduced the detectability of Mn patterns. Secondly, the experimental protocol and statistical treatments were not strictly identical.

Cross *et al.* [3] use pre-administration scans to calculate z-maps at different experimental time points to follow spatio-temporal Mn changes. However, they used isoflurane, an odorous anesthetic, which has an influence on Mn uptake in the olfactory pathway [19]. To resolve this issue, we chose to anaesthetize rats by intra-peritoneal injection of urethane and to run a single MRI acquisition 48 h after Mn injection. Although urethane is toxic [56], meaning the animal has to be sacrificed after anesthesia, it is odor-free and does not affect Mn uptake in the olfactory pathway as much as isoflurane. Finally, the 10µl-1M dose of Mn injected by Cross *et al.* [3] may limit Mn progression in deep brain regions. Recent toxicity research has shown that injecting high doses of Mn can lead to neuronal death and prevent trans-synaptic crossing in distal regions [57].

4.3. Optimization of intersubject registration algorithm configuration using anatomic landmarks

To the best of our knowledge, there are no published studies analyzing variation in brain size and morphology in inbred strains or rats, which could help select an appropriate method for spatial normalization. As a consequence, the degrees-of-freedom of the deformation model is generally chosen arbitrarily [34, 35]. By contrast, we proposed to determine the most efficient method for registering 3D MEMRI T1W datasets derived from different animals. This was achieved by performing a comprehensive comparison, based on landmark registration errors, of candidate deformation models. It appeared that the best deformation model included rotations and translations combined with independent resizing in the 3 directions. This partially contradicts the suggestion by Yu *et al.* [21] that brain size variations among animals of the same age are small enough to be neglected, and that rigid geometric transformations may be sufficient for image registration. This also differs from the strategy developed by Schwarz *et al.* [34] who registered MRI images using only rigid geometric transformations to compute an average template representative of the rat brain. Although in our hands, a 6-parameter model (i.e. without rescaling) gave good results, there was still room for improvement by introducing independent rescaling in the 3 directions. Our results suggest that normalizing by brain size fluctuations may be beneficial for MEMRI image registration. In addition, our results showed that the best cost function for optimizing intersubject registration of MEMRI T1W images was an LSIR. This is coherent with the fact that this cost function was designed for images acquired with the same image modality [46]. In our hands, the mean error of registration of this best deformation algorithm was around the size of a

voxel, which limited detection of Mn enhancement in areas higher than the voxel size. However, the landmarks on different subjects were positioned exclusively by an expert by visual inspection of the T1W image, and a significant proportion of the error calculated for each registration algorithm can be explained by the error inherent to landmark positioning. Consequently, this error of intersubject registration was almost certainly overestimated.

Our results showed that registration accuracy, estimated by landmark distances, initially increased with the complexity of the deformation model, reached a maximum with 9 parameters, and then decreased. However, the cost function diminished as expected with the degrees of freedom (data not shown). The increase of the registration error at some point was likely due to the fact that minimizing the cost function favored a good registration of high-contrast boundaries, at the expense of other regions with lower contrasts, where some of our landmarks were located. Hence, evaluating registration accuracy at landmarks located in both high and low contrast regions prevents erratic behavior away from high contrast boundaries and can be interpreted as indirectly introducing regularization in the deformation model.

This registration error could be further decreased by using complementary strategies. More highly-contrasted anatomical images (e.g. T2-weighted images leading to substantial contrast between brain matters) can be concomitantly acquired in the same subject-frame as T1W images, then realigned with better confidence. Another way to reduce the error of registration would be to boost signal-to-noise ratio and then increase the spatial resolution of the T1W images, e.g. using higher field strength, parallel acquisition, and other optimized T1W sequences (FLASH, MDEFT, MP-RAGE).

4.4. Effect of ROI selection on tracing olfactory pathways using MEMRI

In MEMRI studies, normalization relies on the outline, in all individuals, of the same supposedly Mn-devoid anatomical region in which the signal can consequently only vary by a constant ratio due to the variable gain of the reception chain. Thus, normalization errors result from either a badly delineated ROI or a bad choice of ROI where the signal was modulated by a factor independent of the experimental constant. Simultaneously processing spatial and intensity intersubject normalizations minimized the effect of ROI localization error. Nevertheless, normalization errors can still occur if the ROI intersects regions where the signal does not differ solely by the experimental constant, i.e. where Mn concentration in the ROI is different between groups. The main consequence of this situation is the lower detection of Mn, hence the erroneous detection of regions in which the signal is lower than

would be expected based on Mn concentration. In other words, minimizing the number of these false-positive voxels is a criterion for the choice of the ROI used for intensity normalization. Therefore, in our opinion, any MEMRI study designed to compare two groups of Mn-injected animals should also include a Mn-free group to control for normalization quality.

Our results on ROI choice also revealed that no ROI located within the brain yielded good intensity normalization. Due to the slow Mn transport rate in the brain (~1-6 mm/h: [24, 53, 58]), long diffusion times are required for Mn to be transported to distal regions [18], which increases the possibility of non-specific Mn labeling in regions outside the targeted neuronal pathways. Therefore, choosing ROI solely on the hypothesis that it is supposedly functionally independent of the targeted region is not an adequate strategy. This is illustrated in the present study. Taking the sensorimotor cortex and motor/cingulate cortices as ROI for intensity normalization seemed a relevant choice, as these brain regions are not known to have direct connections with the primary olfactory cortex. However, many false-positive voxels appeared. Injecting Mn in the vicinity of the target region (e.g. through i.c.v. administration) or in the bloodstream coupled to temporary disruption of the blood-brain barrier might help minimize this non-specific enhancement of Mn in the brain.

As suggested by Chuang and Koretsky [18], we used the pituitary as the intensity normalization ROI. In our hands, this triggered the detection of false-positive voxels in the major part of the brain. Indeed, normalization using the pituitary is based on the assumption that the signal in this region is constant whatever the experimental paradigm, whereas it is known that the pituitary can show variable activity [59], notably because it is under the control of a number of hormones.

Using tissues outside the brain might be an adequate method to avoid non-specific enhancement of Mn. In the present study, we found that the temporal muscle and the tongue were good candidates as ROI normalization structures. The temporal muscle has not been reported as having a direct connection with the nasal olfactory epithelium. The number of false-positive voxels did turn out low, but the number of voxels where Mn was detected was also low, probably due to the small size of this ROI and its inhomogeneity. The tongue is in direct relationship with the olfactory epithelium through retronasal communication. However, the tongue gave the best results with respect to intensity normalization (i.e. the lowest number of false-positive voxels and the highest number of voxels where Mn was detected), possibly due to its homogeneous structure and its size.

5. Conclusion

This study presents an original algorithm for performing both spatial and intensity normalization in a single iterative process, and an automatic segmentation method, which was demonstrated to be an efficient preprocessing step. By optimizing the normalization phases required for voxel wise statistical analysis of MEMRI T1W images (i.e. segmentation, spatial normalization, intensity normalization), this algorithm improved the detectability of local variations in Mn concentration in a MEMRI-based tract-tracing experiment of rat olfactory pathways by decreasing potential bias due to normalization. After optimization of spatial registration and localization of the ROI used for intensity normalization, it revealed the presence of Mn up to the posterior entorhinal cortex. The algorithm presented here is generic, as it operates with any cost function and deformation model more adapted for other MEMRI studies and is adaptable to other animal models.

Acknowledgements

This work has been partly funded by the French Research Agency (ANR). The MRI experiments were performed at the MR of biological systems platform at the INRA research center in Clermont-Ferrand, France (www.clermont.inra.fr/rmsb/).

References

1. Lin YJ, Koretsky AP. Manganese ion enhances T-1-weighted MRI during brain activation: An approach to direct imaging of brain function. Magn Reson Med 1997;38(3):378-388.

2. Pautler RG, Silva AC, Koretsky AP. In vivo neuronal tract tracing using manganese-enhanced magnetic resonance imaging. Magn Reson Med 1998;40(5):740-748.

3. Cross DJ, Minoshima S, Anzai Y, Flexman JA, Keogh BP, Kim Y, Maravilla KR. Statistical mapping of functional olfactory connections of the rat brain in vivo. NeuroImage 2004;23(4):1326-1335.

4. Weng JC, Chen JH, Yang PF, Tseng WYI. Functional mapping of rat barrel activation following whisker stimulation using activity-induced manganese-dependent contrast. NeuroImage 2007;36(4):1179-1188.

5. Sloot WN, Gramsbergen JBP. Axonal-Transport of Manganese and Its Relevance to Selective Neurotoxicity in the Rat Basal Ganglia. Brain Res 1994;657(1-2):124-132.

6. Tjalve H, Mejare C, Borgneczak K. Uptake and Transport of Manganese in Primary and Secondary Olfactory Neurons in Pike. Pharmacol Toxicol 1995;77(1):23-31.

7. Newland MC, Cox C, Hamada R, Oberdorster G, Weiss B. The clearance of manganese chloride in the primate. Fundam Appl Toxicol 1987;9(2):314-328.

8. Silva AC, Lee JH, Aoki I, Koretsky AP. Manganese-enhanced magnetic resonance imaging (MEMRI): methodological and practical considerations. NMR Biomed 2004;17(8):532-543.

9. Van der Linden A, Van Camp N, Ramos-Cabrer P, Hoehn M. Current status of functional MRI on small animals: application to physiology, pathophysiology, and cognition. NMR Biomed 2007;20(5):522-545.

10. Aoki I, Tanaka C, Takegami T, Ebisu T, Umeda M, Fukunaga M, Fukuda K, Silva AC, Koretsky AP, Naruse S. Dynamic activity-induced manganese-dependent contrast magnetic resonance imaging (DAIM MRI). Magn Reson Med 2002;48(6):927-933.

11. Chuang KH, Koretsky A. Improved neuronal tract tracing using manganese enhanced magnetic resonance imaging with fast T(1) mapping. Magn Reson Med 2006;55(3):604-611.

12. Ahrens ET, Rothbacher U, Jacobs RE, Fraser SE. A model for MRI contrast enhancement using T1 agents. Proc Natl Acad Sci U S A 1998;95(15):8443-8448.

13. Bearer EL, Falzone TL, Zhang X, Biris O, Rasin A, Jacobs RE. Role of neuronal activity and kinesin on tract tracing by manganese-enhanced MRI (MEMRI). NeuroImage 2007;37(Supplement 1):S37-S46.

14. Canals S, Beyerlein M, Keller AL, Murayama Y, Logothetis NK. Magnetic resonance imaging of cortical connectivity in vivo. NeuroImage 2008;40(2):458-472.

15. Kuo YT, Herlihy AH, So PW, Bell JD. Manganese-enhanced magnetic resonance imaging (MEMRI) without compromise of the blood-brain barrier detects hypothalamic neuronal activity in vivo. NMR Biomed 2006;19(8):1028-1034.

16. Bissig D, Berkowitz BA. Manganese-enhanced MRI of layer-specific activity in the visual cortex from awake and free-moving rats. NeuroImage 2009;44(3):627-635.

17. Chen W, Tenney J, Kulkarni P, King JA. Imaging unconditioned fear response with manganese-enhanced MRI (MEMRI). NeuroImage 2007;37(1):221-229.

18. Chuang KH, Koretsky AP. Accounting for nonspecific enhancement in neuronal tract tracing using manganese enhanced magnetic resonance imaging. Magn Reson Imaging 2009.

19. Chuang KH, Lee JH, Silva AC, Belluscio L, Koretsky AP. Manganese enhanced MRI reveals functional circuitry in response to odorant stimuli. NeuroImage 2009;44(2):363-372.

20. Kivity S, Tsarfaty G, gmon-Levin N, Blank M, Manor D, Konen E, Chapman J, Reichlin M, Wasson C, Shoenfeld Y, Kushnir T. Abnormal olfactory function demonstrated by manganese-enhanced MRI in mice with experimental neuropsychiatric lupus. Ann N Y Acad Sci 2010;1193:70-77.

21. Yu X, Wadghiri YZ, Sanes DH, Turnbull DH. In vivo auditory brain mapping in mice with Mn-enhanced MRI. Nat Neurosci 2005;8(7):961-968.

22. Bock NA, Paiva FF, Nascimento GC, Newman JD, Silva AC. Cerebrospinal fluid to brain transport of manganese in a non-human primate revealed by MRI. Brain Res 2008;1198:160-170.

23. Holt AG, Bissig D, Mirza N, Rajah G, Berkowitz B. Evidence of key tinnitus-related brain regions documented by a unique combination of manganese-enhanced MRI and acoustic startle reflex testing. PLoS One 2010;5(12):e14260.

24. Saleem KS, Pauls JM, Augath M, Trinath T, Prause BA, Hashikawa T, Logothetis NK. Magnetic Resonance Imaging of Neuronal Connections in the Macaque Monkey. Neuron 2002;34(5):685-700.

25. Smith KD, Kallhoff V, Zheng H, Pautler RG. In vivo axonal transport rates decrease in a mouse model of Alzheimer's disease. NeuroImage 2007;35(4):1401-1408.

26. Lebenberg J, Herard AS, Dubois A, Dauguet J, Frouin V, Dhenain M, Hantraye P, Delzescaux T. Validation of MRI-based 3D digital atlas registration with histological and autoradiographic volumes: an anatomofunctional transgenic mouse brain imaging study. NeuroImage 2010;51(3):1037-1046.

27. Ardekani BA, Guckemus S, Bachman A, Hoptman MJ, Wojtaszek M, Nierenberg J. Quantitative comparison of algorithms for inter-subject registration of 3D volumetric brain MRI scans. J Neurosci Methods 2005;142(1):67-76.

28. Woolrich MW, Behrens TEJ, Beckmann CF, Jenkinson M, Smith SM. Multilevel linear modelling for FMRI group analysis using Bayesian inference. NeuroImage 2004;21(4):1732-1747.

29. Snook L, Plewes C, Beaulieu C. Voxel based versus region of interest analysis in diffusion tensor imaging of neurodevelopment. NeuroImage 2007;34(1):243-252.

30. Morgan VL, Pickens DR, Hartmann SL, Price RR. Comparison of functional MRI image realignment tools using a computer-generated phantom. Magn Reson Med 2001;46(3):510-514.

31. Klein A, Andersson J, Ardekani BA, Ashburner J, Avants B, Chiang MC, Christensen GE, Collins DL, Gee J, Hellier P, Song JH, Jenkinson M, Lepage C, Rueckert D, Thompson P, Vercauteren T, Woods RP, Mann JJ, Parsey RV. Evaluation of 14 nonlinear deformation algorithms applied to human brain MRI registration. NeuroImage 2009;46(3):786-802.

32. Howles GP, Qi Y, Johnson GA. Ultrasonic disruption of the blood-brain barrier enables in vivo functional mapping of the mouse barrel field cortex with manganese-enhanced MRI. NeuroImage 2010;50(4):1464-1471.

33. Lu H, Xi ZX, Gitajn L, Rea W, Yang Y, Stein EA. Cocaine-induced brain activation detected by dynamic manganese-enhanced magnetic resonance imaging (MEMRI). Proc Natl Acad Sci U S A 2007;104(7):2489-2494.

34. Schwarz AJ, Danckaert A, Reese T, Gozzi A, Paxinos G, Watson C, Merlo-Pich EV, Bifone A. A stereotaxic MRI template set for the rat brain with tissue class distribution maps and co-registered anatomical atlas: application to pharmacological MRI. Neuroimage 2006;32(2):538-550.

35. Schweinhardt P, Fransson P, Olson L, Spenger C, Andersson JL. A template for spatial normalisation of MR images of the rat brain. J Neurosci Methods 2003;129(2):105-113.

36. Soria G, Wiedermann D, Justicia C, Ramos-Cabrer P, Hoehn M. Reproducible imaging of rat corticothalamic pathway by longitudinal manganese-enhanced MRI (L-MEMRI). NeuroImage 2008;41(3):668-674.

37. Bearer EL, Zhang X, Janvelyan D, Boulat B, Jacobs RE. Reward circuitry is perturbed in the absence of the serotonin transporter. NeuroImage 2009;46(4):1091-1104.

38. Fa Z, Zhang P, Huang F, Li P, Zhang R, Xu R, Wen Z, Jiang X. Activity-induced manganese-dependent functional MRI of the rat visual cortex following intranasal manganese chloride administration. Neurosci Lett 2010;481(2):110-114.

39. Blaffert T, Wiemker R. Comparison of different follow-up lung registration methods with and without segmentation. SPIE Medical Imaging 2004;5370:1701-1708.

40. Hajnal JV, Saeed N, Soar EJ, Oatridge A, Young IR, Bydder GM. A registration and interpolation procedure for subvoxel matching of serially acquired MR images. J Comput Assist Tomogr 1995;19(2):289-296.

41. Brouwer RM, Hulshoff Pol HE, Schnack HG. Segmentation of MRI brain scans using non-uniform partial volume densities. NeuroImage 2010;49(1):467-477.

42. Clarke LP, Velthuizen RP, Camacho MA, Heine JJ, Vaidyanathan M, Hall LO, Thatcher RW, Silbiger ML. MRI segmentation: methods and applications. Magn Reson Imaging 1995;13(3):343-368.

43. Levinski K, Sourin A, Zagorodnov V. Interactive surface-guided segmentation of brain MRI data. Comput Biol Med 2009;39(12):1153-1160.

44. Pal NR, Pal SK. A Review on Image Segmentation Techniques. Pattern Recognition 1993;26(9):1277-1294.

45. Weisenfeld NI, Warfield SK. Automatic segmentation of newborn brain MRI. NeuroImage 2009;47(2):564-572.

46. Woods RP, Grafton ST, Holmes CJ, Cherry SR, Mazziotta JC. Automated image registration: I. General methods and intrasubject, intramodality validation. J Comput Assist Tomogr 1998;22(1):139-152.

47. MRIcron, avalaible from http://www.cabiatl.com/mricro/mricron/index.html/. 2009.

48. Woods RP, Grafton ST, Watson JDG, Sicotte NL, Mazziotta JC. Automated image registration: II. Intersubject validation of linear and nonlinear models. J Comput Assist Tomogr 1998;22(1):153-165.

49. Geng X, Christensen GE, Gu H, Ross TJ, Yang Y. Implicit reference-based group-wise image registration and its application to structural and functional MRI. NeuroImage 2009;47(4):1341-1351.

50. Ashburner J, Friston KJ. Unified segmentation. NeuroImage 2005;26(3):839-851.

51. Chan KC, Fu QL, Hui ES, So KF, Wu EX. Evaluation of the retina and optic nerve in a rat model of chronic glaucoma using in vivo manganese-enhanced magnetic resonance imaging. NeuroImage 2008;40(3):1166-1174.

52. Tucciarone J, Chuang KH, Dodd SJ, Silva A, Pelled G, Koretsky AP. Layer specific tracing of corticocortical and thalamocortical connectivity in the rodent using manganese enhanced MRI. NeuroImage 2009;44(3):923-931.

53. Watanabe T, Michaelis T, Frahm J. Mapping of retinal projections in the living rat using high-resolution 3D gradient-echo MRI with Mn2+-induced contrast. Magn Reson Med 2001;46(3):424-429.

54. Dhuria SV, Hanson LR, Frey WH. Intranasal delivery to the central nervous system: mechanisms and experimental considerations. J Pharm Sci 2010;99(4):1654-1673.

55. Lehallier B, Coureaud G, Maurin Y, Bonny JM. Effects of Manganese dose injected into rat nostrils: implications for in vivo functional study of olfaction using MEMRI. Magn Reson Imaging 2011; In press.

56. Kohn DF, Wixson SK, White WJ, Benson GJ. Anesthesia and analgesia in laboratory animals. New York: Academic Press 1997. -426 p.

57. Thuen M, Berry M, Pedersen TB, Goa PE, Summerfield M, Haraldseth O, Sandvig A, Brekken C. Manganese-enhanced MRI of the rat visual pathway: acute neural toxicity, contrast enhancement, axon resolution, axonal transport, and clearance of Mn(2+). J Magn Reson Imaging 2008;28(4):855-865.

58. Leergaard TB, Bjaalie JG, Devor A, Wald LL, Dale AM. In vivo tracing of major rat brain pathways using manganese-enhanced magnetic resonance imaging and three-dimensional digital atlasing. NeuroImage 2003;20(3):1591-1600.

59. Cui ZJ, Dannies PS. Thyrotropin-releasing hormone-mediated Mn2+ entry in perifused rat anterior pituitary cells. Biochem J 1992;283 (Pt 2):507-513.

Présentation de l'article #3

En préservant la perception olfactive et en normalisant avec précaution les images MEMRI, nous avons montré qu'il est possible de détecter l'accumulation de Mn, 48 h après son injection, depuis le bulbe olfactif jusqu'au cortex entorhinal postérieur. A ce jour, les études ayant injecté le Mn par la voie intranasale pour étudier les zones cérébrales impliquées dans le traitement des odeurs ont pu mettre en évidence des différences fonctionnelles uniquement dans le bulbe olfactif (Chuang *et al.*, 2009b; De Groof *et al.*, 2010). Le but de ce troisième papier est de révéler, grâce au MEMRI, un traitement différentiel d'odeurs dans des zones cérébrales plus profondes que le bulbe olfactif.

Pour atteindre cet objectif, en plus des développements méthodologiques exposés précédemment, nous avons choisi de stimuler des rats pendant une longue période (48h par intermittence) avec des odeurs biologiquement signifiantes. Les mammifères ayant des capacités analytiques limités et le traitement d'une odeur complexe ne correspondant pas à la somme du traitement individuel de chacune des molécules qui la compose (Wilson et Stevenson, 2003), nous avons donc privilégié des odeurs véhiculant des messages particulièrement signifiants à l'animal plutôt que d'étudier séparément des composés mono-moléculaires. Ces odeurs touchent des fonctions essentielles à savoir la prise alimentaire, au moyen d'une odeur chocolatée apprise, et la survie, en utilisant une odeur innée de prédateur.

Les résultats obtenus par MEMRI ont été confrontés avec ceux de Fos, technique fonctionnelle de référence, pouvant être considérée comme l'analogue *ex vivo* de MEMRI (Van der Linden *et al.*, 2007)

Nos résultats montrent que le traitement cérébral d'odeurs est différencié dans le cortex olfactif primaire. Il varie en termes de tailles de populations de neurones recrutés et en termes d'intensité de l'activation de ces neurones. De plus, ce travail souligne qu'un message olfactif crucial, lié à la survie, est traité asymétriquement dans le cerveau.

Ce travail a été soumis pour publication en 2011 à la revue *Cerebral Cortex*.

4. Traitement central d'odeurs biologiquement signifiantes, révélé par MEMRI chez le rat vigile.

Central processing of behaviorally relevant odors in the awake rat, as revealed by Manganese-enhanced MRI

Benoist Lehallier [1], Olivier Rampin [2], Audrey Saint-Albin [2], Nathalie Jérôme [2], Christian Ouali [2], Yves Maurin [2], Jean-Marie Bonny [1*]

(1) UR370 QuaPA, INRA, F-63122 Saint-Genès-Champanelle, France

(2) UR1197 NOeMI, INRA, F-78350 Jouy-en-Josas, France

* Corresponding author

Phone number: (33) 4 73 62 41 52

Fax number: (33) 4 73 62 40 89

E-mail address: bonny@clermont.inra.fr

Abstract

The aim of this study was to investigate, using manganese-enhanced MRI (MEMRI), the activation of central olfactory structures following exposure of awake rats to biologically relevant odors. The activation map obtained after stimulation with the odor released by faeces of male fox, a predator of the rat, was compared to that obtained with the odor of chocolate flavored cereals. Results showed i) a progressive rostro-caudal decrease of Mn enhancement along central olfactory pathways, whatever the odor; ii) a lower Mn enhancement after stimulation by fox faeces odor, as compared to deodorized air, in all olfactory structures and iii) an asymmetric Mn enhancement, lower only in the left hemisphere in rats exposed to fox faeces odor. Fos immunodetection in the piriform cortex confirmed that fox faeces odor (but not chocolate odor) was processed differently from a control odor. However, at variance with MEMRI results, Fos labeling i) was higher following stimulation with fox faeces odor than with chocolate odor and ii) did not reveal any fox faeces odor induced asymmetry. Altogether, both MEMRI and Fos immunolabeling indicate that different biologically relevant odor may be processed differently in olfactory structures. The hypothesis that olfactory processing may rely on both the intensity of activation (revealed by MEMRI) and the size of neuronal populations recruited (revealed by Fos immunohistochemistry) is discussed.

Keywords: rat, olfaction, MEMRI, Fos, functional imaging

Introduction

The question of how a given brain region responds to different odorous stimuli has been addressed through various experimental approaches: electrophysiology (Rennaker *et al.*, 2007; Schoenbaum and Eichenbaum, 1995; Wilson, 2000), Fos activation (Datiche *et al.*, 2001; Illig and Haberly, 2003; Kippin *et al.*, 2003), anatomy (Sosulski *et al.*, 2011), calcium imaging (Stettler and Axel, 2009), functional imaging on animals (Chuang *et al.*, 2009; Kida *et al.*, 2002; Xu *et al.*, 2003; Xu *et al.*, 2005) and humans (Royet *et al.*, 2003; Savic, 2005; Sobel *et al.*, 1998). When analyzing responses in deep olfactory brain regions, it appears that spatial coding of odors in the olfactory bulb disappears to leave place to a blurred organization of activated neurons. Furthermore, this apparent lack of spatial organization is accompanied by an apparent lack of functional selectivity of neurons. Indeed, in the piriform cortex, the response of a given neuron to a monomolecular odorant does not allow to predict its response to this same odorant when administered together with another molecule (Stettler and Axel, 2009). The reductionist approach, based on the implicit assumption that the response of the olfactory system to an odorant mixture can be inferred from its responses to each of the compounds of the mixture, thus leaves space for a more global approach. Indeed, it is generally recognized that mammals have very limited analytical abilities and treat odorous mixtures as perceptual wholes (Wilson and Stevenson, 2003). We have thought worth investigating, more globally, the response of whole brain regions to biologically relevant odors. Functional imaging is perfectly suited for this purpose. Among odors that contribute to basic functions (survival, reproduction and food intake), we have chosen to concentrate on that of fox faeces, which elicits in rats an innate survival response and on that of chocolate flavoured cereals, which stimulates, also in rats, an acquired food intake response.

High field magnetic resonance imaging (MRI) offers various possibilities for the functional imaging of the whole rat brain at an adequate spatial resolution. Blood oxygen level dependent (BOLD) contrast (Bandettini *et al.*, 1992; Kwong *et al.*, 1992; Ogawa and Lee, 1990), used for most human functional studies, yields short lasting signals imposing the stimulus to be delivered during MRI acquisition. Non-compliant rats should be either anaesthetized or acclimatized to being restraint (King *et al.*, 2005; Lahti *et al.*, 1998) before performing MRI acquisitions. Anesthesia significantly affects brain function. Baseline activity at rest decreases with deepening anesthesia (Massimini *et al.*, 2005; Shulman *et al.*, 1999) and, when unconsciousness is triggered by anesthetics, it seems to block brain's ability

to integrate information (Alkire *et al.*, 2008). Alternatively, acclimatizing allows BOLD functional MRI (fMRI) to be applied to conscious animals (Ferris *et al.*, 2006), a strategy used on rats for studying olfaction (Chen *et al.*, 2009; Febo *et al.*, 2009; Febo and Pira, 2011; Huang *et al.*, 2011). However, besides being practically challenging, this approach may be hampered by motion artifacts and by the risk of substituting the adverse effects of anesthesia with those of restraint stress (Martin, 2007).

An interesting alternative to BOLD fMRI is manganese-enhanced magnetic resonance imaging (MEMRI), which can avoid both anaesthesia and restraint during stimulation (Silva *et al.*, 2004). MEMRI is based on the use of manganese (Mn), a calcium analogue, as a surrogate marker for neuronal cell activity. Mn is recruited by activated neurons and subsequently slowly eliminated (i.e. over days). This remanence allows stimulations to be performed on conscious and freely-moving animals and images to be acquired *a posteriori* under anaesthesia. Image contrast depends on intra-neuronal Mn concentration, and reflects neuronal activity throughout the stimulation period. MEMRI can reveal the activation of brain regions following various sensory stimulations on awake animals. So far, MEMRI succeeded at labeling specific activations due to olfactory cue(s) following intravenous Mn administration coupled to mannitol-induced blood-brain-barrier disruption (Chen *et al.*, 2007). Injection of mannitol into the carotid artery requires cumbersome surgery to ensure its perfusion to the brain and prevent its lethal circulation to the heart. Other drawbacks lie in an inhomogeneous disruption of the blood-brain-barrier (Aoki *et al.*, 2004) and in possible early cerebral dysfunction. When targeting olfactory regions, it seems preferable to administer Mn into the nostrils, as previously done in mice (Chuang *et al.*, 2009; Pautler and Koretsky, 2002) and in starlings (De Groof *et al.*, 2010).

In the present work, we have used MEMRI to explore, in the rat olfactory system (i.e. in the olfactory bulb and beyond) the activation elicited by the odors of male fox faeces and of chocolate-flavored cereals. For this purpose, we have made sure that the dose of Mn did not alter olfactory perception and we have allowed its diffusion for a delay long enough to allow Mn to reach distal regions, before MRI acquisition (Lehallier *et al.*, 2011b). Finally, we compared our fMRI maps obtained by MEMRI to the distribution of Fos immunoreactive neurons, since this technique is largely accepted for labeling activated brain regions and has been proposed as the *ex vivo* analogue of MEMRI (Van der Linden *et al.*, 2007).

Methods

The study was in full compliance with the guidelines of the European community (EUVD 86/609/EEC) for the care and use of the laboratory animals.

MEMRI study

Male Brown Norway rats aged 10 week, weighing 215±2.5g were housed individually under a reversed 12 h light / 12 h dark cycle (light on at 20:00). Nine days before the experiment, all the rats were fed with 20 g of laboratory food, excepting those stimulated with the chocolate odor which were fed with a mixture of laboratory food (14 g) and chocolate flavored cereals (6 g, Chocapic™, Nestlé, Switzerland).

3µL of a 100 mM $MnCl_2$-$4H_2O$ solution (Sigma-Aldrich, France) was injected into each nostrils of rats according to the protocol described by Lehallier *et al.* (2011b). Upon wakening (approximately 1 min after Mn administration), rats were put into an empty clean cage with free access to water.

To test the effect of the order of Mn instillation on signal enhancement in the olfactory regions, Mn was first injected into the left nostril and then into the right for 4 animals and in the reverse order for 4 others. MRI scans were acquired 4h after Mn administration, in the absence of any particular olfactory stimulation.

Functional imaging experiments were led using three olfactory stimulations: deodorized air and two odors coming from chocolate flavored cereal and fox faeces. A custom-made device produced a reproducible and constant flow of deodorized air in the rat cage through a sniffing port. Olfactory stimulation was performed by enriching the air flow with the corresponding odor for 5 min every 30 min during 48h. 3 groups of 8 Mn-impregnated rats were formed, each group corresponding to one of the three olfactory stimulations. MRI scans were acquired 48h after Mn administration. A group without Mn injection was also imaged (Mn-free group, n=9).

For both MEMRI experiments, images were acquired on a Bruker (Bruker, GmbH, Ettlingen, Germany) 4.7 T / 40 cm horizontal magnet equipped with a 12-cm gradient coil and interfaced to an Avance console. A 9-cm-diameter linearly-polarized birdcage resonator was used for emission and reception. Animals were placed in a rat-tailored bed equipped with a three point-fixation system (tooth-bar and ear-plugs) and a temperature-controlled warming blanket. Anesthesia was maintained during image acquisition using urethane (1.3g/kg).

Physiological conditions were monitored using breathing and temperature probes. T1-weighted images covering the whole brain were acquired by 3D rapid acquisition with a relaxation enhancement sequence. Centric encoding was used to keep echo time short (=5.5 ms). The others scan parameters were: TR = 500 ms, matrix = 64^3, isotropic voxel size = 500 μm^3, acquisition time = 7 min 30 s. Acquisitions were repeated for 2 h 30 min, corresponding to 20 images for each rat. Each series was first motion-corrected via rigid registration using automated image registration (AIR, version 5.2.6) (Woods *et al.*, 1998) and then averaged. Afterwards, images were successively segmented, normalized using our iterative algorithm for spatial and intensity normalization (Lehallier *et al.*, 2011a) and smoothed using 3D Gaussian filter (FWHM = 0.5 mm). The reference signal for intensity normalization was measured in the tongue.

A two-way analysis of variance (ANOVA, $p < 0.05$) was used to test the effect of the order of Mn instillation on signal enhancement. This comparison was performed on MEMRI signals averaged over manually-defined regions of interest (ROI) delimiting the olfactory bulb for each brain hemisphere.

For the ROI analysis of functional imaging experiments, voxel-wise two-tailed student's t-tests between the unstimulated Mn and the Mn-free groups were first performed. This t-map was thresholded at $p < 0.001$ for highlighting Mn-enhanced regions. The intersection between the latter 3D regions and the coronal planes defined the successive bidimensional ROIs in the rostro-caudal axis. ROI-averaged signals were compared between the Mn-impregnated groups using ANOVA ($p < 0.05$). When there were significant differences, pairwise comparisons were performed using a Tukey's Honest Significant Difference (HSD) test. Statistical t-maps were also contructed to compare, in each voxel, the signal intensity between odor-stimulated and control groups ($p < 0.01$). Finally, anatomical ROIs corresponding to the piriform cortex were manualy delineated in each brain hemisphere according to Paxinos and Watson (2007). Effect of odor stimulation on signal enhancement was estimated using an ANOVA ($p < 0.05$).

C-Fos study

Nine male Brown-Norway rats aged 16 weeks, weighing 323±4 g were housed individually under an inverse light/dark cycle (12 h dark per 24 h starting at 05:15). Rats were fed as described in the MEMRI study. Two days before olfactory stimulation, rats were fasted but still had free access to water.

On the day of olfactory stimulation, the rat was placed during 5 min for habituation in the stimulation arena (LxWxH: 50x30x30 cm3) made of glass with clean sawdust as litter. Odorous samples were presented during 30 min on an aluminum foil put in a receptacle covered with a bolted-on perforated lid. Odorous samples were either the empty foil or a chocolate flake or a sample of male fox faeces (kindly provided by Dr Franck Boué, ANSES, Malzeville, France). Three rats were stimulated on the same day (each with a different odorous sample). Between two sessions, the aluminium foil and the litter were discarded, the arena was thoroughly cleaned and the stimulation room ventilated for 20 min.

At the end of the session, rats were returned to their home cage and deeply anaesthetized 60 min later by an i.p. injection of 1 mL of a 60 mg/mL solution of sodium pentobarbital (CEVA Santé Animale, Libourne, France). They were intracardially perfused with 200 mL Ringer lactate solution (CDM, Lavoisier, France) at 4°C and with 500 mL 10% neutral buffer formalin (Diapath, Microm Microtech, France), pH 7.2-7.4. Brains were dissected out, postfixed overnight in the second perfusion solution and dipped during 24 h in a 15% sucrose solution and during 48 h in a 30% sucrose solution for cryoprotection.

Brains were frozen and sampled using a cryostat (Leica 3050S) in 40 µm thick coronal sections from the olfactory bulbs to the closing of the anterior commissure. Two consecutive sections were collected every 4 sections. One was used for Nissl staining and the following one for Fos immunohistochemistry.

Slices were dried at room temperature, rinsed 2x10 min in phosphate buffered saline (PBS, Sigma-Aldrich, France) and preincubated during 45 min in a moist chamber with 500 µL/slide of 0.25% (v/v) Triton X-100 (Sigma-Aldrich, France) in PBS containing 1.5% (v/v) goat serum (Vector Labs, AbCys, France). Slices were incubated overnight at room temperature with a polyclonal rabbit anti-rat c-Fos antibody (Calbiochem, VWR, France) at a dilution of 1/20000 in PBS-Triton containing 1.5% goat serum (v/v). They were rinsed 3 times in PBS containing 0.1% creamed milk and incubated during 90 min with biotinylated anti-rabbit antibody (Vector Labs, AbCys, France) diluted 1/400 in PBS-Triton containing 0.1% bovine serum albumin. Slices were rinsed 3x10 min with PBS, dipped during 10 min in PBS containing 0.3% H2O2 and rinsed 3x10 min in PBS. They were incubated with the Avidin-Biotin complex (Vectastain, Vector Labs, AbCys, France) during 45 min and rinsed 2x10 minutes in PBS and during 10 min in 50 mM Tris buffer (pH 7.6). Labelling was revealed using nickel-enhanced diamino-benzidine (SK-4100, Vector Labs, AbCys, France).

Section images were digitized with an automatic image digitizer (Nanozoomer, Hamamatsu, France). The piriform cortex was delineated according to Paxinos and Watson

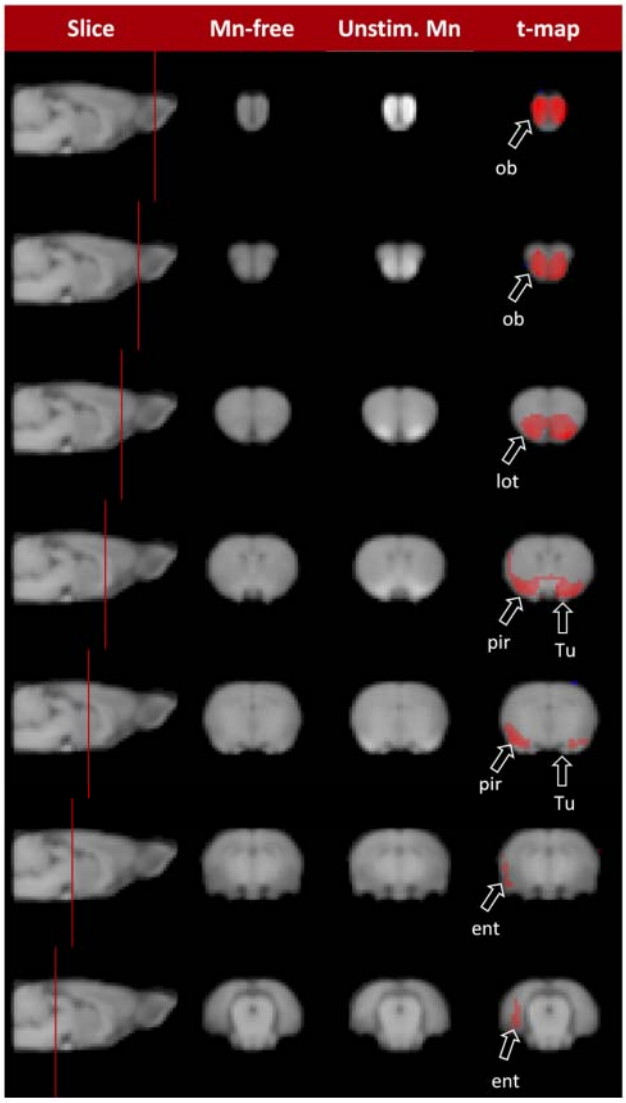

Figure 3.1: Group-averaged images in different coronal slices intercepting primary olfactory cortex for the Mn-free and the unstimulated Mn group. Each image in the first column shows the position of the coronal slice represented in the corresponding row in a sagittal view. Column 2 and 3 represent respectively the Mn-free and the unstimulated Mn group. Column 4 represents statistical t-map overlaid on T1W MEMRI image showing Mn enhancement in the unstimulated Mn group. T-values in red represent voxels whose mean intensity of the unstimulated Mn group was higher than mean intensity of the Mn-free group (two-tailed t-tests, $p<0.001$). Red patterns correspond to significant Mn signal increase due to Mn enhancement. Abbreviations: (ob) olfactory bulb, (lot) lateral olfactory tract, (pir) piriform cortex, (Tu) olfactory tubercle and (ent) entorhinal cortex.

(2007). Fos immunoreactive neurons were identified and numbered using Fiji (http://pacific.mpi-cbg.de/wiki/index.php/Fiji).

Statistical analyzes were performed using SigmaPlot 12 (Systat, Chicago, IL, USA). Normality of distributions was checked using a Shapiro-Wilk test and equality of variances a Levene median test. When both conditions were met, direct pairwise comparisons were done using a t-test and multiple group comparisons a one-way ANOVA followed by a Holm-Sidak pairwise post-hoc comparison. When they were not met, pairwise comparisons were done using a Mann-Whitney rank sum test and multiple comparisons with a Kruskal-Wallis test on ranks.

Results

MEMRI study

The order of Mn instillation (right nostril then left or the reverse) did not significantly affect Mn enhancement in the olfactory bulbs (ANOVA, $p>0.05$). In addition, Mn enhancement in the right and left olfactory bulbs did not significantly differ ($p>0.05$). This suggests that our administration protocol delivers Mn symmetrically.

Figure 1 depicts group-averaged coronal slice images at 7 positions through the rostro-caudal extension of the primary olfactory cortex, for the Mn-free group and the unstimulated Mn group. A statistical t-map resulting from voxelwise comparison of these 2 groups is also presented, which reveals significant contrast enhancements ($p<0.001$) after 48h of Mn progression. Along with the olfactory bulbs, most regions of the primary olfactory cortex (e.g. piriform and entorhinal cortices) were labeled. Interestingly, the olfactory tubercle seemed more weakly labeled (at least at the chosen threshold for t significance). Some other regions were also labeled, such as (along the rostro-caudal axis) the nucleus accumbens, the somatosensory cortex, the amygdala and the insular cortex, the perirhinal cortex and the subiculum.

Figure 2A is a 3D representation of the t-map, thresholded at $p<0.001$. On this figure are also displayed three of the 22 levels that sample rostro-caudally the t-map in order to determine the bidimensional ROIs. Figure 2B shows, at each of these 22 levels, the mean value of T_1-weighted image signal in these ROIs, for the 3 experimental groups (unstimulated Mn (control), chocolate flavored cereal (chocolate) and male fox faeces (fox)). It appeared that, for all stimulations, the T_1-weighted image signal decreased markedly in the olfactory

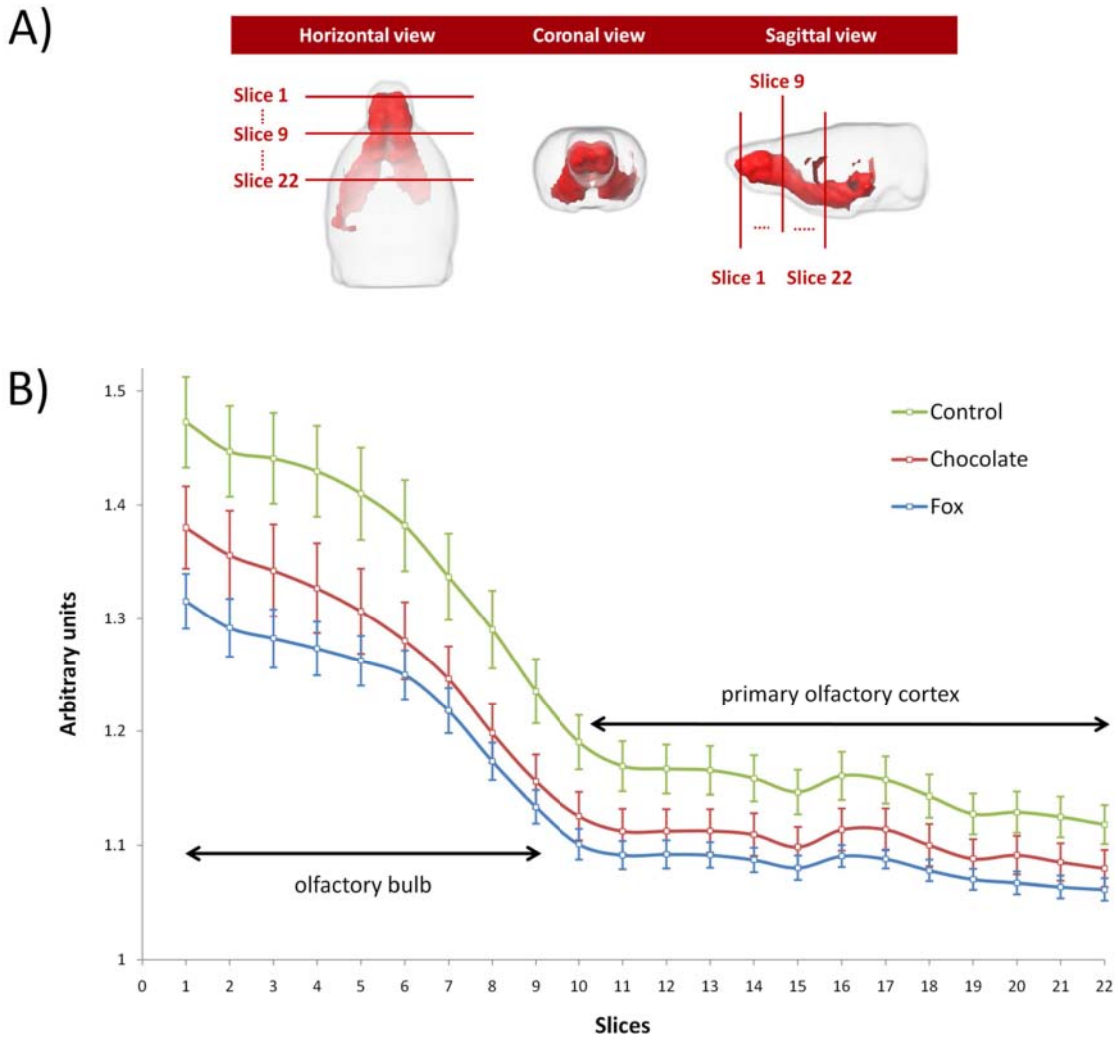

Figure 3.2: Effect of odor stimulation on Mn enhancement along the olfactory pathways. (A) 3D views of the Mn-distribution map represented in figure 1. Mn enhancements were significantly different (ANOVA, $p<0.05$) from the slice 1 to the slice 22 between the Mn-impregnated groups i.e control, chocolate and fox. Group-averaged signal in these slices along a rostro-caudal axis was presented in (B). Each group enhancement (mean ± sem) was normalized by the signal of the Mn-free group.

bulb (slices 1-9) and more moderately in the primary olfactory cortex (slices 10-22). Moreover, a significant link was found between signal intensity and odorous stimulation at each of the 22 rostro-caudal levels (ANOVAs, $p<0.05$) while beyond the 22nd level, no significant difference between groups was found (ANOVA, $p>0.05$). Post-hoc pairwise analysis (using a Tukey HSD test) indicated that fox values differed significantly from control values ($p<0.05$), while chocolate values were not different from either control or fox values.

Figure 3 maps the t value resulting from comparison, in each voxel, of signal intensity between odor-stimulated (chocolate or fox) and control groups. Such comparison at the voxel scale did not highlight difference between chocolate and control ($p<0.01$), consistently to the results obtained by the previous ROI analysis. Moreover, it allowed localizing the differences between fox and control in olfactory regions (e.g. olfactory bulb, lateral olfactory tract, piriform cortex) of the sole left hemisphere ($p<0.01$).

When the comparison between odor-stimulated and control groups is based upon anatomically defined regions (Figure 4), results are similar to those of the voxel-based analysis: in the right hemisphere, no statistically significant difference is found (Figure 4A) while in the left hemisphere, fox stimulated rats displayed a significantly ($p<0.05$) lower signal (Figure 4B).

Fos study

Three rostro-caudal levels in the piriform cortex were analyzed (one coronal section / level / rat). The anterior one was located where the olfactory bulb is no longer separated from the orbital cortex, the posterior one at the closing of the anterior commissure and the central one approximately in the middle of this extension. For each animal and each level, Fos$^+$ neurons were numbered separately in the right and left piriform cortices. Since in no case was a difference detected, neurons numbers were averaged to provide a unique value per level and per rat.

For all olfactory stimulation experiments, Fos$^+$ neurons were observed all along the rostro-caudal extension of the piriform cortex (Figure 5). They were mostly located within layer 2 (Figure 5 B, 5 D and 5 F), although some could be found in layer 3. Almost no labeling was detected in layer 1. Along the medio-lateral axis, Fos$^+$ neurons extended from the rhinal fissure to the limit of the olfactory tubercle, which was much less labeled.

Figure 6 summarizes the results obtained in the 3 groups of 3 rats. Rats stimulated by an empty container (controls) displayed a significant change of Fos labeling in the piriform

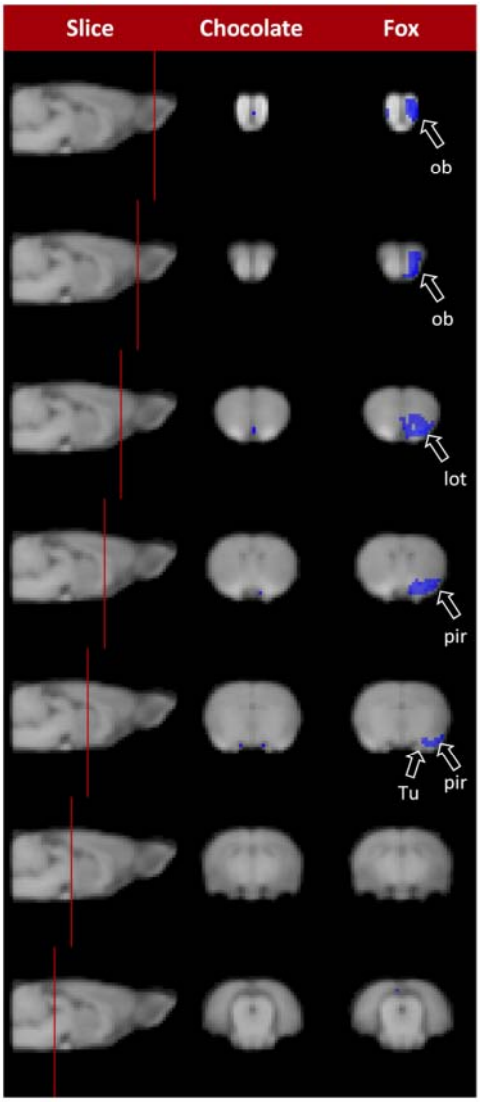

Figure 3.3: Statistical t-maps overlaid on T1 weighted MEMRI images depicting variation of Mn enhancement, in the same slices as those in the figure 2, between odor-stimulated groups and the control group. Column 2 and 3 represent respectively the chocolate and the fox group. T-values in blue represent voxels whose mean intensity of the odor-stimulated is lower than mean intensity of the Control group (two-tailed t-tests, $p<0.01$). Abbreviations: (ob) olfactory bulb, (lot) lateral olfactory tract, (pir) piriform cortex and (Tu) olfactory tubercle.

cortex along the rostro-caudal axis ($p=0.003$). Empty container labeling in the anterior part was significantly lower than in the medial ($p<0.01$) and the posterior ($p<0.01$) ones. Such a rostro-caudal change was not observed in the chocolate and fox groups. The number of Fos^+ neurons in the piriform cortex of the fox group was consistently high. A significant difference with the control group was found at the anterior ($p<0.05$) and posterior ($p<0.05$) levels of the piriform cortex, while no significant difference was found with chocolate stimulated rats at any level.

Discussion

Several studies have shown that, in the absence of any particular olfactory stimulation, Mn administered in the nostrils significantly enhances MR signal in olfactory structures and can therefore be used as a tracer of olfactory pathways (Chuang and Koretsky, 2009; Cross *et al.*, 2004; Pautler *et al.*, 1998). A few studies have attempted to use Mn properties to investigate the activation of olfactory structures following odorous stimulation (Chen *et al.*, 2007; Chuang *et al.*, 2009; De Groof *et al.*, 2010). In the present work, we have tried to compare the activation induced in the primary olfactory cortex by natural odors conveying different messages. In a previous study, we have shown that signal variations induced by 0.1 to 8 µmol Mn are not detectable by mere visual examination of MR images (Lehallier *et al.*, 2011b). This is the reason why we have developed an algorithm to perform both spatial and intensity normalization of MEMRI images (Lehallier *et al.*, 2011a), which allows comparing signal intensity in experimental groups at the voxel scale and facilitates statistical exploitation of MEMRI data. Our normalization procedure, by optimizing Mn detection, allowed us to administer a Mn dose (0.3 µmol) that did not markedly alter olfactory perception. This dose, after 48 h of Mn progression, ensured labeling of the primary olfactory cortex up to its caudal most part. Under these experimental conditions, we were able to detect significant differences between effects induced in deep olfactory regions (i.e. beyond the olfactory bulb) by various odorous stimulations.

In the absence of any particular odorous stimulation, and in agreement with the above mentioned studies, Mn enhancements labeled olfactory structures such as the olfactory bulb and the primary olfactory cortex. Since Mn tracing properties rely upon its uptake into activated neurons and its transport along neurites (Van der Linden *et al.*, 2007), our results suggest that a basal activity exists in olfactory pathways. In keeping with this hypothesis, it has been shown that olfactory receptor neurons do display a varying degree of spontaneous

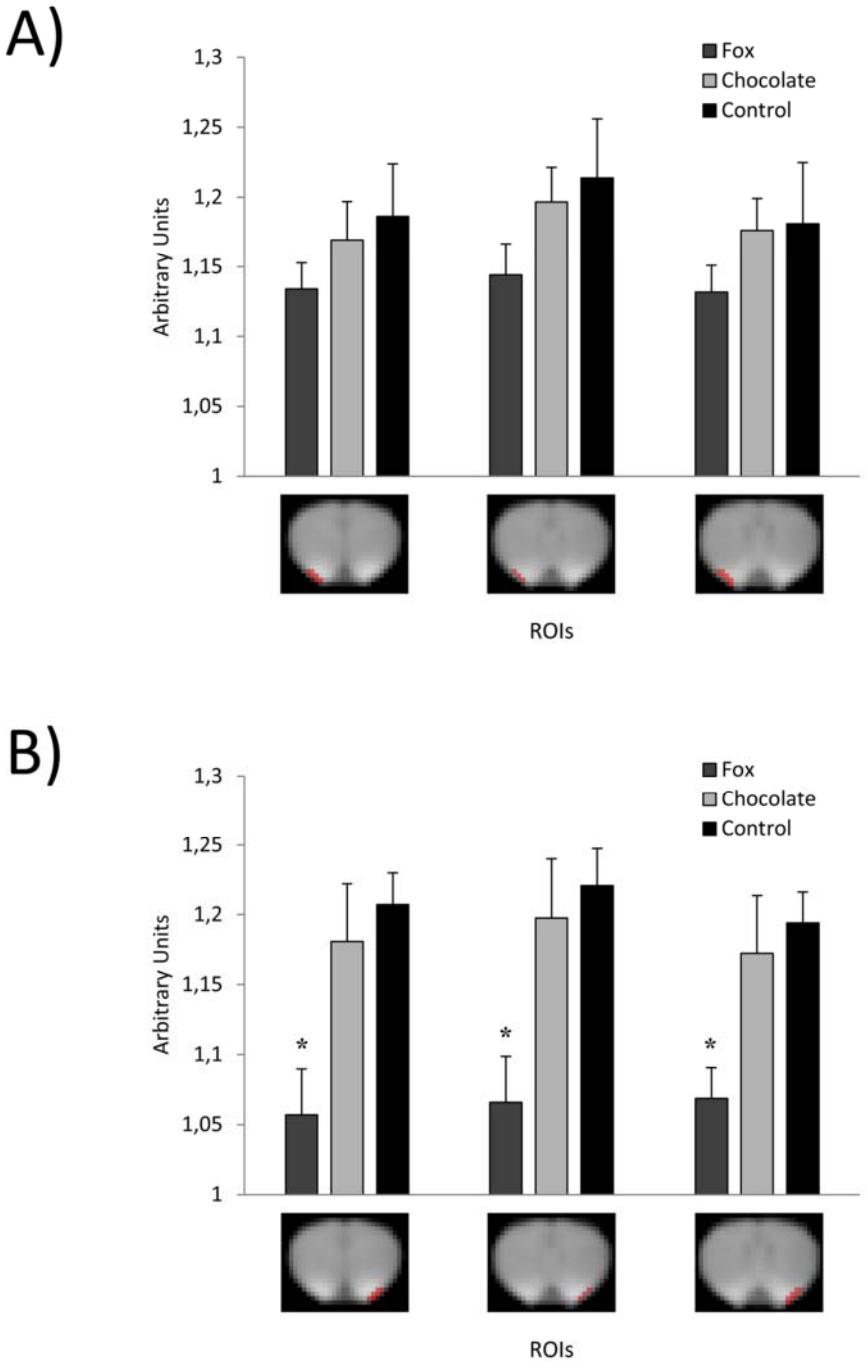

Figure 3.4: Variation of Mn enhancement between odor-stimulated groups and the control group in anatomical ROIs located in three successive slices corresponding to the piriform cortex for (A) the right brain hemisphere and, (B) the left brain hemisphere. Each group enhancement (mean ± sem) was normalized by the signal of the Mn-free group. Means ± s.e.m. are shown. *: $p<0.05$ when compared to the control group.

activity (Reisert, 2010). Moreover, it cannot be excluded that in the absence of a particular odorous stimulation, the environment of our rats contained volatile molecules that were perceived by their olfactory system.

Another characteristic of Mn enhancement was its decrease with the distance from the administration site. This decrease was biphasic: rapid within the olfactory bulb, slower thereafter. Interestingly, the inflection occurred at the junction of the olfactory bulb and of the prefrontal cortex. One possible explanation is that, within the olfactory bulb, the concentration of Mn at a given rostro-caudal plane directly depends on the number of axons of odorant receptor neurons (ORN) crossing this plane to innervate glomeruli at this position or further. Because glomeruli are organized as a single layer envelope in the external part of the olfactory bulb, the number of axons rapidly decreases with the rostro-caudal position, possibly explaining the rapid decrease of Mn enhancements. Beyond the olfactory bulb, since there are no longer any ORN axons, the only neurons carrying Mn are at least one synapse away from the glomerular layer. The efficiency of synapse crossing by Mn may account for the inflection of the Mn enhancement curve. Further on, in the primary olfactory cortex, a single axon sends collaterals to various structures along the olfactory tract, at variance with ORNs that innervate a single glomerulus. This anatomical difference may account for a slower decrease of Mn enhancement in the primary olfactory cortex.

MEMRI experiments also revealed that fox faeces odor was processed differently from chocolate odor and deodorized air. All along the rostro-caudal extent of olfactory pathway, fox faeces odor yielded a significantly lower mean MEMRI signal than that elicited by non-odorized air, while chocolate odor did not. This observation answers our main question: different biologically significant odors yielded different MEMRI signals. Fos immunolabeling in the anterior piriform cortex was performed to corroborate this result. Fos immunolabeling following fox odor stimulation differed significantly from that induced by an empty container in both the rostral and caudal parts of the anterior piriform cortex, while chocolate odor did not. In both MEMRI and Fos experiments, the intensity of chocolate odor effect was between those of fox faeces and control. However, while fox faeces odor yielded a consistently lower MEMRI signal, it induced a consistently higher Fos expression. Since the number of Fos positive neurons is proportional to the intensity of the stimulus (Morgan *et al.*, 1987), our Fos results indicate that fox faeces odor was more potent than chocolate odor or empty container odor at activating olfactory neurons. Consequently, in our MEMRI experiments, the lower signal induced by fox faeces odor should be seen as the consequence of a higher neuronal activation. This interpretation is counter-intuitive since it is generally accepted that Mn uptake

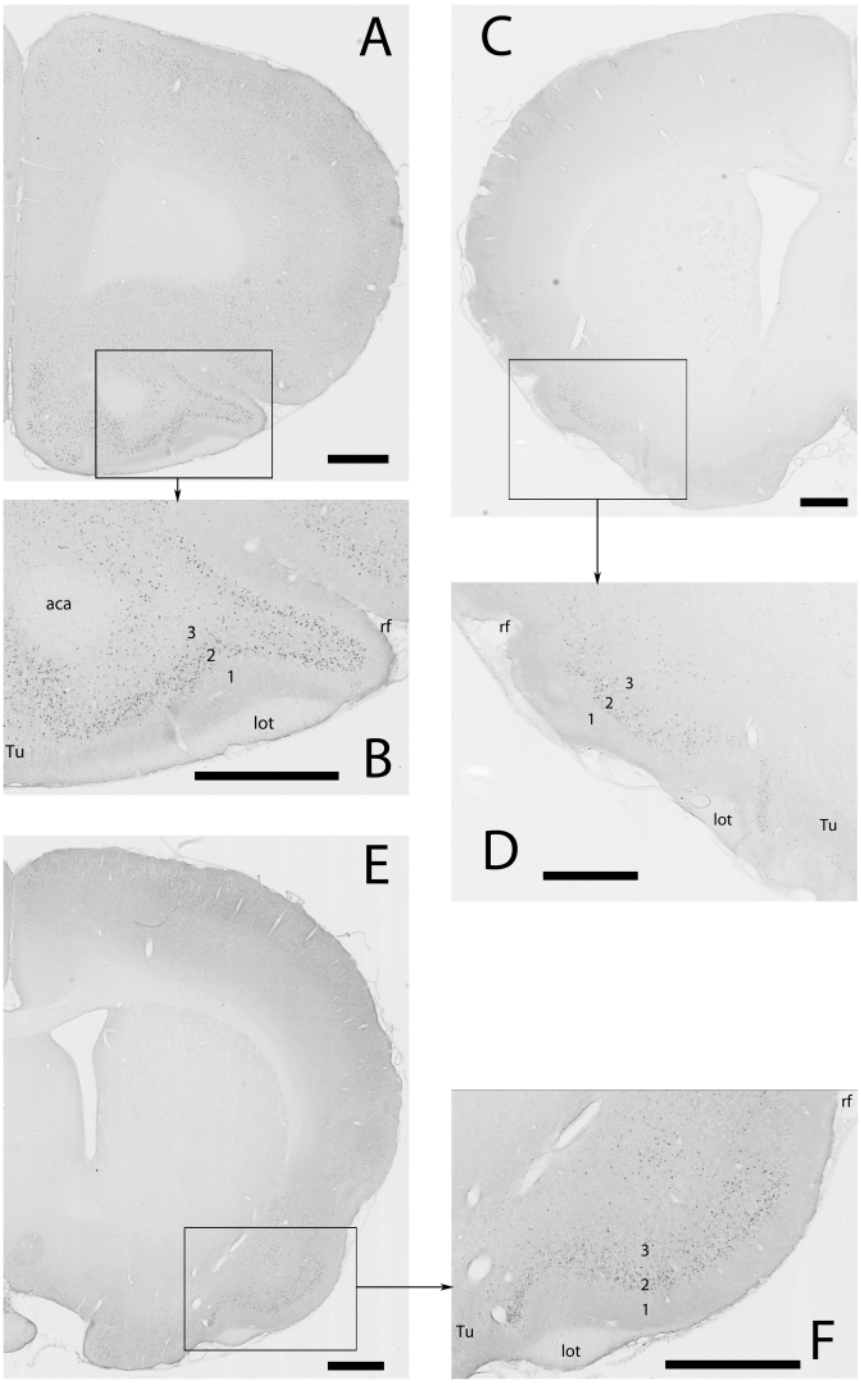

Figure 3.5: Fos immunodetection of neurons activated by olfactory stimulation in the piriform cortex. A, C & E: photomicrographs of the right (C) and left (A, E) sides of the brain. B, D & F: enlargments of the regions delimited by the black rectanges in A, C & E, respectively. A, B: anterior region of the anterior piriform cortex; stimulation: chocolate flavoured cereals C, D: medial region of the anterior piriform cortex; stimulation: empty container E, F: posterior region of the anterior piriform cortex; stimulation: fox faeces. Abbreviations (Tu) olfactory tubercle, (aca) anterior part of the anterior commissure, (lot) lateral olfactory tract, (rf) rhinal fissure, (1), (2), (3): layers 1, 2 and 3 of the piriform cortex. Scale bars: 1 mm.

is proportional to neuronal activation (Van der Linden *et al.*, 2007). However, a higher neuronal activation also elicits a faster axonal transport (Chuang *et al.*, 2009) and probably a higher presynaptic loss. Thus, in our experiments, neuronal release of Mn in olfactory structures might have been accelerated in rats exposed to fox faeces as compared to those exposed to deodorized air. Since the detection of the extracellular Mn is lower than the intracellular one (Nordhoy *et al.*, 2004), a faster transport might have led to a lower MEMRI signal. An alternative possibility is that Mn uptake is lower when the olfactory message is more salient. Indeed, we also observed a lower MEMRI signal in the olfactory bulb of rats exposed to fox faeces odor. A similar result was also obtained in the olfactory bulb of the starling (De Groof *et al.*, 2010). This can be caused, in the olfactory bulb, by activity-dependent lateral inhibitory mechanisms (Arevian *et al.*, 2008), which enhance the salience of a biologically relevant odor over other olfactory signals (for review, see Lledo *et al.*, 2005). Indeed, in the starling, the same odorous stimulation was applied at different periods of the year and it appeared that the MEMRI signal was lower in spring, when the odorous stimulus conveyed an additional biological message related to reproduction (De Groof *et al.*, 2010). The triggering of inhibitory mechanisms would thus be linked to the biological relevance of the odorous signal and would be mediated by the inhibition of neurons that do not process the biologically relevant odorous molecules. This might explain why, in our experiments, fox faeces odor, which signals a predator and triggers in the rat an innate fear response (Rampin *et al.*, 2006; Vernet-Maury, 1980), was more efficient at eliciting inhibitory mechanisms than the odor of chocolate flavored cereals.

When inter-group comparisons were performed on a voxel to voxel basis, a second important observation was that the lower fox-induced MEMRI signal was detected solely in the left hemisphere. In other words, fox-induced MEMRI signal appeared asymmetric. This could not result from an asymmetric availability of Mn. Indeed we verified that Mn administration in the nostrils yielded a symmetric labeling, regardless of the administration order (right nostril then left or the reverse). Moreover, if Mn availability were asymmetric, it would be difficult to explain why chocolate odor or deodorized air yielded a symmetric MEMRI signal. Consequently, the observed asymmetry following fox faeces odor stimulation most likely resulted from an asymmetric processing. Such an asymmetry in odor processing has already been observed in humans (Brand *et al.*, 2001) and in animals (Dantzer *et al.*, 1990). Exposure of awake rats to trimethyl thiazoline (the molecule contained in fox faeces that is primarily responsible for innate fear of rats: Vernet-Maury, 1980) has previously been studied by BOLD fMRI (Febo and Pira, 2011). Careful examination of the results suggests

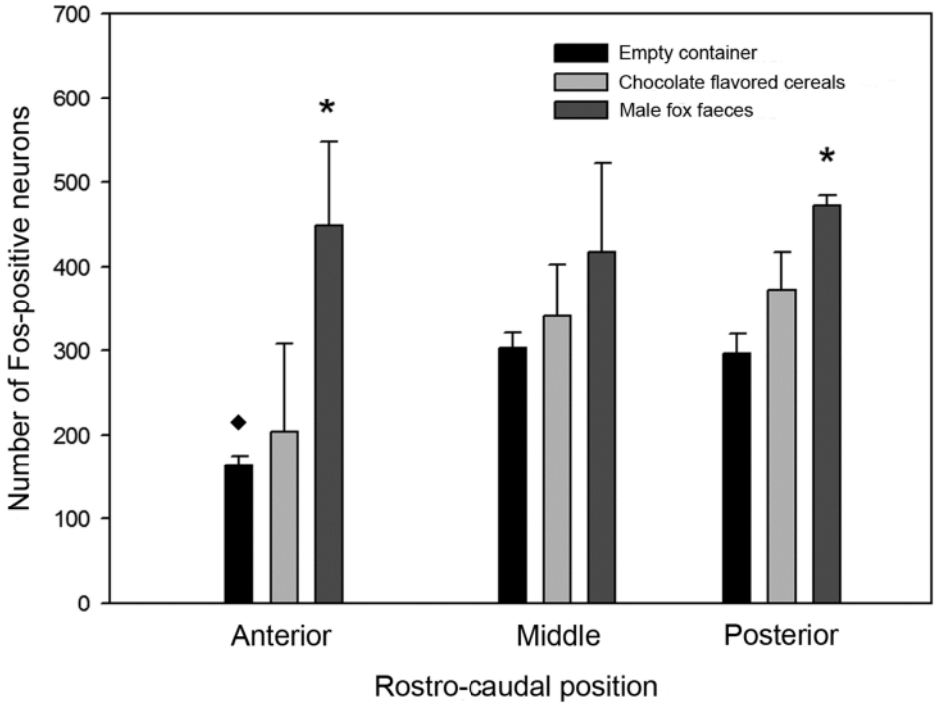

Figure 3.6: Number of Fos-positive neurons at 3 rostro-caudal positions within the anterior piriform cortex of rats stimulated by the odors released by a receptacle either empty or containing chocolate flavored cereals or fox faeces. Means ± s.e.m. are shown. ◆: $p<0.01$ when compared to the two other empty container values; *: $p<0.05$ when compared to the corresponding empty container value.

that brain activation is also asymmetric, although the authors did not particularly stress this point. It remains that, in our hands, Fos experiments did not reveal such an asymmetry in the piriform cortex. The fact that Fos immunodetection does not allow quantifying the intensity of neuronal activation, but only the number of recruited neurons may account for this apparent discrepancy between Fos an MEMRI results. Fos immunodetection will not reveal an asymmetric processing, if this asymmetry relies on a differential degree of activation of equal-sized populations of neurons. On the contrary, the MEMRI signal, which is proportional to the opening of voltage-dependent calcium channels (i.e. to neuronal activity), reflects the quantitative balance of Mn dynamics. Consequently, an asymmetric degree of activation may well be detected by MEMRI and not by Fos immunodetection.

Altogether, our results suggest that odor processing depends on a dual mechanism: the size of the neuronal populations recruited to ensure odor processing and the degree of activation of neurons in these populations. The present experiments indicate that fox faeces odor recruits a larger population of neurons than a less significant odor, such as the empty container, does. This is revealed by Fos immunodetection and not by MEMRI. They also indicate that fox faeces odor triggers a neuronal activation, which is asymmetric in intensity. This is revealed by MEMRI and not by Fos immunodetection.

In conclusion, MEMRI appears to be a powerful technique for the functional imaging of olfactory processes in deep brain regions, under conditions close to natural perception in awake animals. Our results strongly suggest that odor processing depends on the significance of odors. This conclusion is supported by both MEMRI and Fos immunodetection. MEMRI also reveals that a crucial olfactory message is asymmetrically processed in the brain.

Acknowledgements

The MRI experiments were performed at the MR of biological systems platform at the INRA research center in Clermont-Ferrand, France (www.clermont.inra.fr/rmsb/). The authors gratefully acknowledge Dr. Birte Nielsen for careful reading of the manuscript and helpful suggestions.

References

Alkire, M.T., Hudetz, A.G., Tononi, G., 2008. Consciousness and anesthesia. Science 322, 876-880.

Aoki, I., Naruse, S., Tanaka, C., 2004. Manganese-enhanced magnetic resonance imaging (MEMRI) of brain activity and applications to early detection of brain ischemia. NMR Biomed. 17, 569-580.

Arevian, A.C., Kapoor, V., Urban, N.N., 2008. Activity-dependent gating of lateral inhibition in the mouse olfactory bulb. Nat.Neurosci. 11, 80-87.

Bandettini, P.A., Wong, E.C., Hinks, R.S., Tikofsky, R.S., Hyde, J.S., 1992. Time course EPI of human brain function during task activation. Magn Reson.Med. 25, 390-397.

Brand, G., Millot, J.L., Henquell, D., 2001. Complexity of olfactory lateralization processes revealed by functional imaging: a review. Neurosci.Biobehav.Rev. 25, 159-166.

Chen, W., Shields, J., Huang, W., King, J.A., 2009. Female fear: influence of estrus cycle on behavioral response and neuronal activation. Behav.Brain Res. 201, 8-13.

Chen, W., Tenney, J., Kulkarni, P., King, J.A., 2007. Imaging unconditioned fear response with manganese-enhanced MRI (MEMRI). Neuroimage. 37, 221-229.

Chuang, K.H., Koretsky, A.P., 2009. Accounting for nonspecific enhancement in neuronal tract tracing using manganese enhanced magnetic resonance imaging. Magn Reson.Imaging 27, 594-600.

Chuang, K.H., Lee, J.H., Silva, A.C., Belluscio, L., Koretsky, A.P., 2009. Manganese enhanced MRI reveals functional circuitry in response to odorant stimuli. Neuroimage. 44, 363-372.

Cross, D.J., Minoshima, S., Anzai, Y., Flexman, J.A., Keogh, B.P., Kim, Y., Maravilla, K.R., 2004. Statistical mapping of functional olfactory connections of the rat brain in vivo. Neuroimage. 23, 1326-1335.

Dantzer, R., Tazi, A., Bluthe, R.M., 1990. Cerebral lateralization of olfactory-mediated affective processes in rats. Behav.Brain Res. 40, 53-60.

Datiche, F., Roullet, F., Cattarelli, M., 2001. Expression of Fos in the piriform cortex after acquisition of olfactory learning: an immunohistochemical study in the rat. Brain Res.Bull. 55, 95-99.

De Groof, G., Gwinner, H., Steiger, S., Kempenaers, B., Van der Linden, A., 2010. Neural correlates of behavioural olfactory sensitivity changes seasonally in European starlings. PLoS.One. 5, e14337.

Febo, M., Pira, A.S., 2011. Increased BOLD activation to predator stressor in subiculum and midbrain of amphetamine-sensitized maternal rats. Brain Res. 1382, 118-127.

Febo, M., Shields, J., Ferris, C.F., King, J.A., 2009. Oxytocin modulates unconditioned fear response in lactating dams: an fMRI study. Brain Res. 1302, 183-193.

Ferris, C.F., Febo, M., Luo, F., Schmidt, K., Brevard, M., Harder, J.A., Kulkarni, P., Messenger, T., King, J.A., 2006. Functional magnetic resonance imaging in conscious animals: a new tool in behavioural neuroscience research. J.Neuroendocrinol. 18, 307-318.

Huang, W., Heffernan, M.E., Li, Z., Zhang, N., Overstreet, D.H., King, J.A., 2011. Fear induced neuronal alterations in a genetic model of depression: an fMRI study on awake animals. Neurosci.Lett. 489, 74-78.

Illig, K.R., Haberly, L.B., 2003. Odor-evoked activity is spatially distributed in piriform cortex. J.Comp Neurol. 457, 361-373.

Kida, I., Xu, F., Shulman, R.G., Hyder, F., 2002. Mapping at glomerular resolution: fMRI of rat olfactory bulb. Magn Reson.Med. 48, 570-576.

King, J.A., Garelick, T.S., Brevard, M.E., Chen, W., Messenger, T.L., Duong, T.Q., Ferris, C.F., 2005. Procedure for minimizing stress for fMRI studies in conscious rats. J.Neurosci.Methods 148, 154-160.

Kippin, T.E., Cain, S.W., Pfaus, J.G., 2003. Estrous odors and sexually conditioned neutral odors activate separate neural pathways in the male rat. Neuroscience 117, 971-979.

Kwong, K.K., Belliveau, J.W., Chesler, D.A., Goldberg, I.E., Weisskoff, R.M., Poncelet, B.P., Kennedy, D.N., Hoppel, B.E., Cohen, M.S., Turner, R., ., 1992. Dynamic magnetic resonance imaging of human brain activity during primary sensory stimulation. Proc.Natl.Acad.Sci.U.S.A 89, 5675-5679.

Lahti, K.M., Ferris, C.F., Li, F., Sotak, C.H., King, J.A., 1998. Imaging brain activity in conscious animals using functional MRI. J.Neurosci.Methods 82, 75-83.

Lehallier, B., Andrey, P., Maurin, Y., Bonny, J.M., 2011a. Iterative algorithm for spatial and intensity normalization of MEMRI images. Application to tract-tracing of rat olfactory pathways. Magn Reson.Imaging In press.

Lehallier, B., Coureaud, G., Maurin, Y., Bonny, J.M., 2011b. Effects of Manganese dose injected into rat nostrils: implications for in vivo functional study of olfaction using MEMRI. Magn Reson.Imaging In press.

Lledo, P.M., Gheusi, G., Vincent, J.D., 2005. Information processing in the mammalian olfactory system. Physiol Rev. 85, 281-317.

Martin, C., 2007. Anaesthetic use in animal models for neuroimaging. Neuroimage. 38, 1-2.

Massimini, M., Ferrarelli, F., Huber, R., Esser, S.K., Singh, H., Tononi, G., 2005. Breakdown of cortical effective connectivity during sleep. Science 309, 2228-2232.

Morgan, J.I., Cohen, D.R., Hempstead, J.L., Curran, T., 1987. Mapping patterns of c-fos expression in the central nervous system after seizure. Science 237, 192-197.

Nordhoy, W., Anthonsen, H.W., Bruvold, M., Brurok, H., Skarra, S., Krane, J., Jynge, P., 2004. Intracellular manganese ions provide strong T1 relaxation in rat myocardium. Magn Reson.Med. 52, 506-514.

Ogawa, S., Lee, T.M., 1990. Magnetic resonance imaging of blood vessels at high fields: in vivo and in vitro measurements and image simulation. Magn Reson.Med. 16, 9-18.

Pautler, R.G., Koretsky, A.P., 2002. Tracing odor-induced activation in the olfactory bulbs of mice using manganese-enhanced magnetic resonance imaging. Neuroimage. 16, 441-448.

Pautler, R.G., Silva, A.C., Koretsky, A.P., 1998. In vivo neuronal tract tracing using manganese-enhanced magnetic resonance imaging. Magn Reson.Med. 40, 740-748.

Paxinos, G., Watson, C., 2007. The rat brain in stereotaxic coordinates, 6th ed ed. Elsevier, Amsterdam.

Rampin, O., Jerome, N., Briant, C., Boue, F., Maurin, Y., 2006. Are oestrus odours species specific? Behav.Brain Res. 172, 169-172.

Reisert, J., 2010. Origin of basal activity in mammalian olfactory receptor neurons. J.Gen.Physiol 136, 529-540.

Rennaker, R.L., Chen, C.F., Ruyle, A.M., Sloan, A.M., Wilson, D.A., 2007. Spatial and temporal distribution of odorant-evoked activity in the piriform cortex. J.Neurosci. 27, 1534-1542.

Royet, J.P., Plailly, J., on-Martin, C., Kareken, D.A., Segebarth, C., 2003. fMRI of emotional responses to odors: influence of hedonic valence and judgment, handedness, and gender. Neuroimage. 20, 713-728.

Savic, I., 2005. Brain imaging studies of the functional organization of human olfaction. Chem.Senses 30 Suppl 1, i222-i223.

Schoenbaum, G., Eichenbaum, H., 1995. Information coding in the rodent prefrontal cortex. I. Single-neuron activity in orbitofrontal cortex compared with that in pyriform cortex. J.Neurophysiol. 74, 733-750.

Shulman, R.G., Rothman, D.L., Hyder, F., 1999. Stimulated changes in localized cerebral energy consumption under anesthesia. Proc.Natl.Acad.Sci.U.S.A 96, 3245-3250.

Silva, A.C., Lee, J.H., Aoki, I., Koretsky, A.P., 2004. Manganese-enhanced magnetic resonance imaging (MEMRI): methodological and practical considerations. NMR Biomed. 17, 532-543.

Sobel, N., Prabhakaran, V., Desmond, J.E., Glover, G.H., Goode, R.L., Sullivan, E.V., Gabrieli, J.D., 1998. Sniffing and smelling: separate subsystems in the human olfactory cortex. Nature 392, 282-286.

Sosulski, D.L., Lissitsyna, B.M., Cutforth, T., Axel, R., Datta, S.R., 2011. Distinct representations of olfactory information in different cortical centres. Nature 472, 213-216.

Stettler, D.D., Axel, R., 2009. Representations of odor in the piriform cortex. Neuron 63, 854-864.

Van der Linden, A., Van, C.N., Ramos-Cabrer, P., Hoehn, M., 2007. Current status of functional MRI on small animals: application to physiology, pathophysiology, and cognition. NMR Biomed. 20, 522-545.

Vernet-Maury, E., 1980. Trimethyl-thiazoline in fox feces: a natural alarming substance for the rat. In: Van der Starre H (Ed.), 7 ed. IRL, Washington, p. 407.

Wilson, D.A., 2000. Comparison of odor receptive field plasticity in the rat olfactory bulb and anterior piriform cortex. J.Neurophysiol. 84, 3036-3042.

Wilson, D.A., Stevenson, R.J., 2003. The fundamental role of memory in olfactory perception. Trends Neurosci. 26, 243-247.

Woods, R.P., Grafton, S.T., Holmes, C.J., Cherry, S.R., Mazziotta, J.C., 1998. Automated image registration: I. General methods and intrasubject, intramodality validation. Journal of Computer Assisted Tomography 22, 139-152.

Xu, F., Liu, N., Kida, I., Rothman, D.L., Hyder, F., Shepherd, G.M., 2003. Odor maps of aldehydes and esters revealed by functional MRI in the glomerular layer of the mouse olfactory bulb. Proc.Natl.Acad.Sci.U.S.A 100, 11029-11034.

Xu, F., Schaefer, M., Kida, I., Schafer, J., Liu, N., Rothman, D.L., Hyder, F., Restrepo, D., Shepherd, G.M., 2005. Simultaneous activation of mouse main and accessory olfactory bulbs by odors or pheromones. J.Comp Neurol. 489, 491-500.

Chapitre III

Conclusion générale et perspectives

Dans les deux premiers volets du travail réalisé durant cette thèse, nous nous sommes focalisés sur les développements méthodologiques nécessaires à l'utilisation de MEMRI comme méthode d'imagerie fonctionnelle de l'olfaction dans des régions cérébrales plus profondes que le bulbe olfactif chez le rat.

Le premier volet a porté sur l'effet de la dose de Mn injectée dans les narines de rats à la fois sur la perception olfactive et sur le signal mesurable en IRM. Cette étude a montré une altération rapide de la perception olfactive après l'injection de Mn. Elle a, par ailleurs, montré que la relation entre la dose de Mn injectée et le signal détectable en IRM n'était pas linéaire dans la gamme étudiée (1-8 µmol). Nous avons ainsi défini une dose de Mn (0.3 µmol) préservant la perception olfactive tout en assurant un contraste reproductible dans le cortex olfactif primaire.

Le deuxième volet a concerné l'analyse des images MEMRI et plus particulièrement leur normalisation spatiale et en intensité. Aucune méthode générique de normalisation n'émergeant de la littérature, nous avons proposé et validé un algorithme itératif de normalisation de ce type de données. Nous avons, dans ce travail, optimisé le modèle de déformation utilisé pour la normalisation spatiale ainsi que le choix de la région de référence pour la normalisation en intensité. Cette étude a montré qu'un traitement approprié des

données MEMRI révèle l'accumulation de Mn depuis le bulbe olfactif jusqu'au cortex entorhinal postérieur, 48 h après son injection.

S'appuyant sur ces développements méthodologiques, le troisième volet de la thèse a visé à utiliser MEMRI pour mettre en évidence des variations du traitement d'odeurs signifiantes dans le cortex olfactif primaire. Cette étude a montré que le traitement d'une odeur de prédateur est différent de celui d'autres odeurs. Ce résultat est confirmé par les expériences d'immunomarquage Fos. La comparaison des résultats de MEMRI et de Fos nous a conduits à suggérer que le traitement spécifique d'une odeur de prédateur dans le cortex olfactif primaire englobe deux phénomènes distincts. Le premier, détectable en Fos mais pas en MEMRI, concerne le nombre de neurones recrutés par une stimulation olfactive. Le second, non détectable en Fos et mis en évidence par MEMRI, est l'intensité de l'activation de ces neurones. Nous avons ainsi mis en évidence que la taille des populations neuronales recrutées est plus importante pour une odeur de prédateur que pour des odeurs moins signifiantes. D'autre part, pour cette odeur de prédateur, une asymétrie entre les hémisphères cérébraux existe en termes d'intensité d'activation. La méthode idéale qui fournirait l'image globale d'une population de neurones fondée sur l'activité temporelle de chacun d'entre eux n'existant pas, MEMRI permet de démasquer des phénomènes non détectables avec d'autres techniques d'imagerie fonctionnelle comme Fos.

Ce travail a confirmé la pertinence de l'utilisation de MEMRI pour l'étude des mécanismes cérébraux impliqués dans le traitement des odeurs. Nos résultats ont montré qu'il est possible, après injection intra-nasale du Mn, de détecter des variations fonctionnelles d'activité jusque dans la partie caudale du cortex olfactif primaire. Cependant, nous avons observé une dilution de la quantité de Mn détectable le long des voies olfactives. Ce phénomène s'explique probablement par la déperdition de Mn lors du franchissement des synapses. La toxicité du Mn limitant la quantité maximale qu'il est possible d'injecter sans dégrader la perception olfactive, il paraît difficile d'utiliser cette voie d'administration pour étudier l'effet d'odeurs sur des régions cérébrales encore plus profondes. Il a récemment été montré qu'injecter plusieurs petites quantités de Mn entrainait moins d'effets toxiques qu'une unique injection (Soria *et al.*, 2008). Cette stratégie permettrait d'injecter plus de Mn tout en préservant la perception olfactive. Cependant, le choix des fenêtres temporelles consacrées aux stimulations olfactives et à l'imagerie seront des degrés de libertés supplémentaires à optimiser.

Travailler sur d'autres voies d'administration du Mn pourrait permettre d'améliorer l'utilisation de MEMRI pour étudier l'olfaction dans des régions plus profondes que le cortex olfactif primaire. Dans l'absolu, la mise à disposition optimale du Mn serait la plus globale, homogène et instantanée possible. Des équipes travaillent actuellement sur des protocoles moins invasifs que l'injection d'agent hyper-osmotique pour perméabiliser la BHE (à l'aide d'anticorps monoclonaux par exemple, Lu *et al.*, 2010), cependant, aucune méthode ne s'avère encore satisfaisante. L'injection intracérébrale permettrait quant à elle de cibler des structures d'intérêt mais nécessiterait de forts *a priori* sur celles-ci. Cependant, ces deux voies d'administration restent particulièrement invasives. L'administration systémique, sans rupture de la BHE, a été récemment utilisée pour l'étude de régions fonctionnellement impliquées dans l'audition (Yu *et al.*, 2005). Il a également été montré que l'injection systémique du Mn via une pompe osmotique provoque des effets toxiques minimes et permet une accumulation de Mn suffisante pour être détectable en IRM (Eschenko *et al.*, 2010a). Cette stratégie d'administration du Mn paraît la plus adaptée pour étudier, dans les conditions les plus proches de la perception naturelle chez un animal vigile, les régions cérébrales plus profondes que le cortex olfactif primaire impliquées dans le traitement d'odeurs.

Il serait, par ailleurs, possible d'améliorer la technique MEMRI par des progrès en méthodologie IRM. Pour détecter de plus faibles variations de concentration de Mn, il est nécessaire d'augmenter le RSB. Si une solution évidente consiste à augmenter l'amplitude de la polarisation magnétique en utilisant des aimants plus intenses, l'augmentation conjointe du T_1 (Fischer *et al.*, 1990) atténue le gain en RSB. Une solution complémentaire consiste à utiliser un réseau d'antennes réceptrices qui, comme les antennes volumiques, permettent d'imager l'ensemble du cerveau mais en réduisant le bruit recueilli (Cohen-Adad *et al.*, 2011). Par ailleurs, à notre connaissance, les nombreuses séquences pondérées T_1 (par exemple SSFP, MDEFT, RARE, U-FLARE) n'ont pas été comparées en termes de RSB. Actuellement, il n'est donc pas possible de savoir quelles sont les séquences optimales pour les applications MEMRI. Enfin, il a été proposé récemment (Chuang et Koretsky, 2006) de remplacer les séquences pondérées T_1 par des cartes paramétriques T_1. Directement quantitatives, elles ne nécessitent pas de normalisation en intensité. Là encore, la comparaison de l'imagerie « pondérée » et de l'imagerie « quantitative » en termes de RSB reste à traiter pour choisir la meilleure stratégie.

Au-delà des développements méthodologiques liés au MEMRI, ce travail apporte un certain nombre d'éléments concernant le traitement cérébral d'odeurs signifiantes. Nous avons mis en évidence qu'un traitement différencié des odeurs était détectable après 48h de stimulations olfactives intermittentes. De plus, nous avons montré qu'il existe une asymétrie entre les hémisphères cérébraux en termes d'intensité d'activation. Le signal MEMRI dans l'hémisphère gauche est plus faible lorsqu'une odeur de prédateur est utilisée comme stimulation olfactive. Deux hypothèses peuvent expliquer ce résultat. La première est un transport plus rapide du Mn du cortex olfactif primaire vers d'autres régions cérébrales où il se retrouve en quantité insuffisante pour être détecté. La seconde est la mise en jeu de mécanismes d'inhibitions dans le bulbe olfactif (Arevian *et al.*, 2008) qui permettent d'augmenter la discrimination des odeurs (Abraham *et al.*, 2010). Ces mécanismes inhibiteurs diminueraient la quantité globale de Mn entrant dans le cortex olfactif primaire. L'étude de la dynamique de l'entrée du Mn dans les voies olfactives en fonction des différentes odeurs permettrait de valider ou d'infirmer ces hypothèses. Les expériences complémentaires à réaliser nécessiteraient de faire varier le délai entre l'injection du Mn et l'acquisition IRM.

Dans ce travail, nous avons étudié des odeurs ayant trait à la survie et à la prise alimentaire. Parmi les odeurs naturelles véhiculant un message clair pour les animaux, celles liées à la reproduction sont également fortement signifiantes (Rampin *et al.*, 2006). L'étude de Rampin *et al.* (2006) a montré que l'odeur de fèces de femelles en œstrus induit des érections chez le rat. Quand il s'agit de renarde en œstrus, l'odeur de fèces induit simultanément une érection et des comportements de peur. Seuls les comportements de peur sont provoqués par l'odeur de fèces de renarde en dioestrus. Il serait fort intéressant d'étudier en MEMRI, dans les conditions expérimentales que nous avons définies dans cette thèse, le traitement cérébral d'odeurs de fèces de renarde en dioestrus et en œstrus, car ces derniers véhiculent plusieurs messages signifiants pour le rat.

Enfin, puisque l'anesthésie modifie l'activité cérébrale, nous avons étudié l'olfaction sur animal vigile. Cependant, des études en cours montrent qu'une réponse électrophysiologique des neurones du tubercule olfactif à des odeurs biologiquement signifiantes persiste sous anesthésie. Des activations olfactives sont donc certainement mesurables au-delà du bulbe olfactif sous anesthésie. Elles pourraient être mises en évidence par « dynamic activity induced manganese dependent contrast magnetic resonance imaging » (Aoki *et al.*, 2002) en stimulant l'animal dans l'aimant et en acquérant de manière continue des images pondérées

T_1. Ceci offre une perspective supplémentaire pour l'étude de l'olfaction *via* MEMRI dans le cortex olfactif primaire.

Cette thèse avait pour but d'optimiser et d'utiliser MEMRI pour l'étude du traitement cérébral d'odeurs signifiantes dans les conditions les plus proches possibles de la perception naturelle chez un animal vigile. Elle a apporté un certain nombre de nouvelles connaissances que ce soit dans le domaine de la méthodologie MEMRI (articles 1 et 2) que dans celui de la neurobiologie de l'olfaction (article 3), qui ouvrent la voie à une meilleure compréhension du traitement cérébral des odeurs.

Bibliographie

Abraham, N.M., Egger, V., Shimshek, D.R., Renden, R., Fukunaga, I., Sprengel, R., Seeburg, P.H., Klugmann, M., Margrie, T.W., Schaefer, A.T., Kuner, T., 2010. Synaptic inhibition in the olfactory bulb accelerates odor discrimination in mice. Neuron 65, 399-411.

Adrian, E.D., 1942. Olfactory reactions in the brain of the hedgehog. J.Physiol 100, 459-473.

Alexander, G.E., Crutcher, M.D., 1990. Functional architecture of basal ganglia circuits: neural substrates of parallel processing. Trends Neurosci. 13, 266-271.

Alkire, M.T., Hudetz, A.G., Tononi, G., 2008. Consciousness and anesthesia. Science 322, 876-880.

Ambroggi, F., Ishikawa, A., Fields, H.L., Nicola, S.M., 2008. Basolateral amygdala neurons facilitate reward-seeking behavior by exciting nucleus accumbens neurons. Neuron 59, 648-661.

Anderson, A.K., Christoff, K., Stappen, I., Panitz, D., Ghahremani, D.G., Glover, G., Gabrieli, J.D., Sobel, N., 2003. Dissociated neural representations of intensity and valence in human olfaction. Nat.Neurosci. 6, 196-202.

Aoki, I., Naruse, S., Tanaka, C., 2004a. Manganese-enhanced magnetic resonance imaging (MEMRI) of brain activity and applications to early detection of brain ischemia. NMR Biomed. 17, 569-580.

Aoki, I., Tanaka, C., Takegami, T., Ebisu, T., Umeda, M., Fukunaga, M., Fukuda, K., Silva, A.C., Koretsky, A.P., Naruse, S., 2002. Dynamic activity-induced manganese-dependent contrast magnetic resonance imaging (DAIM MRI). Magnetic Resonance in Medicine 48, 927-933.

Aoki, I., Wu, Y.J.L., Silva, A.C., Lynch, R.M., Koretsky, A.P., 2004b. In vivo detection of neuroarchitecture in the rodent brain using manganese-enhanced MRI. NeuroImage 22, 1046-1059.

Apicella, A., Yuan, Q., Scanziani, M., Isaacson, J.S., 2010. Pyramidal cells in piriform cortex receive convergent input from distinct olfactory bulb glomeruli. J.Neurosci. 30, 14255-14260.

Arevian, A.C., Kapoor, V., Urban, N.N., 2008. Activity-dependent gating of lateral inhibition in the mouse olfactory bulb. Nat.Neurosci. 11, 80-87.

Bandettini, P.A., Wong, E.C., Hinks, R.S., Tikofsky, R.S., Hyde, J.S., 1992. Time course EPI of human brain function during task activation. Magn Reson.Med. 25, 390-397.

Bengtsson, S., Berglund, H., Gulyas, B., Cohen, E., Savic, I., 2001. Brain activation during odor perception in males and females. Neuroreport 12, 2027-2033.

Bernabeu, R., Thiriet, N., Zwiller, J., Di, S.G., 2006. Lesion of the lateral entorhinal cortex amplifies odor-induced expression of c-fos, junB, and zif 268 mRNA in rat brain. Synapse 59, 135-143.

Biella, G., De Curtis, M., 2000. Olfactory inputs activate the medial entorhinal cortex via the hippocampus. J.Neurophysiol. 83, 1924-1931.

Blanchard, D.C., Canteras, N.S., Markham, C.M., Pentkowski, N.S., Blanchard, R.J., 2005. Lesions of structures showing FOS expression to cat presentation: effects on responsivity to a Cat, Cat odor, and nonpredator threat. Neurosci.Biobehav.Rev. 29, 1243-1253.

Brand, G., Millot, J.L., Henquell, D., 2001. Complexity of olfactory lateralization processes revealed by functional imaging: a review. Neurosci.Biobehav.Rev. 25, 159-166.

Buck, L., Axel, R., 1991. A novel multigene family may encode odorant receptors: a molecular basis for odor recognition. Cell 65, 175-187.

Bullitt, E., 1990. Expression of c-fos-like protein as a marker for neuronal activity following noxious stimulation in the rat. J.Comp Neurol. 296, 517-530.

Buonviso, N., Revial, M.F., Jourdan, F., 1991. The Projections of Mitral Cells from Small Local Regions of the Olfactory Bulb: An Anterograde Tracing Study Using PHA-L (Phaseolus vulgaris Leucoagglutinin). Eur.J.Neurosci. 3, 493-500.

Butler, R.K., Sharko, A.C., Oliver, E.M., Brito-Vargas, P., Kaigler, K.F., Fadel, J.R., Wilson, M.A., 2011. Activation of phenotypically-distinct neuronal subpopulations of the rat amygdala following exposure to predator odor. Neuroscience 175, 133-144.

Buxton, R.B., Uludag, K., Dubowitz, D.J., Liu, T.T., 2004. Modeling the hemodynamic response to brain activation. Neuroimage. 23 Suppl 1, S220-S233.

Buxton, R.B., Wong, E.C., Frank, L.R., 1998. Dynamics of blood flow and oxygenation changes during brain activation: the balloon model. Magn Reson.Med. 39, 855-864.

Cador, M., Robbins, T.W., Everitt, B.J., 1989. Involvement of the amygdala in stimulus-reward associations: interaction with the ventral striatum. Neuroscience 30, 77-86.

Canals, S., Beyerlein, M., Keller, A.L., Murayama, Y., Logothetis, N.K., 2008. Magnetic resonance imaging of cortical connectivity in vivo. NeuroImage 40, 458-472.

Cassara, A.M., Hagberg, G.E., Bianciardi, M., Migliore, M., Maraviglia, B., 2008. Realistic simulations of neuronal activity: a contribution to the debate on direct detection of neuronal currents by MRI. Neuroimage. 39, 87-106.

Chen, W., Shields, J., Huang, W., King, J.A., 2009. Female fear: influence of estrus cycle on behavioral response and neuronal activation. Behav.Brain Res. 201, 8-13.

Chen, W., Tenney, J., Kulkarni, P., King, J.A., 2007. Imaging unconditioned fear response with manganese-enhanced MRI (MEMRI). Neuroimage. 37, 221-229.

Chuang, K.H., Koretsky, A., 2006. Improved neuronal tract tracing using manganese enhanced magnetic resonance imaging with fast T(1) mapping. Magn Reson.Med. 55, 604-611.

Chuang, K.H., Koretsky, A.P., Sotak, C.H., 2009a. Temporal changes in the T1 and T2 relaxation rates (DeltaR1 and DeltaR2) in the rat brain are consistent with the tissue-clearance rates of elemental manganese. Magn Reson.Med. 61, 1528-1532.

Chuang, K.H., Lee, J.H., Silva, A.C., Belluscio, L., Koretsky, A.P., 2009b. Manganese enhanced MRI reveals functional circuitry in response to odorant stimuli. Neuroimage. 44, 363-372.

Cloquet, H., 1821. Osphrésiologie, Méquignon-Marvis ed, Paris.

Cohen-Adad, J., Mareyam, A., Keil, B., Polimeni, J.R., Wald, L.L., 2011. 32-Channel RF coil optimized for brain and cervical spinal cord at 3 T. Magn Reson.Med. In press.

Couper, J., 1837. On the effects of black oxide of manganese when inhaled into the lungs. Br Ann Med Pharm 1, 41-42.

Cross, D.J., Flexman, J.A., Anzai, Y., Maravilla, K.R., Minoshima, S., 2008. Age-related decrease in axonal transport measured by MR imaging in vivo. Neuroimage. 39, 915-926.

Cross, D.J., Flexman, J.A., Anzai, Y., Morrow, T.J., Maravilla, K.R., Minoshima, S., 2006. In vivo imaging of functional disruption, recovery and alteration in rat olfactory circuitry after lesion. Neuroimage. 32, 1265-1272.

Cross, D.J., Minoshima, S., Anzai, Y., Flexman, J.A., Keogh, B.P., Kim, Y., Maravilla, K.R., 2004. Statistical mapping of functional olfactory connections of the rat brain in vivo. Neuroimage. 23, 1326-1335.

Darquie, A., Poline, J.B., Poupon, C., Saint-Jalmes, H., Le, B.D., 2001. Transient decrease in water diffusion observed in human occipital cortex during visual stimulation. Proc.Natl.Acad.Sci.U.S.A 98, 9391-9395.

Datiche, F., Cattarelli, M., 1996. Reciprocal and topographic connections between the piriform and prefrontal cortices in the rat: a tracing study using the B subunit of the cholera toxin. Brain Res.Bull. 41, 391-398.

Datiche, F., Roullet, F., Cattarelli, M., 2001. Expression of Fos in the piriform cortex after acquisition of olfactory learning: an immunohistochemical study in the rat. Brain Res.Bull. 55, 95-99.

De Groof, G., Gwinner, H., Steiger, S., Kempenaers, B., Van der Linden, A., 2010. Neural correlates of behavioural olfactory sensitivity changes seasonally in European starlings. PLoS.One. 5, e14337.

De Olmos, J.S., Beltramino, C.A., Alheid, G., 2004. Amygdala and extended amygdala of the rat: a cytoarchitectonical, fibroarchitectonical, and Chemoarchitectonical survey. The rat nervous system., Academic Press ed, San Diego, pp. 509-603.

De Olmos, J., Hardy, H., Heimer, L., 1978. The afferent connections of the main and the accessory olfactory bulb formations in the rat: an experimental HRP-study. J.Comp Neurol. 181, 213-244.

Deniau, J.M., Menetrey, A., Charpier, S., 1996. The lamellar organization of the rat substantia nigra pars reticulata: segregated patterns of striatal afferents and relationship to the topography of corticostriatal projections. Neuroscience 73, 761-781.

Deurveilher, S., Semba, K., 2006. Mapping sleep-wake control with the transcription factor c-Fos. In: Springer (Ed.), Immediate early genes in sensory processing, cognitive performance, and neurological disorders, Springer ed, New York, pp. 113-136.

Dielenberg, R.A., Hunt, G.E., McGregor, I.S., 2001. "When a rat smells a cat": the distribution of Fos immunoreactivity in rat brain following exposure to a predatory odor. Neuroscience 104, 1085-1097.

Dielenberg, R.A., McGregor, I.S., 2001. Defensive behavior in rats towards predatory odors: a review. Neurosci.Biobehav.Rev. 25, 597-609.

Dodd, C.A., Ward, D.L., Klein, B.G., 2005. Basal Ganglia accumulation and motor assessment following manganese chloride exposure in the C57BL/6 mouse. Int.J.Toxicol. 24, 389-397.

Doty, R.L., 2003. Introduction and historical perspective. In: Marcel Dekker (Ed.), Handbook of Olfaction and Gustation, Marcel Dekker ed, New York, p. XV-XLV.

Ehrlich, I., Humeau, Y., Grenier, F., Ciocchi, S., Herry, C., Luthi, A., 2009. Amygdala inhibitory circuits and the control of fear memory. Neuron 62, 757-771.

Eichenbaum, H., Schoenbaum, G., Young, B., Bunsey, M., 1996. Functional organization of the hippocampal memory system. Proc.Natl.Acad.Sci.U.S.A 93, 13500-13507.

Eschenko, O., Canals, S., Simanova, I., Beyerlein, M., Murayama, Y., Logothetis, N.K., 2010a. Mapping of functional brain activity in freely behaving rats during voluntary running using manganese-enhanced MRI: Implication for longitudinal studies. NeuroImage 49, 2544-2555.

Eschenko, O., Canals, S., Simanova, I., Logothetis, N.K., 2010b. Behavioral, electrophysiological and histopathological consequences of systemic manganese administration in MEMRI. Magn Reson.Imaging 28, 1165-1174.

Everitt, B.J., Cador, M., Robbins, T.W., 1989. Interactions between the amygdala and ventral striatum in stimulus-reward associations: studies using a second-order schedule of sexual reinforcement. Neuroscience 30, 63-75.

Febo, M., Pira, A.S., 2011. Increased BOLD activation to predator stressor in subiculum and midbrain of amphetamine-sensitized maternal rats. Brain Res. 1382, 118-127.

Febo, M., Shields, J., Ferris, C.F., King, J.A., 2009. Oxytocin modulates unconditioned fear response in lactating dams: an fMRI study. Brain Res. 1302, 183-193.

Fendt, M., Endres, T., Apfelbach, R., 2003. Temporary inactivation of the bed nucleus of the stria terminalis but not of the amygdala blocks freezing induced by trimethylthiazoline, a component of fox feces. J.Neurosci. 23, 23-28.

Ferris, C.F., Febo, M., Luo, F., Schmidt, K., Brevard, M., Harder, J.A., Kulkarni, P., Messenger, T., King, J.A., 2006. Functional magnetic resonance imaging in conscious animals: a new tool in behavioural neuroscience research. J.Neuroendocrinol. 18, 307-318.

Fischer, H.W., Rinck, P.A., Van, H.Y., Muller, R.N., 1990. Nuclear relaxation of human brain gray and white matter: analysis of field dependence and implications for MRI. Magn Reson.Med. 16, 317-334.

Garnero, L., 2001. Imagerie cérébrale fonctionnelle : Techniques et applications, cours. http://www.labos.upmc.fr/center-meg/media/cours%20Line/CoursLine01.pdf.

Ghosh, S., Larson, S.D., Hefzi, H., Marnoy, Z., Cutforth, T., Dokka, K., Baldwin, K.K., 2011. Sensory maps in the olfactory cortex defined by long-range viral tracing of single neurons. Nature 472, 217-220.

Gilad, Y., Przeworski, M., Lancet, D., 2004. Loss of olfactory receptor genes coincides with the acquisition of full trichromatic vision in primates. PLoS.Biol. 2, E5.

Gillet, B., Po, C., Dupont, D., Sébrié, C., Méric, P., 2010. Manganèse et imagerie de résonance magnétique du développement cérébral. Comptes Rendus Chimie 13, 459-465.

Golgi, C., 1875. Sulla fina strruttura dei bulbi olfacrorii. Rivista Sperimentale di Freniatria e Medicina Legale 1, 405-425.

Gottfried, J.A., 2006. Smell: central nervous processing. Adv.Otorhinolaryngol. 63, 44-69.

Gottfried, J.A., Smith, A.P., Rugg, M.D., Dolan, R.J., 2004. Remembrance of odors past: human olfactory cortex in cross-modal recognition memory. Neuron 42, 687-695.

Guthrie, K.M., Gall, C.M., 1995. Functional mapping of odor-activated neurons in the olfactory bulb. Chem.Senses 20, 271-282.

Haberly, L.B., 2001. Parallel-distributed processing in olfactory cortex: new insights from morphological and physiological analysis of neuronal circuitry. Chem.Senses 26, 551-576.

Haberly, L.B., Price, J.L., 1977. The axonal projection patterns of the mitral and tufted cells of the olfactory bulb in the rat. Brain Res. 129, 152-157.

Haberly, L.B., Price, J.L., 1978. Association and commissural fiber systems of the olfactory cortex of the rat. J.Comp Neurol. 178, 711-740.

Hajnal, J.V., Saeed, N., Soar, E.J., Oatridge, A., Young, I.R., Bydder, G.M., 1995. A registration and interpolation procedure for subvoxel matching of serially acquired MR images. J.Comput.Assist.Tomogr. 19, 289-296.

Henriksson, J., Tjalve, H., 2000. Manganese taken up into the CNS via the olfactory pathway in rats affects astrocytes. Toxicol.Sci. 55, 392-398.

Holley, A., Mac, L.P., 1977. [Transduction and coding of olfactory information]. J.Physiol (Paris) 73, 725-848.

Huang, W., Heffernan, M.E., Li, Z., Zhang, N., Overstreet, D.H., King, J.A., 2011. Fear induced neuronal alterations in a genetic model of depression: an fMRI study on awake animals. Neurosci.Lett. 489, 74-78.

Ikemoto, S., 2007. Dopamine reward circuitry: two projection systems from the ventral midbrain to the nucleus accumbens-olfactory tubercle complex. Brain Res.Rev. 56, 27-78.

Illig, K.R., Haberly, L.B., 2003. Odor-evoked activity is spatially distributed in piriform cortex. J.Comp Neurol. 457, 361-373.

Ino, T., Yasui, Y., Itoh, K., Nomura, S., Akiguchi, T., Kameyama, M., Mizuno, N., 1987. Direct projections from Ammon's horn to the septum in the cat. Exp.Brain Res. 68, 179-188.

Inui-Yamamoto, C., Yoshioka, Y., Inui, T., Sasaki, K.S., Ooi, Y., Ueda, K., Seiyama, A., Ohzawa, I., 2010. The brain mapping of the retrieval of conditioned taste aversion memory using manganese-enhanced magnetic resonance imaging in rats. Neuroscience 167, 199-204.

Kang, N., Baum, M.J., Cherry, J.A., 2009. A direct main olfactory bulb projection to the 'vomeronasal' amygdala in female mice selectively responds to volatile pheromones from males. Eur.J.Neurosci. 29, 624-634.

Kelliher, K.R., Liu, Y.C., Baum, M.J., Sachs, B.D., 1999. Neuronal Fos activation in olfactory bulb and forebrain of male rats having erections in the presence of inaccessible estrous females. Neuroscience 92, 1025-1033.

Kida, I., Xu, F., Shulman, R.G., Hyder, F., 2002. Mapping at glomerular resolution: fMRI of rat olfactory bulb. Magn Reson.Med. 48, 570-576.

Kim, J., Choi, I.Y., Michaelis, M.L., Lee, P., 2011. Quantitative in vivo measurement of early axonal transport deficits in a triple transgenic mouse model of Alzheimer's disease using manganese-enhanced MRI. Neuroimage. 56, 1286-1292.

Kippin, T.E., Cain, S.W., Pfaus, J.G., 2003. Estrous odors and sexually conditioned neutral odors activate separate neural pathways in the male rat. Neuroscience 117, 971-979.

Kivity, S., Tsarfaty, G., gmon-Levin, N., Blank, M., Manor, D., Konen, E., Chapman, J., Reichlin, M., Wasson, C., Shoenfeld, Y., Kushnir, T., 2010. Abnormal olfactory function demonstrated by manganese-enhanced MRI in mice with experimental neuropsychiatric lupus. Ann.N.Y.Acad.Sci. 1193, 70-77.

Klein, A., Andersson, J., Ardekani, B.A., Ashburner, J., Avants, B., Chiang, M.C., Christensen, G.E., Collins, D.L., Gee, J., Hellier, P., Song, J.H., Jenkinson, M., Lepage, C., Rueckert, D., Thompson, P., Vercauteren, T., Woods, R.P., Mann, J.J., Parsey, R.V., 2009. Evaluation of 14 nonlinear deformation algorithms applied to human brain MRI registration. Neuroimage. 46, 786-802.

Kwong, K.K., Belliveau, J.W., Chesler, D.A., Goldberg, I.E., Weisskoff, R.M., Poncelet, B.P., Kennedy, D.N., Hoppel, B.E., Cohen, M.S., Turner, R., ., 1992. Dynamic magnetic resonance imaging of human brain activity during primary sensory stimulation. Proc.Natl.Acad.Sci.U.S.A 89, 5675-5679.

Laget, P., 1973. Eléments de neuro-anatomie fonctionnelle: cervelet, mésencéphale et diencéphale, Masson ed, Paris.

LeDoux, J., 2003. The emotional brain, fear, and the amygdala. Cell Mol.Neurobiol. 23, 727-738.

Lei, H., Mooney, R., Katz, L.C., 2006. Synaptic integration of olfactory information in mouse anterior olfactory nucleus. J.Neurosci. 26, 12023-12032.

Levy, L.M., Henkin, R.I., Hutter, A., Lin, C.S., Martins, D., Schellinger, D., 1997. Functional MRI of human olfaction. J.Comput.Assist.Tomogr. 21, 849-856.

Levy, L.M., Henkin, R.I., Lin, C.S., Hutter, A., Schellinger, D., 1999. Odor memory induces brain activation as measured by functional MRI. J.Comput.Assist.Tomogr. 23, 487-498.

Lin, Y.J., Koretsky, A.P., 1997. Manganese ion enhances T-1-weighted MRI during brain activation: An approach to direct imaging of brain function. Magnetic Resonance in Medicine 38, 378-388.

Litaudon, P., Amat, C., Bertrand, B., Vigouroux, M., Buonviso, N., 2003. Piriform cortex functional heterogeneity revealed by cellular responses to odours. Eur.J.Neurosci. 17, 2457-2461.

Lledo, P.M., Gheusi, G., Vincent, J.D., 2005. Information processing in the mammalian olfactory system. Physiol Rev. 85, 281-317.

Lu, H., Demny, S., Zuo, Y., Rea, W., Wang, L., Chefer, S.I., Vaupel, D.B., Yang, Y., Stein, E.A., 2010. Temporary disruption of the rat blood-brain barrier with a monoclonal antibody: a novel method for dynamic manganese-enhanced MRI. Neuroimage. 50, 7-14.

Luskin, M.B., Price, J.L., 1982. The distribution of axon collaterals from the olfactory bulb and the nucleus of the horizontal limb of the diagonal band to the olfactory cortex, demonstrated by double retrograde labeling techniques. J.Comp Neurol. 209, 249-263.

Martel, K.L., Baum, M.J., 2009. A centrifugal pathway to the mouse accessory olfactory bulb from the medial amygdala conveys gender-specific volatile pheromonal signals. Eur.J.Neurosci. 29, 368-376.

Martin, C., 2007. Anaesthetic use in animal models for neuroimaging. Neuroimage. 38, 1-2.

Martin, C., Grenier, D., Thevenet, M., Vigouroux, M., Bertrand, B., Janier, M., Ravel, N., Litaudon, P., 2007. fMRI visualization of transient activations in the rat olfactory bulb using short odor stimulations. Neuroimage. 36, 1288-1293.

Massimini, M., Ferrarelli, F., Huber, R., Esser, S.K., Singh, H., Tononi, G., 2005. Breakdown of cortical effective connectivity during sleep. Science 309, 2228-2232.

Maurin, Y., Banrezes, B., Menetrey, A., Mailly, P., Deniau, J.M., 1999. Three-dimensional distribution of nigrostriatal neurons in the rat: relation to the topography of striatonigral projections. Neuroscience 91, 891-909.

McClintock, M.K., 1971. Menstrual synchorony and suppression. Nature 229, 244-245.

Mendonca-Dias, M.H., Gaggelli, E., Lauterbur, P.C., 1983. Paramagnetic contrast agents in nuclear magnetic resonance medical imaging. Semin.Nucl.Med. 13, 364-376.

Merzenich, M.M., Knight, P.L., Roth, G.L., 1975. Representation of cochlea within primary auditory cortex in the cat. J.Neurophysiol. 38, 231-249.

Mombaerts, P., 2004. Odorant receptor gene choice in olfactory sensory neurons: the one receptor-one neuron hypothesis revisited. Curr.Opin.Neurobiol. 14, 31-36.

Morgan, J.I., Cohen, D.R., Hempstead, J.L., Curran, T., 1987. Mapping patterns of c-fos expression in the central nervous system after seizure. Science 237, 192-197.

Mouly, A.M., Di, S.G., 2006. Entorhinal cortex stimulation modulates amygdala and piriform cortex responses to olfactory bulb inputs in the rat. Neuroscience 137, 1131-1141.

Mouly, A.M., Fort, A., Ben-Boutayab, N., Gervais, R., 2001. Olfactory learning induces differential long-lasting changes in rat central olfactory pathways. Neuroscience 102, 11-21.

Muller, R., Bravo, R., Burckhardt, J., Curran, T., 1984. Induction of c-fos gene and protein by growth factors precedes activation of c-myc. Nature 312, 716-720.

Murray, E.A., Richmond, B.J., 2001. Role of perirhinal cortex in object perception, memory, and associations. Curr.Opin.Neurobiol. 11, 188-193.

Nemitz, J.W., Goldberg, S.J., 1983. Neuronal responses of rat pyriform cortex to odor stimulation: an extracellular and intracellular study. J.Neurophysiol. 49, 188-203.

Newman, R., Winans, S.S., 1980. An experimental study of the ventral striatum of the golden hamster. II. Neuronal connections of the olfactory tubercle. J.Comp Neurol. 191, 193-212.

Nieuwenhuys, R., 1967. Comparative anatomy of olfactory centres and tracts. Prog.Brain Res. 23, 1-64.

Nordhoy, W., Anthonsen, H.W., Bruvold, M., Brurok, H., Skarra, S., Krane, J., Jynge, P., 2004. Intracellular manganese ions provide strong T1 relaxation in rat myocardium. Magn Reson.Med. 52, 506-514.

Ogawa, S., Lee, T.M., 1990. Magnetic resonance imaging of blood vessels at high fields: in vivo and in vitro measurements and image simulation. Magn Reson.Med. 16, 9-18.

Ottoson , D., 1955. Analysis of the electrical activity of the olfactory epithelium. Acta Physiol Scand.Suppl 35, 1-83.

Pautler, R.G., Koretsky, A.P., 2002. Tracing odor-induced activation in the olfactory bulbs of mice using manganese-enhanced magnetic resonance imaging. Neuroimage. 16, 441-448.

Pautler, R.G., Mongeau, R., Jacobs, R.E., 2003. In vivo trans-synaptic tract tracing from the murine striatum and amygdala utilizing manganese enhanced MRI (MEMRI). Magn Reson.Med. 50, 33-39.

Pautler, R.G., Silva, A.C., Koretsky, A.P., 1998. In vivo neuronal tract tracing using manganese-enhanced magnetic resonance imaging. Magn Reson.Med. 40, 740-748.

Petridou, N., Plenz, D., Silva, A.C., Loew, M., Bodurka, J., Bandettini, P.A., 2006. Direct magnetic resonance detection of neuronal electrical activity. Proc.Natl.Acad.Sci.U.S.A 103, 16015-16020.

Philpott, C.M., Bennett, A., Murty, G.E., 2008. A brief history of olfaction and olfactometry. J.Laryngol.Otol. 122, 657-662.

Powell , T.P., Cowan , W.M., Raisman , G., 1963. Olfactory relationships of the diencephalon. Nature 199, 710-712.

Price, J.L., Slotnick, B.M., 1983. Dual olfactory representation in the rat thalamus: an anatomical and electrophysiological study. J.Comp Neurol. 215, 63-77.

Rampin, O., Jerome, N., Briant, C., Boue, F., Maurin, Y., 2006. Are oestrus odours species specific? Behav.Brain Res. 172, 169-172.

Rennaker, R.L., Chen, C.F., Ruyle, A.M., Sloan, A.M., Wilson, D.A., 2007. Spatial and temporal distribution of odorant-evoked activity in the piriform cortex. J.Neurosci. 27, 1534-1542.

Ressler, K.J., Sullivan, S.L., Buck, L.B., 1994. Information coding in the olfactory system: evidence for a stereotyped and highly organized epitope map in the olfactory bulb. Cell 79, 1245-1255.

Rolls, E.T., Kringelbach, M.L., de, A., I, 2003. Different representations of pleasant and unpleasant odours in the human brain. Eur.J.Neurosci. 18, 695-703.

Rolls, E.T., Rolls, J.H., 1997. Olfactory sensory-specific satiety in humans. Physiol Behav. 61, 461-473.

Royet, J.P., Zald, D., Versace, R., Costes, N., Lavenne, F., Koenig, O., Gervais, R., 2000. Emotional responses to pleasant and unpleasant olfactory, visual, and auditory stimuli: a positron emission tomography study. J.Neurosci. 20, 7752-7759.

Sallaz, M., Jourdan, F., 1993. C-fos expression and 2-deoxyglucose uptake in the olfactory bulb of odour-stimulated awake rats. Neuroreport 4, 55-58.

Sanderson, K.J., 1971. The projection of the visual field to the lateral geniculate and medial interlaminar nuclei in the cat. J.Comp Neurol. 143, 101-108.

Savic, I., Gulyas, B., 2000. PET shows that odors are processed both ipsilaterally and contralaterally to the stimulated nostril. Neuroreport 11, 2861-2866.

Savic, I., Gulyas, B., Larsson, M., Roland, P., 2000. Olfactory functions are mediated by parallel and hierarchical processing. Neuron 26, 735-745.

Schaal, B., Coureaud, G., Langlois, D., Ginies, C., Semon, E., Perrier, G., 2003. Chemical and behavioural characterization of the rabbit mammary pheromone. Nature 424, 68-72.

Schoenbaum, G., Eichenbaum, H., 1995. Information coding in the rodent prefrontal cortex. I. Single-neuron activity in orbitofrontal cortex compared with that in pyriform cortex. J.Neurophysiol. 74, 733-750.

Shepherd, G.M., Greer, C.A., Mazzarello, P., Sassoe-Pognetto, M., 2011. The first images of nerve cells: Golgi on the olfactory bulb 1875. Brain Res.Rev. 66, 92-105.

Shipley, M.T., Adamek, G.D., 1984. The connections of the mouse olfactory bulb: a study using orthograde and retrograde transport of wheat germ agglutinin conjugated to horseradish peroxidase. Brain Res.Bull. 12, 669-688.

Shipley, M.T., Ennis, M., Puche, A.C., 2004. Olfactory system. The rat nervous system, Academic Press ed, San Diego, pp. 923-964.

Shulman, R.G., Rothman, D.L., Hyder, F., 1999. Stimulated changes in localized cerebral energy consumption under anesthesia. Proc.Natl.Acad.Sci.U.S.A 96, 3245-3250.

Silva, A.C., Bock, N.A., 2008. Manganese-enhanced MRI: An exceptional tool in translational neuroimaging. Schizophrenia Bulletin 34, 595-604.

Silva, A.C., Lee, J.H., Aoki, I., Koretsky, A.P., 2004. Manganese-enhanced magnetic resonance imaging (MEMRI): methodological and practical considerations. NMR Biomed. 17, 532-543.

Sloot, W.N., Gramsbergen, J.B., 1994. Axonal transport of manganese and its relevance to selective neurotoxicity in the rat basal ganglia. Brain Res. 657, 124-132.

Small, D.M., Jones-Gotman, M., Zatorre, R.J., Petrides, M., Evans, A.C., 1997. Flavor processing: more than the sum of its parts. Neuroreport 8, 3913-3917.

Smith, K.D.B., Kallhoff, V., Zheng, H., Pautler, R.G., 2007. In vivo axonal transport rates decrease in a mouse model of Alzheimer's disease. NeuroImage 35, 1401-1408.

Sobel, N., Prabhakaran, V., Desmond, J.E., Glover, G.H., Goode, R.L., Sullivan, E.V., Gabrieli, J.D., 1998a. Sniffing and smelling: separate subsystems in the human olfactory cortex. Nature 392, 282-286.

Sobel, N., Prabhakaran, V., Hartley, C.A., Desmond, J.E., Glover, G.H., Sullivan, E.V., Gabrieli, J.D., 1999. Blind smell: brain activation induced by an undetected air-borne chemical. Brain 122 (Pt 2), 209-217.

Sobel, N., Prabhakaran, V., Hartley, C.A., Desmond, J.E., Zhao, Z., Glover, G.H., Gabrieli, J.D., Sullivan, E.V., 1998b. Odorant-induced and sniff-induced activation in the cerebellum of the human. J.Neurosci. 18, 8990-9001.

Soria, G., Wiedermann, D., Justicia, C., Ramos-Cabrer, P., Hoehn, M., 2008. Reproducible imaging of rat corticothalamic pathway by longitudinal manganese-enhanced MRI (L-MEMRI). Neuroimage. 41, 668-674.

Sosulski, D.L., Lissitsyna, B.M., Cutforth, T., Axel, R., Datta, S.R., 2011. Distinct representations of olfactory information in different cortical centres. Nature 472, 213-216.

Staubli, U., Fraser, D., Faraday, R., Lynch, G., 1987. Olfaction and the "data" memory system in rats. Behav.Neurosci. 101, 757-765.

Stettler, D.D., Axel, R., 2009. Representations of odor in the piriform cortex. Neuron 63, 854-864.

Stewart, W.B., Kauer, J.S., Shepherd, G.M., 1979. Functional organization of rat olfactory bulb analysed by the 2-deoxyglucose method. J.Comp Neurol. 185, 715-734.

Thuen, M., Berry, M., Pedersen, T.B., Goa, P.E., Summerfield, M., Haraldseth, O., Sandvig, A., Brekken, C., 2008. Manganese-enhanced MRI of the rat visual pathway: acute neural toxicity, contrast enhancement, axon resolution, axonal transport, and clearance of Mn(2+). J.Magn Reson.Imaging 28, 855-865.

Thuen, M., Singstad, T.E., Pedersen, T.B., Haraldseth, O., Berry, M., Sandvig, A., Brekken, C., 2005. Manganese-enhanced MRI of the optic visual pathway and optic nerve injury in adult rats. J.Magn Reson.Imaging 22, 492-500.

Tronel, S., Sara, S.J., 2002. Mapping of olfactory memory circuits: region-specific c-fos activation after odor-reward associative learning or after its retrieval. Learn.Mem. 9, 105-111.

Tusa, R.J., Palmer, L.A., Rosenquist, A.C., 1978. The retinotopic organization of area 17 (striate cortex) in the cat. J.Comp Neurol. 177, 213-235.

Van der Linden, A., Van, C.N., Ramos-Cabrer, P., Hoehn, M., 2007. Current status of functional MRI on small animals: application to physiology, pathophysiology, and cognition. NMR Biomed. 20, 522-545.

van der Zijden, J.P., Wu, O., van der Toorn, A., Roeling, T.P., Bleys, R.L.A.W., Dijkhuizen, R.M., 2007. Changes in neuronal connectivity after stroke in rats as studied by serial manganese-enhanced MRI. NeuroImage 34, 1650-1657.

van Dongen, Y.C., Deniau, J.M., Pennartz, C.M., Galis-de, G.Y., Voorn, P., Thierry, A.M., Groenewegen, H.J., 2005. Anatomical evidence for direct connections between the shell and core subregions of the rat nucleus accumbens. Neuroscience 136, 1049-1071.

Vassar, R., Chao, S.K., Sitcheran, R., Nunez, J.M., Vosshall, L.B., Axel, R., 1994. Topographic organization of sensory projections to the olfactory bulb. Cell 79, 981-991.

Verhagen, J.V., Engelen, L., 2006. The neurocognitive bases of human multimodal food perception: sensory integration. Neurosci.Biobehav.Rev. 30, 613-650.

Vernet-Maury, E., 1980. Trimethyl-thiazoline in fox feces: a natural alarming substance for the rat. In: Van der Starre H (Ed.), 7 ed. IRL, Washington, p. 407.

Voorn, P., Vanderschuren, L.J., Groenewegen, H.J., Robbins, T.W., Pennartz, C.M., 2004. Putting a spin on the dorsal-ventral divide of the striatum. Trends Neurosci. 27, 468-474.

Wesson, D.W., Wilson, D.A., 2010. Smelling sounds: olfactory-auditory sensory convergence in the olfactory tubercle. J.Neurosci. 30, 3013-3021.

West, C.H., Michael, R.P., 1990. Responses of units in the mesolimbic system to olfactory and somatosensory stimuli: modulation of sensory input by ventral tegmental stimulation. Brain Res. 532, 307-316.

Whitsel, B.L., Rustioni, A., Dreyer, D.A., Loe, P.R., Allen, E.E., Metz, C.B., 1978. Thalamic projections to S-I in macaque monkey. J.Comp Neurol. 178, 385-409.

Wilson, D.A., 1997. Binaral interactions in the rat piriform cortex. J.Neurophysiol. 78, 160-169.

Wilson, D.A., Stevenson, R.J., 2003. The fundamental role of memory in olfactory perception. Trends Neurosci. 26, 243-247.

Wyss, J.M., 1981. An autoradiographic study of the efferent connections of the entorhinal cortex in the rat. J.Comp Neurol. 199, 495-512.

Xu, F., Liu, N., Kida, I., Rothman, D.L., Hyder, F., Shepherd, G.M., 2003. Odor maps of aldehydes and esters revealed by functional MRI in the glomerular layer of the mouse olfactory bulb. Proc.Natl.Acad.Sci.U.S.A 100, 11029-11034.

Xu, F., Schaefer, M., Kida, I., Schafer, J., Liu, N., Rothman, D.L., Hyder, F., Restrepo, D., Shepherd, G.M., 2005. Simultaneous activation of mouse main and accessory olfactory bulbs by odors or pheromones. J.Comp Neurol. 489, 491-500.

Yousem, D.M., Maldjian, J.A., Siddiqi, F., Hummel, T., Alsop, D.C., Geckle, R.J., Bilker, W.B., Doty, R.L., 1999. Gender effects on odor-stimulated functional magnetic resonance imaging. Brain Res. 818, 480-487.

Yousem, D.M., Williams, S.C., Howard, R.O., Andrew, C., Simmons, A., Allin, M., Geckle, R.J., Suskind, D., Bullmore, E.T., Brammer, M.J., Doty, R.L., 1997. Functional MR imaging during odor stimulation: preliminary data. Radiology 204, 833-838.

Yu, X., Wadghiri, Y.Z., Sanes, D.H., Turnbull, D.H., 2005. In vivo auditory brain mapping in mice with Mn-enhanced MRI. Nat.Neurosci. 8, 961-968.

Yu, X., Zou, J., Babb, J.S., Johnson, G., Sanes, D.H., Turnbull, D.H., 2008. Statistical mapping of sound-evoked activity in the mouse auditory midbrain using Mn-enhanced MRI. NeuroImage 39, 223-230.

Zald, D.H., Donndelinger, M.J., Pardo, J.V., 1998. Elucidating dynamic brain interactions with across-subjects correlational analyses of positron emission tomographic data: the functional connectivity of the amygdala and orbitofrontal cortex during olfactory tasks. J.Cereb.Blood Flow Metab 18, 896-905.

Zald, D.H., Pardo, J.V., 1997. Emotion, olfaction, and the human amygdala: amygdala activation during aversive olfactory stimulation. Proc.Natl.Acad.Sci.U.S.A 94, 4119-4124.

Zatorre, R.J., Jones-Gotman, M., Evans, A.C., Meyer, E., 1992. Functional localization and lateralization of human olfactory cortex. Nature 360, 339-340.

Zeeni, N., Nadkarni, N., Bell, J.D., Even, P.C., Fromentin, G., Tome, D., Darcel, N., 2010. Peripherally injected cholecystokinin-induced neuronal activation is modified by dietary composition in mice. NeuroImage 50, 1560-1565.

Zelano, C., Montag, J., Johnson, B., Khan, R., Sobel, N., 2007. Dissociated representations of irritation and valence in human primary olfactory cortex. J.Neurophysiol. 97, 1969-1976.

Zhou, W., Chen, D., 2009. Fear-related chemosignals modulate recognition of fear in ambiguous facial expressions. Psychol.Sci. 20, 177-183.

Annexe

Résumé des communications dans des congrès internationaux

Manganese-enhanced fMRI in olfaction: optimisation of Mn dose with minimal deleterious effects upon odour induced behaviour in rats.

B. Lehallier[(1)], A. Ben Moussa[(1)], W. Ben Hassen[(1)], G. Coureaud[(2)], O. Rampin[(3)], B. Schaal[(2)], Y. Maurin[(3)], J.M. Bonny[(1)]

[(1)] UR370 QuaPA, INRA, F-63122 Saint Genès Champanelle, [(2)] CNRS-CESG, Dijon [(3)] UMR 1197 NOPA, INRA, Université Paris Sud, France.

In vivo functional magnetic resonance imaging (fMRI) is a method of choice to identify brain structures activated by odours. BOLD-fMRI, used for most human studies, yields short lasting signals imposing the stimulus to be delivered during MRI acquisition. Hence, investigations on animal models required anaesthesia which alters neural responses to odour. The use of manganese as a contrast agent, which gives rise to a long lasting signal and therefore uncouples stimulation from MRI acquisition, appears to be an adequate strategy. Manganese is injected in nostrils, and odour stimulations are subsequently applied on awake animals. Animals are then anesthetized and MRI is performed *a posteriori* for long periods to improve signal-to-noise ratio. Yet, an important drawback of this technique is the toxic effect of manganese which may alter locomotor behaviour and/or olfactory perception. The purpose of our study was to find the maximal manganese dose providing a good contrast in fMRI studies while simultaneously preserving a normal behaviour in animals.

Five groups of three adult rats received increasing doses of Mn in both nostrils (0, 0.3, 1, 3, 8 µmol) 25' before being tested for behavioural performances in an open-field. The open-field arena was equipped with a sniffing port through which a familiar food odour was delivered for 5' every 30'. Animals were videorecorded during 120' in the arena. Latency, frequency and duration of locomotor activity and sniffing behaviour were quantified.

Our results show that, within the dose range studied, locomotor activity without odour stimulation was not affected by manganese, while frequency and duration of odour-induced behaviours were dose-dependently decreased. These results allow determining the optimal manganese dose sparing olfactory perception while simultaneously ensuring a good contrast in fMRI studies. Toxic effects of manganese have thus to be considered before functional interpretation of the activation maps obtained by Mn enhanced fMRI.

Dynamic MEMRI in olfaction: optimisation of Mn dose with minimal deleterious effects upon odour induced behaviour in rats.

B. Lehallier[(1)], A. Ben Moussa[(1)], W. Ben Hassen[(1)], G. Coureaud[(2)], O. Rampin[(3)], B. Schaal[(2)], Y. Maurin[(3)], J.M. Bonny[(1)]

[(1)] UR370 QuaPA, INRA, F-63122 Saint Genès Champanelle, [(2)] CNRS-CESG, Dijon [(3)] UMR 1197 NOPA, INRA, Université Paris Sud, France.

Purpose/Introduction

In vivo functional magnetic resonance imaging (fMRI) is a method of choice to identify brain structures activated by odours. BOLD-fMRI, used for most human studies, yields short lasting signals imposing the stimulus to be delivered during MRI acquisition. Hence, investigations on animal models required anaesthesia which alters neural responses to odour. Manganese enhanced MRI (MEMRI) which gives rise to a long lasting signal and therefore uncouples stimulation from MRI acquisition, appears to be an adequate strategy. Manganese is injected in nostrils, and odour stimulations are subsequently applied on awake animals. Animals are then anesthetized and MRI is performed *a posteriori* for long periods to improve signal-to-noise ratio. Yet, an important drawback of MEMRI technique is the toxic effect of manganese which may alter locomotor behaviour and/or olfactory perception (1). The purpose of our study was to find the maximal manganese dose providing a good contrast in fMRI studies while simultaneously preserving a normal behaviour in animals. Using this optimal dose, contrast enhancement was analysed by dynamic imaging in order to detect regions elicited by odour.

Subjects and methods

Five groups of three adult rats received increasing doses of Mn in both nostrils (0, 0.3, 1, 3, 8 µmol) 25' before being tested for behavioural performances in an open-field. The open-field arena was equipped with a sniffing port through which a familiar food odour was delivered for 5' every 30'. Animals were videorecorded during 120' in the arena. Latency, frequency and duration of locomotor activity and sniffing behaviour were quantified.

For imaging sessions, rats received 0.3 µmol of Mn and were stimulated by odour 5' every 30' for 240'. Afterwards, dynamic MRI was performed at 4.7T under anaesthesia by 3D T1-weighted RARE every 7'30" for 180'. Signal variations over time were analysed using independent component analysis (ICA) under FSL platform.

Results

Our results show that, within the dose range studied, locomotor activity without odour stimulation was not affected by manganese, while frequency and duration of odour-induced behaviours were dose-dependently decreased.

Using a dose preserving odour-induced behaviours, an uptake of manganese was observed in olfactory bulb and lateral olfactory tract. ICA revealed a signal increase over time (during the imaging run) in these regions.

Discussion/Conclusion

These results allow determining the optimal manganese dose sparing olfactory perception while simultaneously ensuring detection of manganese enhancement by rapid 3D MRI. Using such dose (0.3 µmol) and 40' of discontinuous odour for 240', MEMRI demonstrates manganese transport across synapses from olfactory mucosa to deep mitral cells during the period of odour stimulation. The signal increase over time is explained by anterograde progression of manganese in neurons activated by odour which persists under anesthaesia. Our objective is now to correlate this dynamic enhancement with odour characteristics and nutritional state.

Even if MEMRI is able to produce enhancement patterns depending on odorant in olfactory bulb (2), we demonstrate that toxic effects of manganese on olfactory ability have to be considered before functional interpretation of the activation maps obtained by this promising technique.

References

(1) Finkelstein *et al.*, Neurotoxicology (2007) 28:1003-14

(2) Chuang *et al.*, Neuroimage (2009) 44:363-72

Methods for groupwise analysis of functional MEMRI data

Benoist Lehallier[a], Philippe Andrey[b], Jasmine Burguet[b], Yves Maurin[b], Jean-Marie Bonny[a]

[a] UR370 QuaPA, INRA, F-63122 Saint-Genès-Champanelle, France

[b] UR 1197 NOeMI, INRA, F-78350 Jouy-en-Josas, France

(benoit.lehallier@clermont.inra.fr)

This study addressed the functional mapping of deep brain regions activated by odours in rats. For this purpose, manganese-enhanced MRI (MEMRI) was chosen. This method uses manganese (Mn) as an exogenous contrast agent (1). Manganese, a calcium analogue, is recruited by activated neurons and then slowly eliminated. This allows stimulations to be performed on conscious animals and images to be acquired under anaesthesia. Image contrast depends on intra-neuronal Mn concentration, and so reflects neuronal activity throughout the stimulation period. However, Mn remanence prevents control and activation state images being obtained in a single-subject experiment. Images have to be acquired through multi-subject studies and spatial variation of Mn concentration assessed by groupwise image comparison. Two image processing steps are crucial for such an analysis: (i) brain segmentation and (ii) inter-subject normalization. We have developed an original image processing sequence comprising (i) a semi-supervised brain segmentation method based on fast adjustment of an average three-dimensional brain model obtained from 20 manual segmentations and (ii) an iterative algorithm normalizing images in both spatial and intensity dimensions, independently of an a priori image target. This latter algorithm integrates the AIR package intra-modal inter-subject registration method (2), which was optimized by exhaustively searching for the best cost function/deformation model pair. Preliminary results indicate that our image processing sequence, associated with a voxelwise statistical test for comparing means, highlights deep brain regions involved in odour processing.

1. Van der Linden A., Van Camp N., Ramos-Cabrer P., Hoehn M., NMR in Biomedicine, 20, 522-545 (2007)

2. Woods R.P., Grafton S.T., Watson J.D.G., Sicotte N.L., Mazziotta J.C., Journal of Computer Assisted Tomography, 22, 153-165 (1998)

Functional Manganese Enhanced MRI Reveals Deep Brain Regions Activations In Response to Odorant Stimuli In Rats

Benoist Lehallier[a], Gérard Coureaud[b], Olivier Rampin[c], Benoist Schaal[b], Yves Maurin[c], Jean-Marie Bonny[a]

[a] *UR370 QuaPA, INRA, F-63122 Saint-Genès-Champanelle, France*
[b] *Equipe d'Ethologie Développementale et Psychologie Cognitive, UMR 6265 CNRS/INRA/UB/Agrosup Dijon, France*
[c] *UR 1197 NOeMI, INRA, F-78350 Jouy-en-Josas, France*
benoit.lehallier@clermont.inra.fr

This study addresses the functional mapping of deep brain regions activated by alimentary and pheromonal odours in rats. For this purpose, manganese-enhanced MRI (MEMRI) was chosen. This method uses manganese (Mn) as an exogenous contrast agent (1). Manganese, a calcium analogue, is recruited by activated neurons and then slowly eliminated. This allows olfactory stimulations to be performed during several hours on conscious animals and images to be subsequently acquired under anaesthesia. Image contrast depends on intra-neuronal Mn concentration, and therefore reflects neuronal activity throughout the stimulation period. However, a major drawback of this technique is the toxic effect of manganese, which may alter locomotor behaviour and/or olfactory perception. Firstly, we defined the maximal manganese dose which could be injected into nostrils (2) to provide a good contrast in fMRI studies while simultaneously preserving odour induced behaviour in animals. Also, Mn remanence prevents control and activation state images from being obtained in a single-subject experiment. Images have to be acquired through multi-subject studies and spatial variation of Mn concentration assessed by groupwise image comparison. We have developed an original image processing sequence comprising (i) a semi-supervised brain segmentation method based on fast adjustment of an average three-dimensional brain model obtained from 20 manual segmentations and (ii) an iterative algorithm normalizing images in both spatial and intensity dimensions, independently of an *a priori* image target. Preliminary results obtained from large cohorts of rats indicate that the combination of (i) an optimal dose preserving odour induced behaviour with (ii) an image processing chain for segmentation and normalization and with (iii) a voxelwise statistical test for comparing means, highlights deep brain regions involved in odour processing.

1. Van der Linden A. *et al.*, *NMR in Biomedicine*, 20, 522-545 (2007)

2. Lehallier B. *et al.*, Manganese-enhanced fMRI in olfaction: optimisation of Mn dose with minimal deleterious effects upon odour induced behaviour in rats. XIX *Ecro Congress* (2009)

Benoist Lehallier

Traitement cérébral d'odeurs biologiquement signifiantes, révélé chez le rat par imagerie RMN fonctionnelle du manganèse

Résumé : L'objectif de cette thèse est d'utiliser MEMRI (manganese-enhanced magnetic resonance imaging) pour étudier le traitement d'odeurs signifiantes dans le cortex olfactif primaire de rats dans les conditions les plus proches de la perception naturelle. MEMRI est une méthode fondée sur la détection d'un agent de contraste fonctionnel et rémanent de l'activité neuronale, le manganèse, qui a prouvé son efficacité pour montrer le traitement différencié d'odeurs dans le bulbe olfactif chez l'animal vigile. Cependant, cette technique a été surtout utilisée pour tracer les voies neuronales, mais relativement peu pour explorer des fonctions sensorielles. C'est pourquoi nous avons conduit deux études visant l'une à définir les conditions d'application du manganèse et l'autre à optimiser le traitement des images MEMRI, avant d'aborder la question biologique proprement dite. S'appuyant sur ces développements méthodologiques, nous avons ensuite utilisé MEMRI pour étudier les variations du traitement d'odeurs signifiantes (odeurs de nourriture et de prédateur comparées à une situation de contrôle) dans le cortex olfactif primaire de rats. Nous avons montré que le traitement cérébral d'une odeur de prédateur est différent de celui de la situation de contrôle dans le cortex olfactif primaire. Nous avons confirmé ce résultat par immunomarquage Fos dans le cortex piriforme. Mis ensembles, les résultats de MEMRI et Fos suggèrent que le traitement cérébral d'une odeur peut varier en termes de taille de populations de neurones recrutés ainsi qu'en termes d'intensité de l'activation de ces neurones. Enfin, les résultats MEMRI montrent qu'un message olfactif crucial, pour la survie, est traité asymétriquement dans le cerveau. Les avancées méthodologiques et scientifiques qu'apporte cette thèse ouvrent la voie à une meilleure compréhension du traitement cérébral des odeurs.
Mots-clés : MEMRI, olfaction, rat, manganèse, toxicité, normalisation, cortex olfactif primaire

Central processing of behaviorally relevant odors in the awake rat, as revealed by Manganese-enhanced MRI

Abstract: The aim of this thesis was to use MEMRI (manganese-enhanced magnetic resonance imaging) for studying the processing of behaviorally significant odors in the rat primary olfactory cortex, under conditions close to natural perception in awake animals. MEMRI is a method based on the detection of a functional and remanent contrast agent, manganese, which has proved to be valuable for studying odor processing in the olfactory bulb. However, this method has mainly been used to trace neuronal pathways, but seldom to explore sensory functions. Here, we have conducted two studies to define the conditions of application of manganese and to optimize processing of MEMRI images. Based on these methodological developments, we have then used MEMRI to investigate the activation of central olfactory structures following exposure of awake rats to biologically relevant odors (food and predator odors compared to a control situation). MEMRI revealed that a predator odor is processed differently from the control situation in the primary olfactory cortex. Fos immunolabeling in the anterior piriform cortex corroborated this result. Altogether, MEMRI and Fos results suggest that olfactory processing may rely on both the intensity of activation and the size of neuronal populations recruited. Finally, MEMRI revealed that an olfactory message, crucial for survival, is asymmetrically processed in the brain. Methodological and scientific advances brought by this thesis will be useful for better understanding brain olfactory processing.
Keywords: MEMRI, olfaction, rat, manganese, toxicity, normalization, primary olfactory cortex

Université Blaise Pascal – Ecole Doctorale des Sciences de la Vie et de la Santé
Laboratoire STIM – U.R. 370 – INRA de Theix
63122 Saint Genès Champanelle